FUNCTIONAL ANNOTATION OF THE PIEBALD DELETION REGION OF MOUSE CHROMOSOME 14

A Dissertation

Presented to the Faculty of the Graduate School

of Cornell University

In Partial Fulfillment of the Requirements for the Degree of

Doctor of Philosophy

by

James Augustus Hagarman

February 2010

FUNCTIONAL ANNOTATION OF THE PIEBALD DELETION REGION OF MOUSE CHROMOSOME 14

James Augustus Hagarman, Ph. D.

Cornell University 2010

We currently know a great deal about the mouse genome, including sequence, genomic location and expression patterns for many genes. However, the function of individual genes is unknown in many cases. Understanding gene function is critical to assess a gene's relationship to human health and disease. Forward genetic screens are a classic strategy to evaluate animals for phenotypes of interest and link a gene to a biological function. The piebald deletion complex is a set of overlapping chromosomal deficiencies on distal mouse chromosome 14 created during the specific locus test. We have surveyed the functional genetic content of the piebald deletion region in an essential gene mutagenesis screen of 952 genomes to recover seven lethal mutants. The screen uses the deletion resource and the spotted coat color of the piebald mouse to identify developmentally critical genes within an ~19Mb interval of the distal region of mouse chromosome 14. The ENU-induced mutations were mapped to defined genetic intervals using the piebald deletion panel. Lethal mutations identified included a loss-of-function allele of *Phr1* resulting in respiratory distress at birth and a locus required for establishment of the left-right embryonic axis.

We further characterized the ENU-induced mutation disrupting left-right patterning as an allele of Progesterone induced blocking factor 1 (*Pibf1)* by positional cloning and the characterization of a second allele. We show that the phenotype of

Pibf1-deficient embryos is consistent with disrupted Hedgehog signaling. We also find that PIBF1 localizes to the ciliary axoneme and that loss of *Pibf1* disrupts the formation of both cilia and microvilli suggesting a role in the organization of the cytoskeleton. Thus, our studies identify *Pibf1* as a gene important for cytoskeletal organization, ciliogenesis and signal transduction. A functional map of the piebald region integrates experimental genetic data from the deletion panel, mutagenesis screen, and the targeted disruption of specific genes. A comparison of several genomic intervals targeted in regional mutagenesis screens suggests that the piebald region is characterized by a low gene density and high essential gene density with a distinct genomic content and organization that supports complex regulatory interactions and promotes evolutionary stability.

BIOGRAPHICAL SKETCH

James Hagarman, the son of Holly V. Brown and James A. Hagarman, was born August 12, 1973 in Abington, PA. The author grew up in West Chester, PA where he graduated from Henderson High School in 1991. He attended the Pennsylvania State University and completed his degree in Biology, B.S. (1995). After completing his degree he enlisted in the US Army and served until 2001. He then worked at The Jackson Laboratory, first as a laboratory animal technician, then as a research assistant in the lab of Dr. Timothy P. O'Brien. He joined Dr. O'Brien's lab as a graduate student in the Functional Genomics program offered through the University of Maine and The Jackson Laboratory. In 2005, the O'Brien lab moved to Cornell University. Jim completed his Ph.D. in the field of Molecular and Integrative Physiology in the fall of 2009 for his thesis titled "Functional annotation of the piebald deletion region of mouse chromosome 14."

ACKNOWLEDGMENTS

I would like to thank the current and past members of the O'Brien lab for thoughtful discussion and valuable support: Ian Welsh, Kevin Peterson, Yingying Zhao, Randy Babiuk, Lindsay Shopland, and Mark Riccio. I would especially like to thank Ian, who was primarily responsible for training me in the techniques used in my research. I would like to recognize my committee members Paula Cohen, Maria Garcia-Garcia, Teresa Gunn and John Schimenti for important suggestions and feedback during the progress of my studies. Thank you also to the members of the Roberson and Cohen labs for creating a positive work environment and being generous with assistance as well as reagents. Finally, I would like to thank my advisor, Tim O'Brien, for his unwavering support during my scientific development.

TABLE OF CONTENTS

Biographical Sketch iii
Acknowledgements iv
Table of Contents v
List of Figures vii
List of Tables viii

Chapter 1: Introduction 1
1.1 The mouse as a model for human disease and development 1
1.2 Disrupting genes to understand gene function 2
1.3 Mutagenesis in the mouse 3
1.3.1 ENU mutagenesis 4
1.3.1.1 Genome-wide screens 5
1.3.1.2 Regional screens 7
1.4 The specific locus test 9
1.5 Deletion complexes as genetic resources 10
1.6 Summary of research chapters 11

Chapter 2: An essential gene mutagenesis screen across the highly conserved piebald deletion region 14
2.1 Introduction 14
2.2 Materials and methods 16
2.3 Screen design 18
2.4 Results 18
2.4.1 Screen yield 18
2.4.2 Deletion mapping of ENU-induced mutations 20
2.4.3 Initial characterization of ENU-induced alleles 23
2.4.4 Genetic characterization of ENU-induced alleles 25
2.4.5 An ENU-induced mutation in *Phr1* 28

Chapter 3: An evolving functional map of the piebald deletion region 31
3.1 Introduction 31
3.2 Materials and methods 31
3.3 A functional map of the piebald deletion region 33
3.4 Regional functional organization of the genome 37
3.4.1 Essential gene density 38
3.3.2 Comparisons of genomic organization between genomic regions 39
3.5 Discussion 41

Chapter 4: Cloning and characterization of an ENU-induced mutation

in Progesterone Induced Blocking Factor 1 44
4.1 Introduction 44
4.2 Materials and methods 46
4.3 The phenotype of ENU 128-7 mutants 48
4.4 Positional cloning of ENU 128-7 48
4.4.1 Genetic confirmation of *Pibf1* as the gene responsible for the phenotype of ENU 128-7 mutants 53
4.5 *Pibf1* is expressed in multiple embryonic regions patterned by Hedgehog signaling 53
4.6 Altered left/right patterning in *Pibf1*$^{128-7}$ mutant embryos 57
4.7 Midline defects in *Pibf1*$^{128-7}$ embryos 59
4.8 Embryological defects in *Pibf1*$^{128-7}$ mutant embryos confirm a defect in SHH signaling 62
4.8.1 Vascular defects in *Pibf1*$^{-/-}$ mutants 63
4.8.2 Somite defects in *Pibf1*$^{-/-}$ embryos 65
4.8.3 Disrupted neural crest development in *Pibf1*$^{-/-}$ embryos 66
4.8.4 Patterning of ventral neural tube progenitors is disrupted in *Pibf1*$^{-/-}$ embryos 68
4.9 *Pibf1* functions in SHH target cells downstream of *Ptch1* 69
4.10 *Pibf1*$^{128-7}$ mutants have a severe reduction, but not a complete loss of Hedgehog signaling 72

Chapter 5: PIBF1 and cytoskeletal organization 74
5.1 Introduction 74
5.2 Materials and methods 75
5.3 Cilia are disrupted in *Pibf1*$^{128-7}$ mutants 76
5.4 PIBF1 is localized to the cilia 77
5.5 Cilia loss contributes to, but does not fully explain the left/right patterning defects in *Pibf1*$^{128-7}$ mutant embryos 77
5.6 Identifying PIBF1 as a component of the ciliome 79
5.7 Future studies of *Pibf1* function 82
5.7.1 *Pibf1* and cell polarity 82
5.7.2 Investigating the role of *Pibf1* in microtubule stability 84
5.7.3 Compartmentalization of signaling molecules 86

Chapter 6: Summary and Conclusions 88

Bibliography 91

LIST OF FIGURES

Figure 1.1 Genome-wide and regional genetic screens 6
Figure 1.2 Piebald mice display white spotting due to loss of *Ednrb* function 12
Figure 2.1 An ENU mutagenesis screen to recover recessive lethal mutations within the piebald deletion region 19
Figure 2.2 Developmental defects characteristic of embryos homozygous for the ENU-induced 128-7 mutation 24
Figure 2.3 Summary of pairwise complementation crosses involving ENU-induced mutations recovered in the piebald region screen 26
Figure 2.4 The ENU-induced 274-4 mutation disrupts *Phr1* and results in respiratory distress at birth 29
Figure 3.1 Functional map of the piebald deletion region 34
Figure 3.2 Genomic organization of chromosomal intervals targeted in regional ENU-mutagenesis screens 40
Figure 3.3 Multispecies comparison of conserved syntenic segments across chromosomal intervals targeted in ENU-mutagenesis screens 42
Figure 4.1 ENU 128-7 mutants exhibit multiple defects in embryonic development caused by a mutation in *Pibf1* 49
Figure 4.2 The point mutation in intron 2 of *Pibf1* is at the lariat branch point site and leads to a splicing defect in 128-7 mutant embryos 52
Figure 4.3 *Pibf1* gene trap allele fails to rescue the lethality of the ENU-induced mutation 54
Figure 4.4 *Pibf1* expression pattern 56
Figure 4.5 Proper expression of left-right patterning genes is lost in *Pibf1* mutant embryos 58
Figure 4.6 Premature degeneration of the notochord in *Pibf1* embryos 60
Figure 4.7 Patterning of HH signaling-dependent tissues is disrupted in *Pibf1* Mutants 64
Figure 4.8 Ventral neural tube patterning is disrupted in *Pibf1* mutants 70
Figure 4.9 Double mutant analysis shows *Pibf1* functions in SHH-responsive cells downstream of *Ptch1* 71
Figure 5.1 Loss of *Pibf1* causes a defect in cilia formation and PIBF1 localizes to the ciliary axoneme 78
Figure 5.2 *Pibf1* is conserved between mouse and *Trypanosome Brucei* 81

LIST OF TABLES

Table 2.1 Deletion mapping of ENU-induced lethal mutations 21
Table 2.2 Gene content of genomic intervals defined by piebald deletions used for complementation mapping ENU-induced mutations 22
Table 3.1 Regional comparison of gene and essential gene densities in the mouse genome 37
Table 3.2 Gene content and organization of genomic regions surveyed in mouse mutagenesis screen 39

CHAPTER 1

INTRODUCTION

1.1 The mouse as a model for human disease and development

The human and mouse lineages diverged between 65 and 85 million years ago (Lee, 1999). In spite of this, the mouse is the pre-eminent model for human physiology and disease. Its size, short generation time and suitability for genetic manipulation make it ideal for the laboratory environment (Kile and Hilton, 2005). In addition, well-characterized inbred strains exist, allowing researchers to minimize genetic variation in their studies. The numerous inbred mouse strains minimize noise and artifact during experimentation, providing a consistent and uniform animal model. Mouse models currently exist that allow research into many of the most clinically relevant human diseases, from down syndrome, cystic fibrosis and glaucoma to complex behavioral diseases such as schizophrenia and autism. Mouse models give insight into the etiology of such diseases as well as identify possible therapeutic targets.

The publication of the human genome sequence in 2001, followed by the mouse in 2002, provided an unprecedented level of detail of the genetic sequences upon which the phenotype of an individual is built (Venter et al., 2001; Waterston et al., 2002). 40% of the human genome can be aligned to the mouse genome at the nucleotide level and over 90% of the mouse and human genomes may be partitioned into regions of conserved synteny, allowing comparative genomics to link the work of basic and clinical researchers (Waterston et al., 2002). While the function of genes may sometimes be inferred from sequence similarity, conserved protein domains or expression patterns, the complexity of mammalian systems requires empirical study.

The mouse provides an excellent opportunity to understand gene function through experimentation.

1.2 Disrupting genes to understand gene function

Although scientists have long studied inbred strains and spontaneous mutations in mice, breakthroughs in molecular biology have revolutionized mouse genetics. The analysis of DNA sequence allows the identification and positioning, not only of genes, but also of various functional elements controlling genomic functions such as gene expression. However, building such a catalog is only the first step toward understanding the role of the genome in biology. Many aspects of gene function cannot be deduced from sequence analysis alone. Collecting genetic variants in model organisms that perturb gene function can give insight into a gene's role and make important contributions to functional genomics through the examination of the resulting phenotype (Nadeau et al., 2001).

Early studies on variation took advantage of the fact that most strains are of hybrid origin and that recessive alleles may remain undetected for many generations, or on the occurrence of new spontaneous, dominant alleles (Sturtevant, 1965). Herman Muller was the first to demonstrate the mutagenic action of x-rays and provided the first example of the artificial induction of mutation in *Drosophila* in 1927 (Muller, 1927). The induction of mutations by chemical means was shown in 1941 when Auerbach and Robson showed that mustard gas is mutagenic (Sturtevant, 1965). Although a comprehensive list of mutations known to affect embryogenesis was compiled in 1970, genetic screens to identify such mutations weren't carried out until more recently (Wright, 1970). In the 1980s researchers screened the *Drosophila* genome for mutations disrupting segment number and polarity, and in the 1990s successfully mutagenized and screened the zebrafish genome, assigning 894 mutants to 372 complementation groups involved in a spectrum of mutant phenotypes (Haffter

et al., 1996; Nusslein-Volhard and Wieschaus, 1980). These screens in lower organisms set the stage for mutagenesis in the mouse and for exploring gene function in a mammalian system.

1.3 Mutagenesis in the mouse

The functional annotation of the mammalian genome is an ongoing project in the biomedical sciences community. The majority of efforts to uncover gene function in the mouse involve designing targeted vectors for, or inserting gene traps into, the mouse genome. Such methods are called 'reverse genetic' approaches because they start with the disrupted gene, however there is no guarantee that the resulting mouse will display an interesting phenotype. Efforts such as the knockout mouse project (KOMP) and the international gene trap consortium (IGTC) are generating large numbers of mouse mutants. The IGTC alone has over 435,000 cell lines that represent mutations in 38% of annotated genes (http://www.genetrap.org/). Knockouts have proven indispensable for understanding gene function, but provide a reductionist view. Conditional knockouts allow us to control gene expression in a tissue- or time-specific manner as well as titrate the amount of gene product up or down, but suffer drawbacks based on the efficiency of the recombinase. In addition, conditional knockouts generally fail to offer an opportunity to change the structure or activity of the protein. The ultimate realization of functional annotation is multiple mutations in every gene. These allelic series can be highly informative. The range of effects generated will give a more complete view of gene function in complex mammalian tissues.

As an example, although implicated in many physiological processes, embryos lacking the BRG1 subunit of the mammalian SWI/SNF-related complexes die as blastocysts, preventing a thorough understanding of the gene's function (Bultman et al., 2000). However, a chemically-induced mutation within the catalytic ATPase domain allows mutant embryos to develop normally until midgestation, when the

development of the erythroid lineage is disrupted leading to anemia and death (Bultman et al., 2005). The mutant protein is stable, assembles into SWI/SNF-related complexes and exhibits normal ATPase activity, but loses the ability to remodel nucleosomes. The ENU-induced mutation establishes a role for *Brg1* during organogenesis as well as demonstrating that the ATPase activity and chromatin remodeling functions of the protein may be decoupled, which would have been impossible to discover by simply knocking out the gene.

1.3.1 ENU mutagenesis

An effective way to generate mouse mutants that give insight into diverse gene function is through the application of phenotype-based genetic screens using the high-efficiency chemical mutagen N-ethyl-N-nitrosourea (ENU). ENU is an alkylating agent and its mechanism involves the donation of an ethyl group to DNA leading to mispairing (Favor, 1999). The most relevant DNA adducts are O^2-ethylthymine and O^4-ethylthymine (Allen, 1990). This is consistent with the observation that most base pair substitutions occur at A/T sites. Because ENU generates primarily point mutations it has the potential to generate an allelic series including hypomorphic, hypermorphic and neomorphic mutations that can provide novel insights into gene function. As determined in the specific locus test, ENU creates mutations in the mouse germline at a rate 12 times that of X-rays and over 200 times the spontaneous rate, inducing mutations at a frequency of one per locus in every 700 gametes (Hitotsumachi et al., 1985). A more recent, sequence-based assessment of ENU mutation frequency for a fractionated treatment protocol found a mutation frequency of one sequence change per 10^6 bp (Quwailid et al., 2004).

Present day mutagenesis screens use genetically engineered mouse strains and selective breeding strategies to perform a variety of screens. These can be genome-wide or regionally directed, recover dominant or recessive mutations, and/or isolate

mutants in specific areas of biology. Thus, ENU provides a complementary approach to gene targeting with the potential to create mutations that give insights unavailable through reverse genetic approaches. A complete functional annotation of the mammalian genome will only be accomplished with a combination of gene- and phenotype-based and large- and small-scale approaches.

1.3.1.1 Genome-wide screens

A genome-wide screen identifies dominant and recessive phenotypes of interest scattered throughout the genome and offers the most powerful approach for the isolation of new mutants to researchers interested in specific biological processes (Figure 1.1 A). A general strategy for genome-wide screens is as follows: G_0 mice are injected with ENU and crossed to wildtype females. The G1 offspring may then be screened for dominant phenotypes. G1 mice are crossed to wildtype females and the resulting G2 females mated back to the G1 male. G3 animals are produced that have a 25% probability to be homozygous for any recessive mutation present in the G2 female. In this way recessive mutations may be recovered in the G3 generation.

A number of genome-wide screens are being done to identify genes important in clinically relevant domains. These include visual, auditory, metabolic and behavioral function. The Neuroscience Mutagenesis Facility (NMF) at The Jackson Laboratory has so far screened over 28,000 G3 mice representing over 1600 distinct mutagenized pedigrees (Goldowitz et al., 2004). This includes more than 40 neurological mutant mouse lines. The NMF uses a series of high-throughput screens to detect mutations, including monitoring physiological and behavioral parameters over time. This screen provides a tool that may lead to a greater understanding of neurological disease.

Genome-wide screens also provide a way to identify important developmental

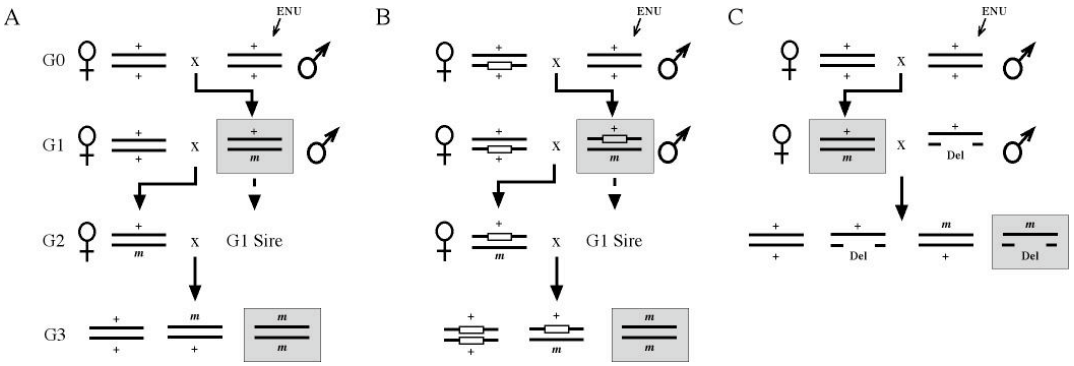

Figure 1.1 Genome-wide and regional genetic screens. (A) A conventional strategy for a genome-wide genetic screen takes three generations of breeding and can uncover both dominant and recessive mutations. An alternative approach to make mice homozygous for ENU-induced mutations in the G3 generation is through brother-sister mating of the G2 generation. (B) A balancer screen. The inversion is represented by the open box. Additional elements have been used to increase the efficiency of the screen, such as visible markers to identify the balancer or a recessive lethal mutation in the balancer to eliminate the need for genotyping of carriers. (C) A deletion screen. The primary advantage of the deletion-based regional screen is that one fewer generation of breeding is required and recessive mutations may be identified in the G2 generation. The class of animals examined for dominant phenotypes is shown in the shaded box in the G1 generation for each screen. The class of animals examined for recessive phenotypes is shown in the shaded box in either the G2 (deletion-based screen) or G3 (genome-wide & balancer screens) generation.

genes. Kathryn Anderson's lab at the Sloan-Kettering Institute has conducted a genome-wide screen for embryonic lethal mutations in the mouse (Kasarskis et al., 1998). They screened 380 lines of mice and identified 43 recessive mutations that map to single loci and cause morphological abnormalities in midgestation embryos (Garcia-Garcia et al., 2005). Among other valuable mouse mutants to come out of the screen were *wimple* and *flexo,* which were used to show that intraflagellar transport and cilia were essential for mammalian Hedgehog signaling (Huangfu et al., 2003).

In addition to those described above, large-scale genome-wide screens are being performed at the Neurogenomics Project at Northwestern University (http://genome.northwestern.edu/neuro/), the Reproductive Genomics Program at The Jackson Laboratory (http://reproductivegenomics.jax.org/index.html), the Mouse Heart, Lung, Blood, and Sleep Disorder Center at The Jackson Laboratory (http://pga.jax.org/index.html), the Australian Phenomics Facility at The Australian National University (http://www.apf.edu.au/index.shtml), the Beutler lab at The Scripps Research Institute (http://mutagenetix.scripps.edu/default.cfm?page=start), the Institute of Experimental Genetics at the German Research Center for Environmental Health (http://www.helmholtz-muenchen.de/en/ieg/group-functional-genetics/enu-screen/index.html), the Functional Genomics Section at MRC Harwell (http://www.har.mrc.ac.uk/research/mutagenesis/), and the Mutagenesis and Genomics Team at The Riken Institute in Japan (http://www.brc.riken.jp/lab/gsc/mouse/). That so many resources are being devoted to forward genetic screens in the mouse is a testament to their value in the scientific community.

1.3.1.2 Regional screens

Genetic screens may also be performed that focus on exploring the functional content of a defined chromosomal interval. A distinct advantage of a regional screen is that mapping is simplified. Regional screens use either marked balancer

chromosomes, which are several Mb inversions, or comparably large chromosomal deletions. Either way, the low-resolution mapping step used to localize induced mutations to a large chromosomal interval is eliminated. Spontaneous inversions exist that contain markers useful in genetic screens, such as the *rump white (Rw)* inversion on proximal Chr 5 that has a change in coat color caused by misexpression of the *Kit* receptor (Hough et al., 1998). In addition, Cre-*lox P* technology has allowed the creation of engineered mouse balancer chromosomes (Zheng et al., 1999). Balancer screens are three-generation screens similar to genome-wide screens and can identify mutations across the genome, but the balancer represses recombination and enriches for mutations in the interval spanned by the inversion (Figure 1.1 B). Regional screens using balancer chromosomes have been performed on chromosomes 11, 4 and 5 and have identified 147 mutations while screening 2289 genomes (Hentges et al., 2007; Kile et al., 2003; Wilson et al., 2005). Balancer screens still require high-resolution mapping to define the interval containing the mutation to a manageable size, typically 1-2 Mb. This can require hundreds to thousands of informative meioses, although a strategy to create local sets of chromosomal deletions for use in complementation tests has been described (Schimenti et al., 2000; Wilson et al., 2005).

Deletion-based regional screens have an additional advantage in that they require only two generations of breeding to produce test-class mice (Figure 1.1 C). In addition, the availability of a deletion complex can simplify fine mapping of ENU-induced mutations and facilitate positional cloning efforts. Deletion screens have been successfully run to isolate mutants linked to the albino and pink-eyed dilution regions using deletion complexes created during the specific locus test (SLT) (Rinchik and Carpenter, 1999; Rinchik et al., 2002). Rinchik and Carpenter performed a screen centered on the albino locus screening 4557 gametes and identified 31 new mutants arranged into 10 complementation groups. Mutations generated in this screen

identified the *Picalm* gene as necessary for hematopoiesis (fit1) (Potter et al., 1997) and created *Fah* mutants that are mouse models for acute and chronic forms of human tyrosinemia (Aponte et al., 2001). The largest collection of deletion complexes currently available are those that map to the loci involved in the SLT, however methods for generating deletion complexes at defined regions of the genome in ES cells have been developed that could be used to generate reagents for use in screens in addition to being tools strictly for mapping (You et al., 1997).

1.4 The specific locus test

Mutagenesis took off in the beginning of the atomic age due to intense interest in the effects of radiation on the human germline. The Oak Ridge National Laboratory became the pre-eminent center in the field of mammalian mutagenesis and Dr. William Russell made major contributions to forward genetics in the mouse. In 1947 Dr. Russell arrived at Oak Ridge National Laboratory with the goal of calculating a rate for heritable gene mutations induced by radiation. His research centered on the creation of a unique mouse strain called the T-stock mouse. In the SLT, the T-stock mouse, homozygous for mutations in seven easily identifiable traits (non-agouti, brown, chinchilla, dilute, pink-eye, piebald and short ear), was used in a simple one-generation screen to identify mutations linked to each locus. In the screen, male wildtype mice were irradiated and mated to T-stock females. A mutation at any one of the seven T-stock loci was immediately recognized in the offspring. With seven mutations packed into a single mouse, the T-stock mouse provided a valuable tool for genetic analysis, and because the screen only took one generation of breeding Dr. Russell was able to collect a volume of data rarely matched by today's geneticists. In his first paper Dr. Russell examined over 85,000 progeny and recovered 53 alleles for the seven loci (Russell, 1951).

The SLT has a rich genetic legacy, creating hundreds of mouse mutants and contributing greatly to our knowledge of DNA damage and repair. Among other accomplishments, Dr. Russell identified ENU as the most potent mutagen in the mouse. After testing over 20 chemicals, only three had shown clear-cut mutagenic potential in mouse spermatogonia (Russell et al., 1979). The most effective, procarbazine, produced 1/3 the number of mutations as acute radiation. By contrast, an acute dose of ENU produced 15 times as many mutations as procarbazine. Along with his wife Liane, Dr. Russell also showed that mammals are more sensitive to radiation than *Drosophila* and that in mice the mutation rate due to radiation was dependent on dose, in contrast to flies (Russell et al., 1958). This led to the hypothesis that in mammals some mutations could be repaired. As a final example of the usefulness of the SLT, radiation-induced translocations between the X-chromosome and autosomes generated in the SLT led to variegated patterning in offspring and provided support for the theory of X-inactivation (Russell, 1961).

1.5 Deletion complexes as genetic resources

One consequence of years of chemical and radiation experiments with T-stock mice was the generation of a large collection of deletions at the SLT loci. These independently induced alleles were organized by complementation tests into sets of overlapping, nested deletions (Russell, 1971). The deletion complexes provide a framework to create a detailed physical map of the region and can be used as tools to genetically identify functional loci. The dilute-short ear locus contains over 200 spontaneous, chemical- and radiation-induced alleles (Rinchik et al., 1986). Pairwise complementation crosses of this collection of alleles have been used to identify functional domains associated with pigment, skeletal patterning, neurological and lethal phenotypes. This approach allowed the identification of 9 loci and arranged

them, proximal to distal, on a physical map of the region. Thus, the genetics of the deletion series helped refine the functional annotation of the region.

A similar analysis was performed in the albino region of chromosome 7 using the *c-4FR60Hd* and *c-5FR60Hg* deletion lines. The analysis identified two novel loci, *eed* and *exed*, mapping to the distal part of the two albino deletions (Niswander et al., 1989). In *exed* mutants extraembryonic ectoderm does not develop, and primitive streak development and mesoderm production fails. The *eed* locus is required to form embryonic ectoderm. Mutants displayed a gross morphological abnormality at E8.5 due to a failure of the mesoderm to organize into somites. The *eed* locus was later shown to code for the mouse homolog of the *Drosophila* polycomb group gene *extra sex combs* (Schumacher et al., 1996). Polycomb group genes are responsible for the long-term maintenance of spatially restricted expression patterns of homeotic genes (Simon, 1995). Embryos lacking *eed* display disrupted A-P patterning of the primitive streak and lack a node, notochord and somites. The deletion-based genetic analysis of the albino region made possible the discovery of this global regulator of A-P patterning.

1.6 Summary of research chapters

My graduate work has focused on the functional annotation of a region of distal mouse chromosome 14 defined by the piebald deletion complex. The piebald deletion complex is a set of overlapping, nested deletions centered on the Endothelin Receptor B (*Ednrb*) locus on distal mouse chromosome 14. The *Ednrb* locus is one of the original seven loci used by Bill Russell in the SLT. *Ednrb* is required for the development of neural crest derived melanocytes and partial loss of *Ednrb* function leads to white spotting covering ~20% of the coat (Figure 1.2). Studies in chapter 2 take advantage of the spotted coat color of piebald mutants and the large chromosomal deletions created in the SLT to conduct a regional ENU mutagenesis screen on mouse

Figure 1.2 Piebald mice display white spotting due to loss of *Ednrb* function. White spotting in piebald mice is due to defective migration of neural crest-derived melanocytes. The black (bottom) mouse is homozygous for a spontaneous allele (*Ednrb*^{s}) containing an insertion of a transposon in intron 1 leading to 75% reduction in expression and white spotting covering ~20% of the coat. The brown (top) mouse carries one *Ednrb*^{s} allele while the second allele has a deletion (*Ednrb*$^{s\text{-}l}$) leading to complete loss of *Ednrb* function. *Ednrb*$^{s\text{-}l}$/*Ednrb*$^{s\text{-}l}$ homozygotes are almost completely white and are lethal as juveniles from megacolon due to loss of neural crest-derived enteric ganglion. *Ednrb*^{s}/*Ednrb*^{s} homozygotes were used in our mutagenesis screen.

chromosome 14 centered on the *Ednrb* locus. 952 pedigrees were screened, resulting in the recovery of seven lethal mutations, results that are comparable to other deletion-based screens. In chapter 3 I provide an integrated view of the genetic content and genomic organization of the piebald region in comparison with other genomic regions surveyed by regional mutagenesis screens. The comparisons highlight variations in the functional composition of genomic regions and reveal interesting relationships between essential gene density, structural organization and chromosome evolution. In chapter 4 I present a detailed characterization of an ENU-induced mutation in Progesterone induced blocking factor 1 (*Pibf1)*, one of the seven mutants recovered from our mutagenesis screen. I show that *Pibf1* is required for Hedgehog signaling and ciliogenesis. Finally, in chapter 5 I present data showing that *Pibf1* provides a potential functional link between microtubule- and actin-based cytoskeletal organization and the formation of structures that effect cell signaling during development and propose future experiments to explore that link. These studies uncover the function of individual genes while also helping us understand the genomic organization of the piebald region, in order build a more complete account of the functional genetic content of distal mouse chromosome 14.

CHAPTER II

AN ESSENTIAL GENE MUTAGENESIS SCREEN ACROSS THE HIGHLY CONSERVED PIEBALD DELETION REGION[1]

2.1 Introduction

Our lab is using the SLT-derived piebald deletion complex to annotate the distal region of mouse chromosome 14, map genes important for mammalian development and investigate the genomic architecture of the region. We have previously mapped the breakpoints of the deletions within the piebald complex using SSLP markers and have used complementation crosses to identify a number of developmentally essential loci within the region (O'Brien et al., 1996; Roix et al., 2001). Along with our genetic studies we have used computational and comparative genomic analysis to annotate the gene content and organization of distal mouse chromosome 14 (Peterson et al., 2002). The phenotypes of deletion homozygotes vary and include early lethality, defects in mesodermal supply, respiratory distress at birth and craniofacial malformations. We have identified candidate genes for several of these phenotypes (Roix et al., 2001).

Homozygous *Ednrb*$^{s\text{-}15DttMb}$ mutants (hereafter SLT-induced deletions are abbreviated using allele names, i.e. *Ednrb*$^{s\text{-}15DttMb}$ = *15DttMb*) fail to establish proper respiratory rhythm, become cyanotic and die of respiratory distress within thirty minutes of birth. The respiratory distress phenotype maps to a 480kb interval containing four genes. Of those four genes, *Sce1* mutants produce viable offspring and *Ednrb* mutants display juvenile lethality due to megacolon at ~3 weeks of age

[1] Hagarman, J.A. and O'Brien, T.P. (2009). An essential gene mutagenesis screen across the highly conserved piebald deletion region of mouse chromosome 14. *Genesis*. 47(6), 392-403. Reproduced with permission from *Genesis*, accepted for publication 13 January 2009.

(Hosoda et al., 1994). Within the respiratory distress interval is the candidate gene *Phr1*, the mouse ortholog of the *Drosophila highwire* gene. *Highwire* is a negative regulator of synaptic growth with homology to a family of ubiquitin ligases (DiAntonio et al., 2001). Mutant flies display synaptic overgrowth and defects in neurotransmitter release. Staining the diaphragm of *15DttMb* mutants shows they contain dysmorphic neuromuscular junctions comparable with the synaptic defects seen in *Drosophila highwire* mutants (Burgess et al., 2004). On the basis of conserved abnormal neuronal morphology we have proposed that *Phr1* is a candidate gene for the respiratory distress phenotype of *15DttMb* mutant mice.

Mice homozygous for the *36Pub* deletion are missing ~6Mb that when absent results in craniofacial malformations including cleft palate. The morphogenesis of the palate requires the coordinated growth, remodeling and fusion of the palatal shelves. This is dependent on epithelial-mesenchymal interactions requiring proper FGF signaling (Hilliard et al., 2005). The interval deleted from *36Pub* mutants contains *Spry2*, an antagonist of FGF signaling (Klein et al., 2006; Shim et al., 2005). Mice carrying a targeted disruption of *Spry2* fail to complement the *36Pub* deletion and a *Spry2*-BAC transgene rescues the clefting defect, demonstrating *Spry2* is required for proper palate morphogenesis (Welsh et al., 2007).

In order to identify candidate genes for additional deletion phenotypes, uncover novel developmentally important genes, and to extend our functional annotation of the piebald region we have performed a regional essential gene mutagenesis screen centered on the *Ednrb* locus. Our survey of 952 genomes recovered seven lethal mutants. Deletion mapping and allelism tests define four distinct complementation groups. Molecular and phenotypic studies demonstrate that these seven mutations likely correspond to novel essential genes and allelic variants of previously known essential genes that perform critical developmental functions such

as patterning the left-right embryonic axis and establishing the breathing rhythm required for survival at birth. We also provide an integrated view of the genetic content and genomic organization of the piebald region in comparison with genomic regions surveyed by regional mutagenesis screens targeting chromosomes 5, 7 and 11. Our comparisons highlight variations in the functional composition of genomic regions and reveal interesting relationships between essential gene density, structural organization and chromosome evolution.

2.2 Materials and methods

ENU Mutagenesis

(C57Bl/6J x SSL/Le)N_2 mice were generated as previously described (Hagge-Greenberg et al., 2001). G0 mice were injected with 3 x 65 mg/kg ENU and mated to C57Bl/6J females after a sterility period of ~8 weeks. G1 females were mated to *24Pub* male carriers and G2 offspring assayed for the presence of the test class, which contains the mutated SSL/Le chromosome in *trans* to the *24Pub* deletion. We considered a line to contain a lethal mutation when it produced zero piebald offspring out of 30 total G2 offspring. Any G1 female that produced a spotted pup in its first two litters was discarded. If a spotted pup was produced after the second litter it was genotyped to check for recombination.

Mice

SSL/Le and C57Bl/6J mice were obtained from The Jackson Laboratory and maintained as inbred stocks. All deletion stocks were obtained as heterozygous carriers on a (101/R1 x C3H/R1)F1 background. The deletion mice were then moved to a C57Bl/6J or cByB6F1/J background. Deletion heterozygous mice were identified by PCR using microsatellite markers proximal and distal to the deletions to identify 101/C3H and C57Bl/6J or cByB6F1/J polymorphisms. The markers used were: *4Pub,*

1XMLP - D14Mit225, *185*, *9*; *24Pub - D14Mit225*, *Dist4*; *48Uthc, 36Pub, 15DttMb - D14Mit265*, *177*; *1Acrg - D14Mit 225*, *94*. The *Dist4* primers are F 5'-CAG GGA TGT CTA ATC AGG AAG-3' and R 5'-GAA TGC CTG ATC TGG TCC TC-3'.

Mice carrying ENU-induced mutations were maintained as heterozygotes on a C57Bl/6J background. Mice were PCR genotyped with the microsatellite markers *D14Mit225*, *8*, *197*, and *95* to identify the mutated *s* chromosome. All markers are polymorphic between C57Bl/6J and SSL/Le and together they span the *24Pub* deletion.

Deletion mapping and testing allelism

To fine map the ENU-induced mutations carriers were crossed to a series of deletions centered on the *Ednrb* locus. Mutants were first crossed to the *1XMLP* deletion that spans the distal 10.7 Mb of the *24Pub* deletion from 99.7 Mb to 110.4 Mb. A deletion was defined as complementing if ENU/Del compound heterozygous spotted offspring (confirmed by genotyping with genetic markers) were produced and survive to wean. Additional deletions including *15DttMb*, *1Acrg*, and either *36Pub* or *48UThc* were also used in complementation tests. Complementation crosses are expected to yield 25% compound heterozygous offspring. We defined failure to complement as no spotted pups in 20 offspring. ENU mutations that map to the same region were intercrossed to assay for allelism with the same standard of no spotted pups in 20 offspring defining failure to complement.

Phenotype characterization

Timed matings were established between *24Pub* deletion and ENU-induced mutation heterozygous mice. Mutant offspring (ENU/*24Pub*) were identified by PCR genotyping of yolk sacs using markers as described for colony maintenance. Starting

at midgestation (embryonic day = E10.5) successive halving was used to assign mutant offspring to a gestational window and ultimately define a time of lethality. Each litter was examined for resorptions and progeny with gross morphological defects. Offspring were delivered by Cesarean section at E18.5 to investigate late gestation lethality and early postnatal survival. ENU-induced mutation heterozygous mice were intercrossed for phenotypic comparison between ENU homozygous and ENU/*24Pub* compound heterozygous mutants.

2.3 Screen design

We have established conditions and instituted a regional ENU mutagenesis screen using the piebald deletion stocks (Figure 2.1) (Hagge-Greenberg et al., 2001). Our screen takes advantage of the piebald coat color of SSL/Le inbred strain of mice, which is homozygous for an insertion (*s*) disrupting the function of the Endothelin receptor B (*Ednrb*) gene leading to failure in the migration of neural crest derived melanocytes. Piebald mice are mutagenized with 3 injections of 65mg/kg ENU. After a sterility period mutagenized mice are mated to C57Bl/6J females to generate G1 females carrying one mutagenized chromosome 14. Each G1 female represents a unique mutagenized genome. The G1 females are then crossed to *24Pub* males that carry a ~19Mb deletion. 25% of G2 offspring from this cross carry a mutagenized piebald region opposite the *24Pub* deletion and have a piebald coat color. A recessive lethal mutation within the region spanned by the *24Pub* deletion will result in the absence of the spotted class of mouse. This is an efficient way to screen for recessive lethal mutations in the piebald region.

2.4 Results

2.4.1 Screen yield

To perform the screen 103 G0 males were treated with a 195 mg/kg, fractionated dose of ENU (3 x 65 mg/kg weekly). The 65 G0 males (63%) that

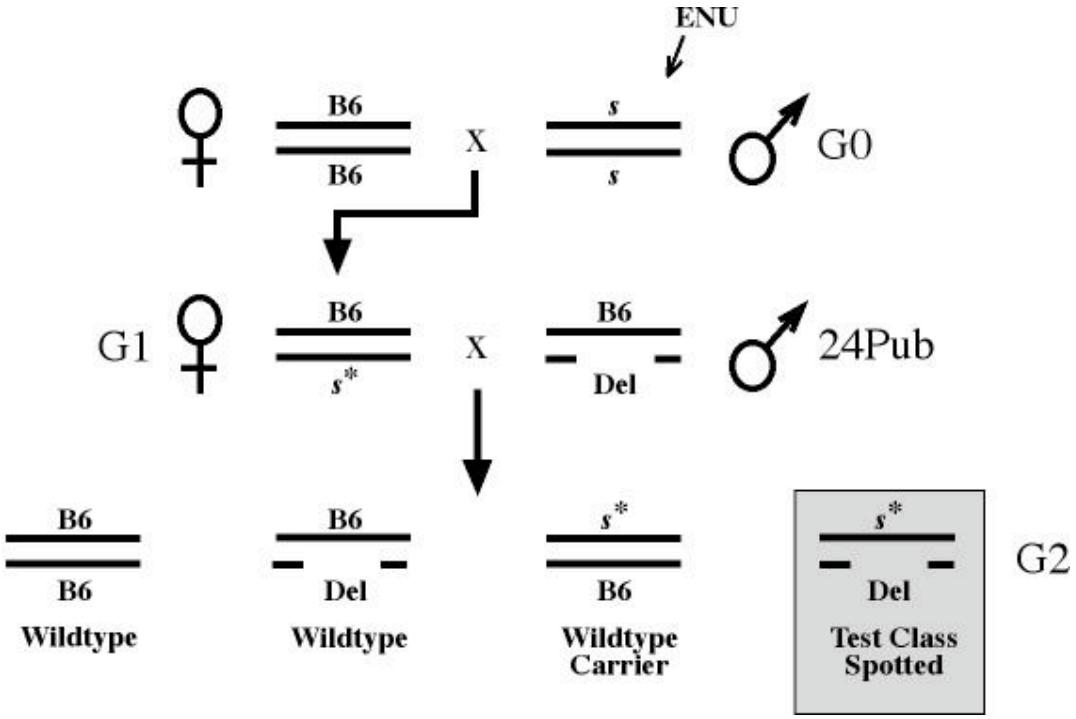

Figure 2.1 An ENU mutagenesis screen to recover recessive lethal mutations within the piebald deletion region. ENU-treated G0 male piebald mice are mated to C57Bl/6J females to produce G1 females that potentially carry a mutation linked to the *Ednrb*^{s} allele. G1 females are then crossed to *24Pub* males carrying a ~19Mb deletion. Four classes of G2 progeny are produced, 25% of which inherit the deletion in combination with the ENU-treated piebald chromosome and have the piebald coat color. The other 75% of offspring are black. Lethal mutations are identified by the loss of the spotted test class. Note that the carrier class of mouse may be identified by PCR.

returned to fertility produced an average of 17 G1 females. Two G0 males produced 1 G1 female while 10 G0 males produced >30 G1 females, with the maximum being 65 G1 females produced by a single male. Thus, the majority of pedigrees in our screen likely represented uniquely mutagenized genomes. However, there is some risk of redundant sampling given that a limited number of spermatogonial stem cells reestablish fertility in ENU treated mice.

We screened a total of 952 pedigrees in test crosses between G1 females and *24Pub* deletion heterozygous males. Pedigrees that produced spotted progeny in their first or second litter (~10 – 16 offspring) were discarded. Failure to produce spotted offspring among 30 G2 progeny was considered evidence of a recessive lethal mutation ($P = 0.0001$). We isolated seven recessive lethal mutations yielding 1 mutant mouse line for every 136 genomes screened. Our results are comparable with the SLT deletion-based ENU mutagenesis screens covering the albino and pink-eyed dilution regions of chromosome 7 that realized mutation recovery rates of 1/147 and 1/111, respectively (Rinchik and Carpenter, 1999; Rinchik et al., 2002).

2.4.2 Deletion mapping of ENU-induced mutations

A regionally directed mutagenesis screen using a chromosomal deficiency permits the efficient recovery of recessive mutations. In addition, the mutations are assigned to a defined genomic interval. The panel of overlapping chromosomal deficiencies at the piebald locus affords efficient further genetic localization of mutations using complementation mapping. We selected deletions from our previously characterized set of 20 piebald region deficiencies nested within the *24Pub* deletion interval for complementation mapping of the ENU-induced mutations (Roix et al., 2001).

For each mutation complementation mapping was initiated using the *1XMLP* deletion (Table 2.1). The proximal breakpoint of the *1XMLP* deletion is distal to the

Table 2.1 Deletion mapping of ENU-induced lethal mutations

Mutation	*24Pub*	*1XMLP*	*36Pub*	*15DttMb*	*1Acrg*
128-7	0/54 (0)	7/27 (26)			
174-16	0/57 (0)	15/54 (28)			
183-15	0/62 (0)	9/61 (14)			
251-1	2/63 (3)	10/56 (18)			
274-4	0/52 (0)	0/10 (0)	0/27 (0)	0/21 (0)	0/23 (0)
283-1	1/90 (0)	4/26 (15)			
289-5	0/62 (0)	6/26 (23)			

Ratio of spotted to total progeny classified at weaning (percentage).

proximal breakpoint of the *24Pub* deletion and the distal breakpoint of *1XMLP* extend beyond the distal end of *24Pub* (see Figure 3.1). Therefore, the *1XMLP* deletion partitions the *24Pub* deletion interval into two regions. Mutations complemented by the *1XMLP* deletion are localized to an 8.7 Mb proximal segment and failure to complement localizes mutations to a 10.7 Mb distal segment of the *24Pub* region surveyed in the screen. The *1XMLP* deletion complemented six of the ENU-induced mutations (128-7, 174-16, 183-15, 251-1, 283-1 and 289-5) localizing the search for candidate genes to the 8.7 Mb critical interval defined by the *24Pub* and *1XMLP* proximal breakpoints (Table 2.1 and see Figure 3.1). Higher resolution mapping of these mutations was not afforded by any remaining piebald deletions. Current annotations assign 10 RefSeq genes to the chromosomal interval containing these six ENU-induced mutations (Table 2.2).

The *1XMLP* deletion failed to complement one ENU-induced mutation (274-

Table 2.2 Gene content of genomic intervals defined by piebald deletions used for complementation mapping ENU-induced mutations

Deletion mapping interval (Mb)	Gene	Position (Mb) and strand	Targeted mutation	Phenotype	Reference
24Pub-Proximal to *1XMLP*-Proximal *D14Mit219* (91.6) - *D14Mit264* (100.3)	*Pcdh9*	93.4 -			
	4921530L21Rik	96.3 +			
	Klhl1	96.5 -	Viable	loss of motor control	He et al., 2006
	Dach1	98.2 -	Lethal	failure to thrive at birth	Davis et al., 2001
	2410129H14Rik	99.4 -			
	6720463M24Rik	99.4 +			
	Dis3	99.5 -			
	Pibf1	99.5 +			
	Klf5	99.7 +	Lethal	embryo lethal prior to E8.5	Shindo et al., 2002
	Klf12	100.3 -			
1XMLP-Proximal to *36Pub*-Proximal *D14Mit264* (100.3) - *D14Mit38* (102.8)	*1700110M21Rik*	101.6 -			
	Tbc1d4	101.8 -			
	Commd6	102.0 -			
	Uchl3	102.0 +	Viable	Unremarkable	Kurihara et al., 2000
	Lmo7	102.1 +			
15DttMb-Proximal to *1Acrg*-Distal *D14Mit38* (102.8) - *D14Mit94* (104.5)	*Kctd12*	103.4 -			
	Irg1	103.4 +			
	Cln5	103.5 +	Viable	Neurodegeneration	Kopra et al., 2004
	Fbxl3	103.5 -	Viable	Circadian rhythm defect	Godinho et al., 2007
	Phr1	103.6 -	Lethal	Respiratory distress at birth	Bloom et al., 2007
	Sce1	103.9 +	Viable	Unremarkable	Baden et al., 2005
	Slain1	104.0 +			
	Ednrb	104.2 -	Lethal	Juvenile lethal, ENS defect	Hosoda et al., 1994
1Acrg-Distal to *24Pub*-Distal *D14Mit94* (104.5) - *D14Mit95* (110.4)	*Pou4f1*	104.8 -	Lethal	Failure to thrive at birth	Xiang et al., 1996
	Rnf219	104.9 -			
	Rbm26	105.5 -			
	Ndfip2	105.6 +			
	Spry2	106.3 -	Lethal	Failure to thrive at wean	Shim et al., 2005
	Trim52	106.5 +			
	Slitrk2	109.3 -			

4), placing this mutation within the 10.7 Mb interval defined by the *1XMLP* proximal and *24Pub* distal breakpoints. Several piebald deletions provide an opportunity to refine the map position of this mutation. Complementation crosses with the *36Pub*, *15DttMb* and *1Acrg* deletions all failed to produce spotted progeny (Table 2.1). These results localize the ENU-induced mutation 274-4 to a critical interval defined by the *15DttMb* proximal and *1Acrg* distal breakpoints. There are 8 RefSeq genes annotated to this 1.7 Mb region of chromosome 14 (Table 2.2).

2.4.3 Initial characterization of ENU-induced alleles

Our screen detected essential genes as a mutation that results in lethality and loss of the visibly marked class of spotted mice. Thus, a gene required for viability at or before birth or survival approaching wean would be uncovered as an essential gene in our survey. We performed an initial characterization to determine the time of lethality and morphological defects associated with each ENU-induced mutation when heterozygous with the *24Pub* deletion used to uncover essential genes.

The mutations recovered result in lethality spanning a wide range of developmental stages, from peri-implantation/gastrulation stages to juvenile lethality. Three of the mutant lines (128-7, 174-16, 183-15) fail to survive gestation, while the remaining four mutant lines (251-1, 274-4, 283-1, 289-5) survive to birth. Three of the lines that complete gestation, 251-1, 283-1 and 289-5 are grossly normal at birth, but fail to thrive and die prior to weaning. The remaining line, 274-4, fails to establish a normal breathing rhythm at birth. Caesarean delivery at E18.5 established that newborn mice genotyping as 274-4/*24Pub* die of respiratory distress.

Three of the ENU-induced mutations when heterozygous with the *24Pub* deletion result in gestational lethality. Embryos genotyping as 183-15/*24Pub* are absent at E7.5 suggesting that this mutation disrupts a gene required for pre-implantation development, implantation or gastrulation. A total of 27 embryos were recovered from four litters at E7.5 with only 1 resorption site (4%), suggesting homozygous mutants are dying prior to implantation. A second mutation, 174-16 results in lethality in late gestation between E16.5 and E18.5. Identifying abnormalities, such as cardiovascular defects, responsible for the late gestational lethality of 174-16/*24Pub* mutants will require further investigation. A final mutation, 128-7, results in midgestational lethality. Embryos genotyping as 128-7/*24Pub* die at

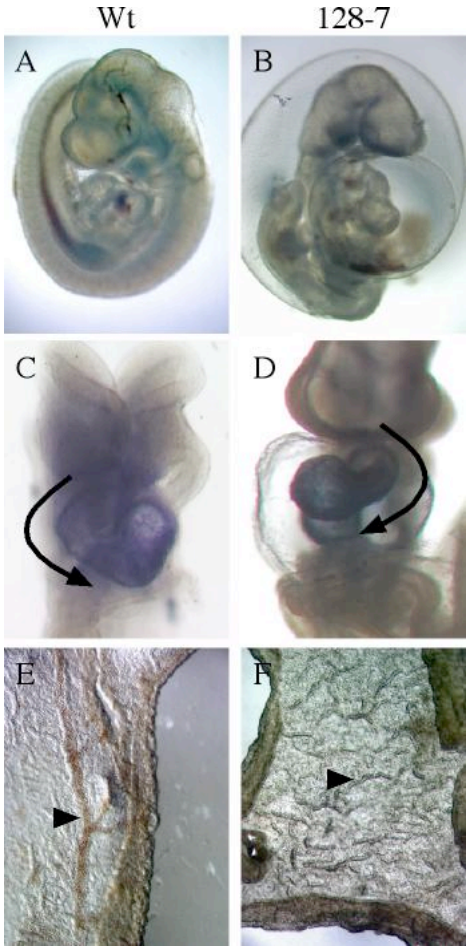

Figure 2.2 Developmental defects characteristic of embryos homozygous for the ENU-induced 128-7 mutation. Lateral (A and B) and frontal (C and D) views of age-matched wildtype (Wt) and 128-7 mutant embryos at E10.5. Mutant embryos fail to complete embryonic turning, head and branchial arches are dysmorphic, and the pericardium is swollen and contains blood (B). Wildtype embryos (C) exhibit rightward looping morphogenesis during heart development. The direction of heart looping morphogenesis is randomized in 128-7 mutants. Heart looping morphogenesis is reversed in the 128-7 mutant embryo shown in (D). Embryos in (C and D) are labeled for *Nkx2.5* expression to enhance visualization of the heart tube. At E10.5 the yolk sac of wildtype embryos (E) has formed a well-developed vasculature (arrows) compared with 128-7 mutant embryos (F), which fail to form mature blood vessels in the yolk sac (arrows).

~E10.5 and show incomplete and variable direction of heart looping and embryonic turning, suggesting a defect in the patterning of the left-right axis (Figure 2.2 A-D). In addition, the mid- and hindbrain regions and branchial arches of the mutant are reduced in size and have an abnormal morphology. The pericardium is swollen and often contains blood (Figure 2.2 B). The development of the yolk sac blood vessels is arrested at the vascular plexus stage while in wild type littermates mature vitelline vessels are visible (Figure 2.2 E, F arrowheads). Thus, the lethality of 128-7/*24Pub* mutants is likely related to cardiovascular defects associated with abnormal heart looping morphogenesis and blood vessel development.

2.4.4 Genetic characterization of ENU-induced alleles

Each of the ENU-induced mutations was identified owing to the lethal phenotype observed when heterozygous with the ~19 Mb *24Pub* deletion. Thus, the lethality associated with these compound heterozygotes potentially results from the ENU-induced mutation disrupting a single gene together with the complete loss of function for that gene when ablated by the deletion allele. Lethality might also reflect a synthetic phenotype resulting from the ENU-induced mutation together with haploinsufficiency for a number of genes removed by the *24Pub* deletion. Therefore, homozygosity for an ENU-induced mutation may present a different phenotype compared to the lethal phenotype of the ENU-induced mutation when heterozygous with the *24Pub* deletion.

We established the phenotype of mice homozygous for each ENU-induced mutation. Three of the ENU-induced mutations when homozygous (128-7, 183-15, 274-4) resulted in a lethal phenotype as seen when heterozygous with the *24Pub* deletion (Figure 2.3). The fully penetrant lethal phenotype suggests these mutations most likely correspond to a null allele of an essential gene. In contrast, four of the ENU mutations when homozygous (174-16, 251-1, 283-1, 289-5) displayed a

	128-7	174-16	183-15	251-1	274-4	283-1	289-5
128-7	0/109						
174-16	6/25	0/58					
183-15	3/20	8/33	0/38				
251-1	5/18	5/21	6/29	4/25			
274-4	nd	nd	nd	nd	0/39		
283-1	5/26	4/21	4/24	8/28	nd	4/24	
289-5	5/24	9/33	4/23	4/21	nd	7/22	8/15

Figure 2.3 Summary of pairwise complementation crosses involving ENU-induced mutations recovered in the piebald region screen. Each matrix element represents an intercross between mice heterozygous for the independently isolated ENU-induced mutation. The numbers in each box are the ratio of spotted offspring to total offspring. The ENU-induced mutation 274-4 maps to a unique genetic interval and was not crossed to the other ENU-induced mutant lines (not determined, nd). Homozygosity for a specific ENU-induced mutation either resulted in fully penetrant lethality (grey) or viability (red) that likely reflects instances where the ENU-induced mutation generated a hypomorphic allele.

phenotype different from that seen when heterozygous with the *24Pub* deletion. Unlike the late gestational lethality (E16.5-18.5) of 174-16/*24Pub* mutants, mice homozygous for the 174-16 mutation survive gestation and die within three weeks of birth. For the remaining three ENU-induced mutations (251-1, 283-1, 289-5) heterozygosity with the *24Pub* deletion results in failure to thrive after birth and fully penetrant juvenile lethality. However, in each instance homozygous mutants are viable. Thus, four of the ENU-induced mutations recovered in our screen (174-16, 251-1, 283-1, 289-5) potentially correspond to hypomorphic alleles. Alternatively, these mutations could represent partial or complete loss of function alleles that result in lethality when combined with the multi-gene haploinsufficiency presented by the *24Pub* deletion chromosome.

Six of the seven mutations recovered in our screen (all but 274-4) map within the same genetic interval defined by the *24Pub* and *1XMLP* proximal deletion breakpoints. We performed pair-wise crosses between each of these six mutant lines to determine whether failure to complement provided genetic evidence that the mutations correspond to different alleles of the same gene (Figure 2.3). Formally, non-allelic non-complementation precludes an absolute determination of allelism. Nevertheless, the crosses between the mutant lines define complementation groups and provide an estimate of the number of essential genes mutated in the screen. Each pair-wise combination of the six ENU-induced mutations passed the complementation test and produced viable spotted pups. However, since three of the mutant lines (251-1, 283-1, 289-5) potentially correspond to hypomorphic alleles and mice homozygous for these mutations are viable, we cannot conclude that our genetic studies define six complementation groups. Complementation between the three fully penetrant lethal mutations (128-7, 174-16, 183-15) and the phenotypic differences between these mutant lines provides evidence that the 128-7, 174-16, and 183-15 mutations disrupt

different genes. Therefore, together with the 274-4 mutation that maps to a distinct genomic region, our genetic studies indicate that we have uncovered at least four and as many as seven complementation groups corresponding to essential genes.

2.4.5 An ENU-induced mutation in Phr1

Complementation mapping using the piebald deletion panel localized the ENU-induced mutation 274-4 to a 1.7 Mb critical interval between the *15DttMb* proximal and *1Acrg* distal breakpoints. There are 8 genes annotated to this chromosomal region, including the gene *Phr1* (*PAM*, *highwire*, *rpm-1*) that we have established as a candidate gene for the respiratory distress phenotype presented by mice homozygous for the *15DttMb* deletion (Burgess et al., 2004). *Phr1* (current symbol *Mycbp2*) is the mouse ortholog of the human gene *PAM* (Protein associated with Myc) and is homologous to *highwire* (*hiw*) in *Drosophila* and the *C. elegans* gene regulator of presynaptic morphology (*rpm-1*).

Phr1 encodes a large (4,708 aa) multi-domain protein with a ring zinc finger domain associated with ubiquitin ligase activity (Figure 2.4). *Phr1* functions to regulate presynaptic differentiation and activity. *Highwire* mutants in *Drosophila* display synaptic overgrowth and defects in neurotransmitter release (DiAntonio et al., 2001). In *C. Elegans*, *rpm-1* has a conserved role as a regulator of synapse formation and growth (Zhen et al., 2000). We previously established that nerve terminal morphology and innervation are defective at the neuromuscular junction in the *15DttMb* deletion mutant diaphragm providing evidence that *Phr1* plays an evolutionarily conserved role in synapse formation in mammals and is necessary for respiratory function at birth (Burgess et al., 2004). Studies using our *15DttMb* deletion mutant and a conditional knockout allele have confirmed the role of *Phr1* in synaptogenesis and revealed an additional role in axon guidance (Bloom et al., 2007).

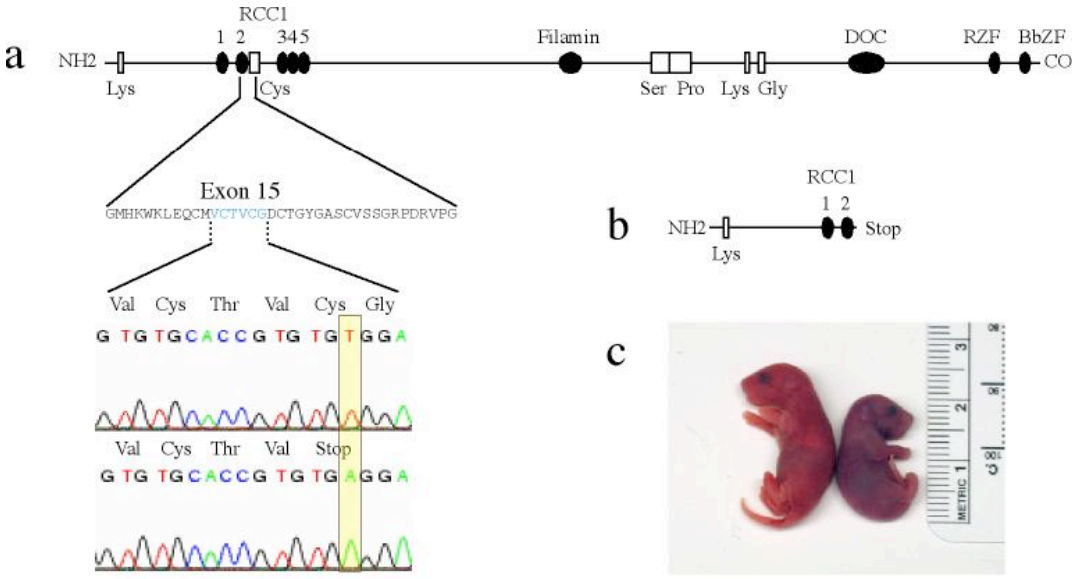

Figure 2.4 The ENU-induced 274-4 mutation disrupts *Phr1* and results in respiratory distress at birth. (A) Multiple conserved domains (UniProtKB/Swiss-Prot) contained in the protein encoded by the *Phr1* locus include lysine (Lys), cysteine (Cys), serine (Ser), proline (Pro), and glycine (Gly) rich amino acid regions, 5 regulator of chromosome condensation (RCC1) homology repeats, a filamin repeat, DOC domain, RING-type zinc finger (RZF), and B box-type zinc finger BbZF. Sequence analysis of transcripts produced by 274-4 mutants revealed a T to A transversion at nucleotide position 2,599 within exon 15 of the 85 exon *Phr1* gene. (B) The cysteine (TGT) to stop codon (TGA) nonsense mutation at amino acid position 772 is predicted to truncate the full length 4,746 amino acid protein following the second RCC1 homology domain. (C) *Phr1*$^{274\text{-}4}$ mutants are smaller than their wildtype littermates and die of respiratory distress shortly after birth.

Mice homozygous for the 274-4 mutation are viable at birth. However, they immediately fail to establish a normal breathing rhythm and die of respiratory distress within ~30 minutes (Figure 2.4). Mutants also exhibit a hunched posture and small size compared to wildtype littermates, averaging 0.85 g compared to 1.17 g for wildtype littermates. The phenotype of 274-4 mutants is identical to the respiratory distress, low birth weight and abnormal posture seen in *15DttMb* deletion homozygous mutants (O'Brien et al., 1996). Given the phenotypic similarity between the 274-4 and *15DttMb* mutants and the genetic data supporting *Phr1* as the gene disrupted in the *15DttMb* deletion leading to respiratory distress, we evaluated the 233 Kb *Phr1* locus for mutations that would lead to loss of function. Sequence analysis of overlapping cDNA clones revealed a T to A transversion at nucleotide position 2,599 of the ~15 Kb *Phr1* transcript expressed in homozygous 274-4 mutants. The resulting nonsense mutation (cysteine to stop codon) in exon 15 of the 86 exon *Phr1* gene is predicted to encode a severely truncated protein and further establishes *Phr1* as an essential gene required for normal respiratory activity at birth (Figure 2.4).

CHAPTER III

AN EVOLVING FUNCTIONAL MAP OF THE PIEBALD DELETION REGION[1]

3.1 Introduction

Our ENU mutagenesis screen had three primary objectives. First, to generate mutants and identify essential genes. This was described in the previous chapter. A second was to characterize the mutants to uncover novel gene function. We will present those results in chapters 4 & 5. A third goal of our screen was to functionally annotate the piebald region in order to gain insight into the organization of the genomic region spanned by the deletion complex. Phenotypic traits uncovered by the ENU mutagenesis screen, the deletion panel, and targeted mutations of individual genes each provide insights into the functional genetic content of the region. We integrated our genetic map of the ENU-induced lethal loci uncovered in the mutagenesis screen with the functional genetic data from the targeted disruption of specific genes and our previous genetic studies that used the deletion panel to uncover and map lethal traits across the piebald region (O'Brien et al., 1996; Roix et al., 2001). In addition we compared the genetic composition, genomic organization and evolutionary stability of the piebald region with four other genomic regions surveyed by ENU mutagenesis and have revealed significant regional variation in the functional content and structure of the genome.

3.2 Materials and methods

Essential gene density estimation

---

[1] Hagarman, J.A. and O'Brien, T.P. (2009). An essential gene mutagenesis screen across the highly conserved piebald deletion region of mouse chromosome 14. *Genesis*. 47(6), 392-403. Reproduced with permission from *Genesis*, accepted for publication 13 January 2009.

Lethal mutations remaining undetected in a screen were estimated by using a Poisson distribution, $P(k|\lambda) = (\lambda^k/k!)\, e^{-\lambda}$, to describe the recovery of randomly mutated essential loci. For undetected mutations, k=0 and the probability is given by $P(0|\lambda) = 1/e^{\lambda}$. Multiple rates ($\lambda$) were used as a simple approach to account for the variability in mutation rate between different loci. Estimates were calculated using four rates (λ = 0.5, 1, 2 and 4) to represent loci ranging from lower to higher mutability and reflecting a bias toward the recovery of multiple alleles at a relatively low frequency. For a probability $P(0|\lambda)$, the number of undetected essential genes was given by (P/1 - P) x L, where L is the number of lethal complementation groups recovered in a mutagenesis screen. Undetected essential gene estimates were combined with the number of lethal complementation groups to arrive at an estimate of the total number of essential genes. Essential gene density was based on the RefSeq annotation of the total number of genes in the genomic region covered by the screen.

Annotation of genomic regions

Markers defining the proximal (P) and distal (D) endpoints of the chromosomal regions surveyed in each screen were based on mouse genome coordinates (Build 37, July 2007) as follows: piebald deletion region, (P) *D14Mit219* and (D) *D14Mit95*; albino deletion region, (P) *D7Mit350* and (D) *D7Mit351* (from (Wilson et al., 2005)); pink-eyed dilution deletion region, (P) *Lhb* and (D) *D7Mit84* (from (Rinchik et al., 2002)); *Trp53-Wnt3* inversion region, (P) *Trp53* and (D) *Wnt3* (from (Kile et al., 2003)); rump-white inversion region, (P) *Dpp6* and (D) *Kit* (from (Wilson et al., 2005)). Gene number and genomic coordinates used to evaluate regional variation in gene density and distribution were based on Refseq annotations obtained from the UCSC mouse genome (Build 37, July 2007) Table Browser using the "Refseq genes" track and eliminating redundancies. We defined a "gene desert" as

a region ≥ 500kb lacking a Refseq gene annotation. Syntenic regions were generated using the UCSC mouse genome Table Browser based on the “net” track for each species in the "comparative genomics" group with the mouse as the reference genome and filtering for “top” alignments, excluding alignments less than 500 Kb.

3.3 A functional map of the piebald deletion region

Five lethal traits have been characterized using the set of piebald deletions that encompass the 19 Mb region targeted by our mutagenesis screen (Figure 3.1). The earliest lethal trait, failure to develop beyond the gastrulation stage (E7.5), is observed in embryos homozygous for the large *24Pub* deletion. Six of the ENU-induced lethal mutations map to the proximal region of the *24Pub* deletion. Five of these mutations (128-7, 174-16, 251-1, 283-1, 289-5) result in lethality after E7.5 and potentially represent essential genes masked by the early lethality characteristic of *24Pub* deletion mutants. However, the 183-15 ENU-induced mutation results in failure to develop beyond E7.5 as seen in *24Pub* deletion mutants and potentially disrupts an early acting essential gene uncovered by the *24Pub* deletion.

The *1Acrg* deletion uncovers a second lethal trait in the piebald region (Kurihara et al., 2002). Embryos homozygous for the *1Acrg* deletion fail to sustain a supply of mesoderm resulting in posterior truncation, laterality and heart morphogenesis defects and ultimately midgestation lethality (E10.5) (Welsh and O'Brien, 2000). Our screen did not uncover an ENU-induced mutation mapping to the *1Acrg* critical region. Six RefSeq genes are localized to the ~2 Mb *1Acrg* critical interval (see Table 2.2; *Klf12* maps within the *1Acrg* deletion breakpoint interval and therefore is considered a candidate). Mice homozygous for an 800 Kb deletion ($Lmo7^{d800}$) that results in the joint loss of two of these genes, *Uchl3* and *Lmo7*, do not display the *1Acrg* mutant phenotype (Semenova et al., 2003). Therefore, any one of the four remaining genes in the interval is the essential locus uncovered by the *1Acrg*

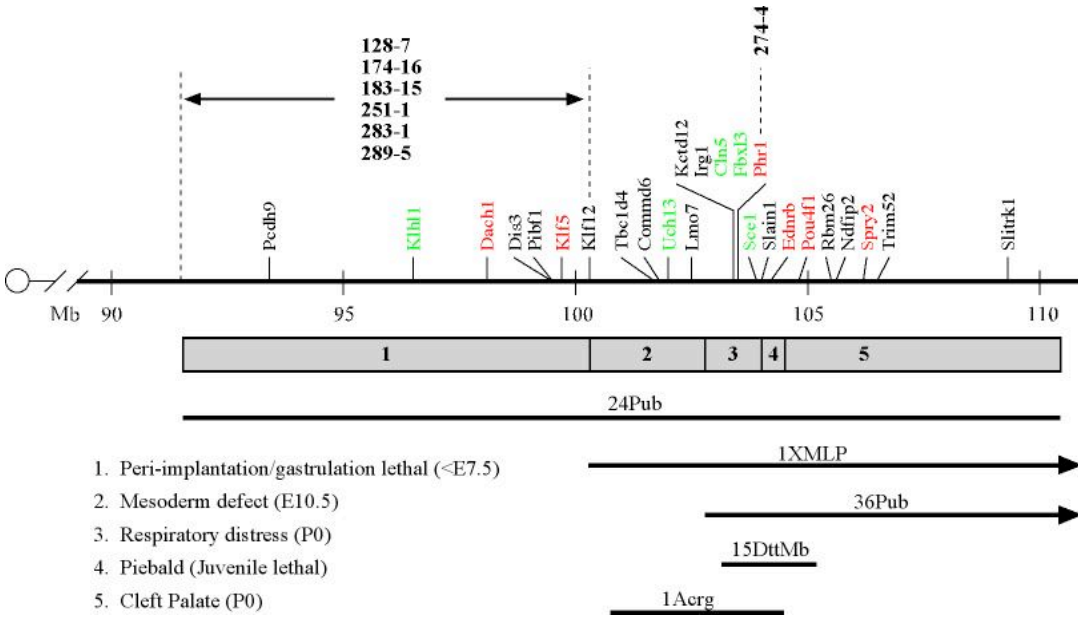

Figure 3.1 Functional map of the piebald deletion region. Genes mapping within the ~19 Mb *24Pub* deletion interval are shown above the chromosome. Genes shown to be essential (red) or nonessential (green) by targeted disruption are indicated. The seven ENU-induced mutations corresponding to novel or known essential loci and their map position are shown above the chromosome. Critical intervals associated with lethal traits uncovered by the piebald deletion panel are shown below the chromosome together with the deletions used for complementation studies to localize the ENU-induced mutations to specific deletion intervals.

deletion or the *1Acrg* mutant phenotype represents a contiguous gene syndrome and would not be expected to be recovered as an ENU-induced point mutation. The phenotype of the 128-7 ENU-induced mutation is similar to that of the *1Acrg* deletion mutant. However, complementation testing established that 128-7/*1Acrg* compound heterozygotes survive to wean indicating that the 128-7 and *1Acrg* phenotypes are genetically distinct.

The three remaining lethal traits uncovered by the piebald deletions include respiratory distress associated with *15DttMb* deletion mutants (O'Brien et al., 1996), juvenile lethality resulting from enteric defects owing to the deletion of the *Ednrb* gene (Hosoda et al., 1994), and cleft palate associated with *36Pub* deletion mutants attributable to the loss of the FGF signaling antagonist *Spry2* (Welsh et al., 2007). Our screen did not recover additional alleles of *Ednrb* or *Spry2*. However, we did recover an ENU-induced allele (274-4) of the *Phr1* gene responsible for the *15DttMb* deletion mutant respiratory distress and lethality at birth.

Targeted disruption has been used to examine the function of 11 of the 30 RefSeq genes annotated to the *24Pub* deletion region covered in the screen (Figure 3.1 and Table 2.2). Of these eleven genes, six are required for development and survival and five are not essential genes. The ENU-induced $Phr1^{274-4}$ allele corresponds to one of the six genes in the region shown to be essential by targeted disruption. Two of the essential genes revealed by gene targeting, *Dach1* and *Klf5*, map within the proximal *24Pub* genetic interval containing six of the ENU-induced lethal mutations recovered in our screen. *Dach1* is the mouse homologue of the *Drosophila* gene *dachshund* and homozygous mutant mice survive to birth, become cyanotic and die within 24 hours (Backman et al., 2003; Davis et al., 2001). *Klf5* is a member of the Kruppel-like transcription factor family and homozygous mutants fail to develop beyond E8.5 (Shindo et al., 2002). Our genetic data suggest that four of the six ENU-induced

mutations (174-16, 251-1, 283-1, 289-5) result in a hypomorphic phenotype and survive beyond the time of lethality observed for *Dach1* or *Klf5* mutants. Therefore, these ENU-induced mutations potentially represent hypomorphic alleles of either *Dach1* or *Klf5*. Although further characterization is required, given the similar time of lethality (prior to E8.5) the ENU-induced 183-15 mutation potentially represents a loss of function allele of *Klf5*. In contrast, differences in the time of lethality suggested that rather than an allele of *Dach1* or *Klf5*, the fully penetrant ENU-induced 128-7 mutation represented a novel essential gene.

Given factors such as differences in mutability between loci and phenotypic variation owing to screens performed on different and mixed genetic backgrounds, a particular mutagenesis screen is unlikely to exhaust the genetic complexity of a particular phenotypic domain. Accordingly, three of the six known essential genes in the piebald region (*Ednrb*, *Pou4f1*, *Spry2*) were not detected in our screen. Lethality associated with the *1Acrg* deletion also represents a potential essential gene that remains undetected. The combination of data from our mutagenesis screen, deletion panel, and the targeted disruption of individual genes provide genetic evidence for at least seven distinct essential genes. Although unlikely, it is possible that the ENU-induced mutations correspond to seven complementation groups and uncover an additional six novel essential genes. Thus, together with the deletion panel, the genetic data suggest as many as thirteen essential genes mapping within the *24Pub* deletion interval. While additional experimental studies are needed to determine the full complement of essential genes, these studies are building toward a more complete account of the functional genetic content of the piebald region of distal chromosome 14.

Table 3.1 Regional comparison of gene and essential gene densities in the mouse genome

Region	Piebald	Albino	Pink-eye	Rump-white	Trp53-Wnt3
Chromosome (Mb region)	14 (91.6 - 110.4)	7 (90.7 - 104.0)	7 (52.7 - 66.4)	5 (27.1 - 76.0)	11 (69.4 - 103.7)
Interval size (Mb)	18.8	13.3	13.7	48.9	34.3
Total gene number[1]	30	70	100	252	702
Gene density (genes/Mb)	1.6	5.3	7.3	5.1	20.5
Pedigrees in ENU screen	952	4557	1218	1003	785
ENU-induced lethal lines	7	19	10	37	45
Complementation groups[2]	4	8	6	35	40
Estimated number lethal genes	6 (4 - 10)	12 (8 - 20)	9 (6 - 15)	54 (36 - 87)	63 (41 - 102)
Essential gene density	20% (13 - 33%)	17% (11 - 28%)	9% (6 - 15%)	21% (14 - 34%)	9% (6 - 14%)
[1] Gene number based on annotated Refseq genes from UCSC browser Build 37, July 2007					
[2] Minimum complementation groups for piebald (see text) and maximum complementation groups for rump-white (J. Schimenti, pers. comm.)					

3.4 Regional functional organization of the genome

We screened 952 ENU mutagenized genomes to survey the 19 Mb genomic region uncovered by the large *24Pub* deletion for essential genes. Given that only 30 RefSeq genes are annotated to the *24Pub* deletion interval and that targeted disruption has established that 5 of these genes are not essential for survival (see Table 2.2), we anticipated that the screen would recover a modest number of lethal mutations. Overall, we isolated and established heritability for seven ENU-induced mutations that resulted in lethality before or shortly after birth. A comparison of several highly successful regional mutagenesis screens in the mouse (Table 3.1) provides alternative measures of the recovery of lethal lines on the basis of pedigrees screened (e.g. ~1/240 for albino vs. ~1/17 for *Trp53-Wnt3*) and on the basis of the number of genes in the target interval (e.g. ~1/4 for albino vs. ~1/16 for *Trp53-Wnt3*). Each measure illustrates the efficacy of a mutagenesis screen and the lethal mutant yield of 1/136 on the basis of pedigrees and of ~1/4 on the basis of the number of genes for the piebald region screen is comparable to the results obtained in the albino region screen (Rinchik and Carpenter, 1999).

3.4.1 Essential gene density

In addition to generating mouse models for the study of gene activity during development a regionally directed mutagenesis screen provides an experimental approach for the functional annotation of a defined genomic interval. A functional genetic survey of a defined segment of the genome adds another layer to the computational and experimental methods being used to arrive at a comprehensive understanding of the genome. A comparison of the genetic composition, genomic organization and evolutionary stability of the piebald region with four other genomic regions surveyed using ENU mutagenesis reveals significant regional variation in the functional content and structure of the genome. One notable feature of the piebald region is its low gene density (Table 3.1). At 1.6 genes/Mb the piebald region of chromosome 14 has a 3 to 13-fold lower gene density than the four genomic regions surveyed in the chromosome 5, 7 and 11 screens. The average gene density across the mouse genome is 6.7 genes/Mb, or more than four times that of the piebald region. The rump white, albino and pink-eye regions of chromosomes 5 and 7 are much closer to the genomic average at between 5.1 and 7.3 genes/Mb, and the Trp53-Wnt3 region is extremely gene dense, at 20.5 genes/Mb.

Despite an overall low gene density the piebald region has a high essential gene density. We estimated the total number of essential genes based on the number of lethal loci and complementation groups generated in each regional ENU mutagenesis screen (Table 3.1). The simple multiple rate Poisson model we used undoubtedly assumes the significant uncertainty associated with screen-based estimates of essential genes (Pollock and Larkin, 2004). However, our screen-based estimate of 20% (13 - 33%) is comparable to the experimental data indicating an essential gene density of at least 23% and potentially as high as 43% for the piebald region. This is in contrast to the low essential gene density of the Trp53-Wnt3 region,

Table 3.2 Gene content and organization of genomic regions surveyed in mouse mutagenesis screens

Region	Piebald	Albino	Pink-eye	Rump white	Trp53-Wnt3
Chromosome (Mb region)	14 (91.6 - 110.4)	7 (90.7 - 104.0)	7 (52.7 - 66.4)	5 (27.1 - 76.0)	11 (69.4 - 103.7)
Interval size	18.8	13.3	13.7	48.9	34.3
Number gene clusters (% of region)	11 (24)	4 (67)	4 (67)	14 (57)	3 (93)
Number gene "deserts" (% of region)	12 (76)	3 (33)	3 (33)	13 (43)	2 (7)
Avg. gene cluster size	409 Kb	2.2 Mb	2.3 Mb	2.0 Mb	10.6 Mb
Avg. gene "desert" size	1.2 Mb	1.5 Mb	1.5 Mb	1.6 Mb	1.2 Mb
Avg. gene size (Total gene number)	116 Kb (30)	67 Kb (70)	59 Kb (100)	68 Kb (252)	26 Kb (702)
Gene size distribution - number (%):					
< 25 Kb	14 (47)	44 (63)	64 (64)	111 (44)	536 (76)
25 - 50 Kb	4 (13)	8 (11.4)	16 (16)	54 (21)	89 (12)
50 - 75 Kb	3 (10)	7 (10)	5 (5)	23 (9)	33 (5)
75 - 100 Kb	0	3 (4.2)	4 (4)	22 (9)	18 (3)
> 100 Kb	9 (30)	8 (11.4)	11 (11)	42 (17)	26 (4)

which has an essential gene density of only 9%, in contrast to its extremely high gene density. It is also striking that the two genomic regions that have gene densities higher than the genomic average, pink-eye and Trp53-Wnt3, have essential gene densities of 9%, while the three genomic regions with gene densities below the genomic average, piebald, albino and rump-white, have essential gene densities between 17% and 21%.

3.4.2 Comparisons of genomic organization between genomic regions

The piebald region exhibits a distinct structural organization marked by gene clusters separated by Mb-scale gene deserts (Peterson et al., 2002). The ~19 Mb *24Pub* deletion interval is partitioned into 11 gene cluster and 12 "gene desert" domains (regions ≥ 500 Kb lacking a RefSeq annotated gene) that cover 76% of the region (Table 3.2 and Figure 3.2). The average gene cluster size of 409 Kb for the piebald region is 5 to 26-fold smaller than the average gene cluster size characteristic of the chromosome 5, 7 and 11 regions. Not only does the piebald region lack large contiguous genic regions, a higher proportion of large genes with an average size of

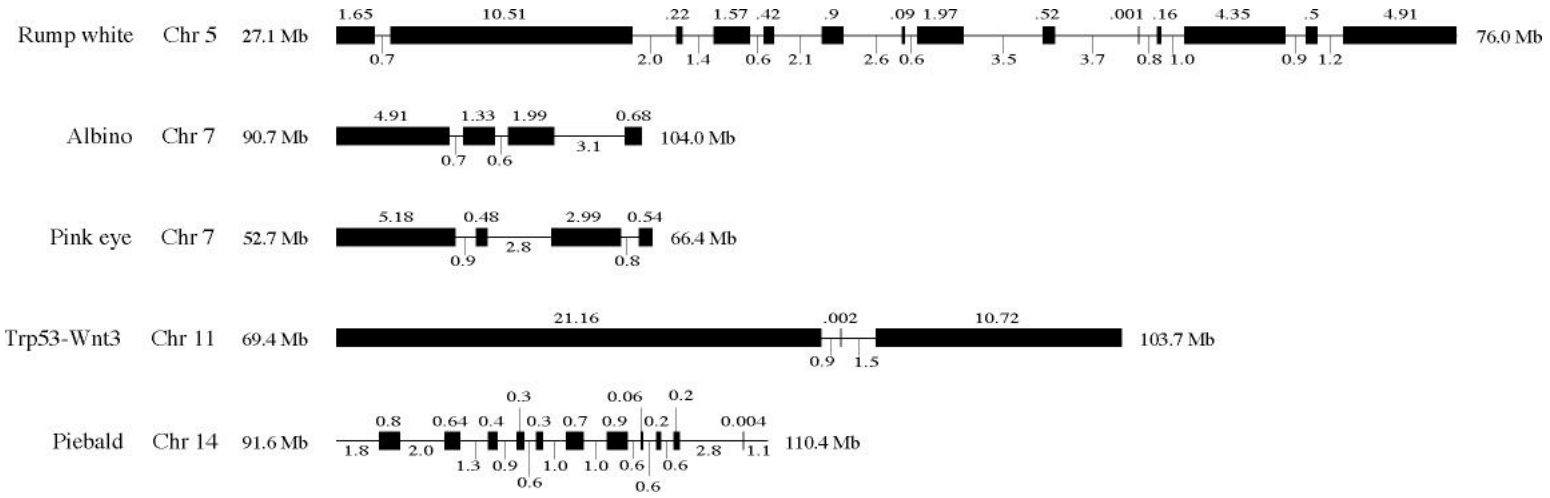

Figure 3.2 Genomic organization of chromosomal intervals targeted in regional ENU-mutagenesis screens. Gene clusters (contiguous genic regions) are displayed as a thick line with their size (Mb) indicated above the cluster. "Gene desert" regions (defined as a region ≥ 500 Kb lacking a Refseq gene annotation) are displayed as a thin line with their size (Mb) indicated below the chromosome.

116 Kb and 30% exceeding 100 Kb also distinguishes the gene content and organization of the piebald region (Table 3.2). A "piebald region-like" organization is present in a distinct domain of one of the other regions we analyzed. The rump-white region contains a central core that is partitioned into 9 gene clusters and 10 gene deserts that look surprisingly similar to the piebald region (Figure 3.2). Two domains of large gene clusters surround this central, piebald-like domain. In addition, in the "piebald region-like" part of the rump-white interval, the size of the gene clusters drops to 650kb, close to the size of the clusters in the piebald region. These similarities suggest that the piebald region and the core of the rump-white region share a common genomic organization.

Despite its low gene density the evolutionary stability of the piebald region is maintained across several mammals and chicken (Figure 3.3). The piebald region is encompassed by a single homologous synteny block compared with several breakpoints marking inversions and rearrangements across the chromosome 5, 7 and 11 regions. Notably, a large central region within the rump-white inversion from 40 - 64 Mb on chromosome 5 also shows significant evolutionary stability, similar to piebald. This region corresponds to the part of the rump-white region that has a genomic structure similar to the piebald region, namely the cluster/desert organization (see Figure 3.2).

3.5 Discussion

Our genetic and genomic analysis of the piebald region provides insights into regional variation in the genetic content and structure of chromosomes. In contrast to chromosomal regions with a high gene density, low essential gene density, or features such as repetitive sequences or increased gene density associated with evolutionary breakpoints (Murphy et al., 2005); the piebald region is characterized by a low gene density, high essential gene density, distinct genomic organization and high

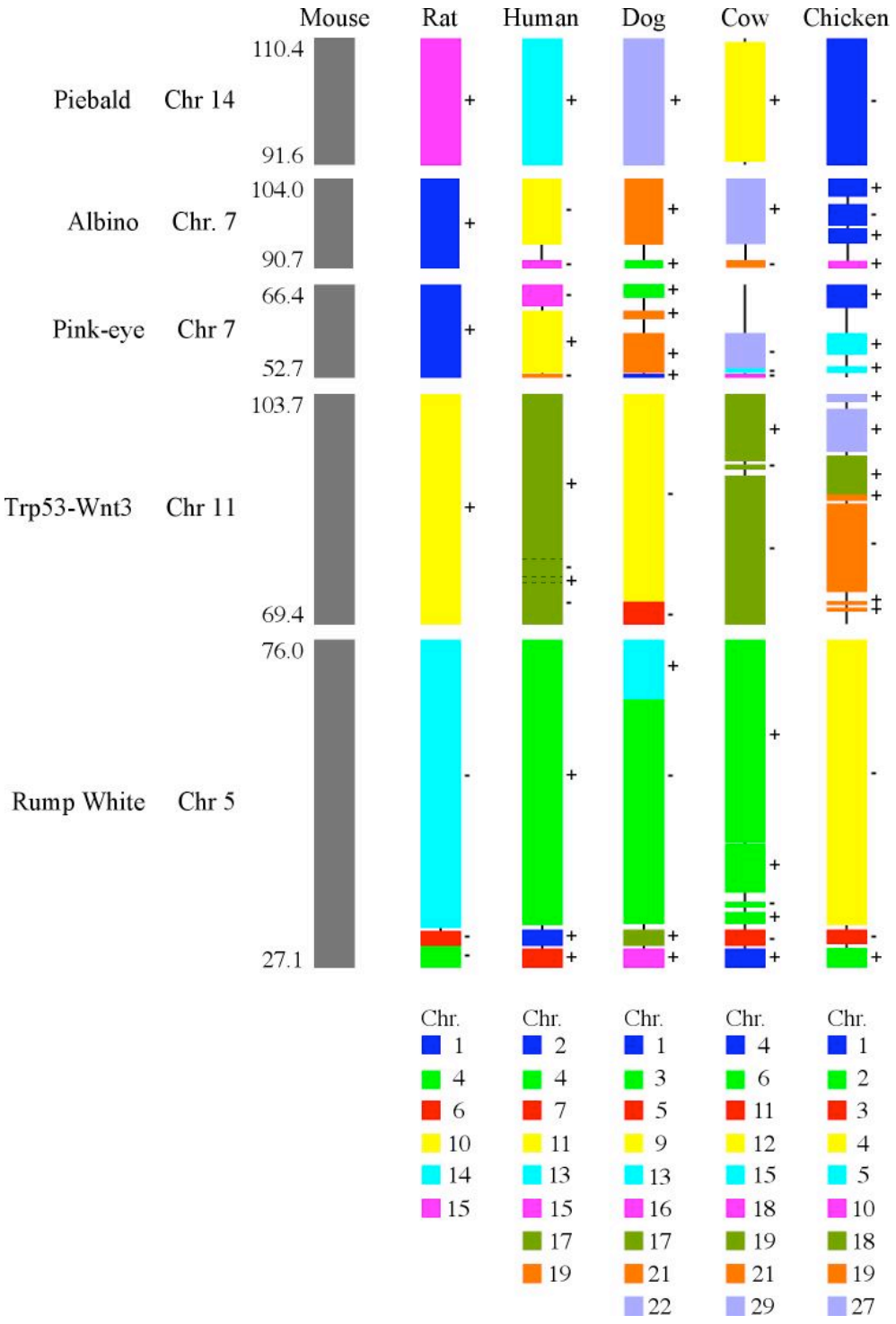

Figure 3.3 Multispecies comparison of conserved syntenic segments across chromosomal intervals targeted in ENU-mutagenesis screens. Chromosomal region coordinates (Mb) in the mouse genome are indicated. Mouse is used as the reference genome, sequence alignment gaps are shown as a solid black line, and syntenic blocks with the same (+) or inverted (-) orientation relative to the mouse are indicated. Note that the color-coding of chromosomes is different for each species.

evolutionary stability. Although factors that contribute to chromosome evolution are poorly understood, a high essential gene density potentially promotes evolutionary stability (Hentges et al., 2007). However, even with a high essential gene density, the overall low gene density of the piebald region suggests that additional features are also likely to be important. The unique structure and stability of the piebald region might also reflect a high level of regulatory complexity. In keeping with their essential function, numerous genes in the piebald region are expressed in intricate and dynamic patterns throughout development. The region also contains an extensive number of noncoding conserved sequence elements that are likely to perform structural and regulatory functions (Peterson et al., 2002). For example, sequences highly conserved from pufferfish to mammals act as distant enhancers positioned hundreds of Kb from the *Dach1* transcription start site (Nobrega et al., 2003; Poulin et al., 2005). Genomic organization and evolutionary stability might also reflect higher-order properties such as a distributed regulatory architecture owing to shared enhancer elements and sequence features that mediate physical interactions to shape the relative positioning of genes in the nucleus. Supporting this concept, we have established that the folded structure of the piebald chromosomal region in the interphase nucleus is based on the clustered organization of the genes in the primary genomic sequence (Shopland et al., 2006). Thus, dynamic interactions between multiple gene clusters across a region with a high regulatory complexity and essential gene density suggest a functional basis for the distinct genomic organization and evolutionary stability of the piebald region of distal chromosome 14. Continued efforts to establish and compare the genetic content, structure and activity of defined chromosomal regions will reveal important properties of genome organization and function.

CHAPTER IV

CLONING AND CHARACTERIZATION OF AN ENU-INDUCED MUTATION IN PROGESTERONE INDUCED BLOCKING FACTOR 1[1]

4.1 Introduction

Having completed the ENU mutagenesis screen and used the data from it to try to gain insight into the organization of the region, the next goal for the project was to use the mutants generated in the screen to better understand the functions of individual genes in the region. We chose to focus on ENU 128-7 because it is the only mutant generated in the screen with an observed phenotype that was novel for the genes in the region. Also, since the mutant embryos had an obvious defect in left/right patterning, and since the pathway controlling the establishment of asymmetry is well defined, there were a number of experiments that provided a way to explore the underlying defect. A important requirement for establishment of the left/right axis is the Hedgehog signaling pathway.

Hedgehog (HH) signaling is an important developmental signaling pathway used to establish cell fate, promote proliferation and mediate apoptosis (Dessaud et al., 2008; Hooper and Scott, 2005; Ingham, 2008; Jacob and Lum, 2007). HH ligands may act as short- or long-range morphogens and disrupted HH signaling in humans leads to defects in the CNS and limbs, cleft palate, as well as a predisposition for various types of tumors. After translation, HH precursor enters the secretory pathway and is modified by autoproteolysis catalyzed by the C-terminal end of HH (Lee et al., 1994). The N-terminal signaling peptide (SHH-N) is further modified by C-terminal covalent linkage of cholesterol and addition of a palmitate moiety on the N-terminus

[1] Hagarman, J.A. and O'Brien, T.P. *Pibf1* is an essential gene in the mouse involved in cytoskeletal organization required for ciliogenesis and Hedgehog signaling. In preparation.

(Pepinsky et al., 1998; Porter et al., 1996). Release of modified SHH-N requires the transmembrane protein Dispatched, and secreted SHH has been shown to form a gradient in the neural tube (Burke et al., 1999; Chamberlain et al., 2008). The cholesterol and palmitate modifications mediate the binding of HH to lipoproteins and are required for long-range signaling and the establishment of HH gradients (Panakova et al., 2005). In addition, heparan sulfate proteoglycans (HSPGs) in the extracellular matrix mediate the trafficking of HH, and loss of genes required for the biosynthesis of HSPGs reduce the range of HH signaling (Lin, 2004).

Secreted SHH ligand binds to its receptor, the 12-pass transmembrane protein Patched (PTCH1) at the target cell. Binding by SHH alleviates PTCH1 inhibition of the 7-pass transmembrane protein Smoothened (SMO). SMO activates a signal transduction cascade that modulates the activity of the GLI transcription factors. The three members of the GLI family of zinc-finger transcription factors exist in both activator (GLI^A) and repressor (GLI^R) forms. GLI1 and GLI2 are primarily transcriptional activators. GLI^R function is largely provided by GLI3, which also may serve as a transcriptional activator depending on SMO activity. Elucidating the mechanism of SHH signal transduction is a major focus of developmental biology.

PIBF1 was first identified as a 34 kDa immunomodulatory molecule isolated from pregnancy lymphocytes (Szekeres-Bartho et al., 1989; Szekeres-Bartho et al., 1985). Secreted PIBF1 acts as a signaling ligand that activates the JAK/STAT signaling pathway, preventing the activation of NK cells and playing a role in modulating the cytokine profile of T cells in pregnant women (Szekeres-Bartho et al., 1997a; Szekeres-Bartho and Wegmann, 1996). Loss of PIBF1 results in a Th2 biased shift in the cytokine profile and an increase in spontaneous abortion (Szekeres-Bartho et al., 1997a; Szekeres-Bartho et al., 1997b). In this manner PIBF1 has an anti-abortive effect and is a player in immunomodulation during normal pregnancy. In

addition to the secreted 34 kD isoform PIBF1 also exists in a full-length 90 kD isoform that is overexpressed in highly proliferative cells (Polgar et al., 2003). By immunocytochemistry and western blot full-length PIBF1 localizes to the centrosome while the smaller 34 kDa isoform is dispersed diffusely in the cytoplasm (Lachmann et al., 2004). Treatment of cells with the microtubule-disrupting agent nocodazole results in the time-dependent loss of PIBF1, suggesting that PIBF1 is not an integral component of the centrosome but rather a microtubule-associated protein. The function of the intracellular full-length PIBF1, the dominant form in proliferating cells, has not yet been addressed.

4.2 Materials and methods

Mice

The ENU-induced *Pibf1* mutation was generated as described (Hagge-Greenberg et al., 2001). The mutation was created on the SSL/Le background and is maintained on an inbred C57Bl/6J background. Mice are genotyped using microsatellite markers D14Mit225 and D14Mit8 that lie proximal and distal to the mutation, respectively, to identify polymorphisms between the SSL/Le and C57Bl/6J strains. The RRH031 ES Cell line containing a gene trap insertion in intron 10 of *Pibf1* was obtained from the Mutant Mouse Regional Resource Centers at UC-Davis. Germline mutant mice were generated by ES Cell microinjection using the service at the Cornell University Life Sciences Core Laboratories Center. Gene trap mice are genotyped using standard *Neo* primers. *Ptch1*^{tm1Mps} mice were obtained from The Jackson Laboratory.

Genetic mapping and molecular identification of *Pibf1*

The ENU-induced mutation was mapped by complementation crosses to the *Ednrb*$^{s\text{-}24Pub}$ and *Ednrb*$^{s\text{-}1XMLP}$ deletion lines as previously described. RNA was

prepared from mutant and wildtype embryos using either Trizol (≥E10.5) or the Qiagen RNeasy micro RNA isolation kit (<E10.5) and reverse transcription performed using SSII reverse transcriptase. PCR products were purified using EXOSAP-IT and sequenced by the Cornell Life Sciences Core Laboratories Center. The lariat branch point site in intron 2 was cloned as previously described (Vogel et al., 1997). Briefly, whole-embryo RNA was transcribed using a gene specific primer close to the splice donor site at the beginning of the intron. The resulting RT product contained synthetic DNA sequences made from the lariat intermediate that could then be amplified by PCR and sequenced to identify the branch point site.

Tissue processing and histochemistry

Embryos were dissected in cold PBS and fixed in 4% PFA overnight. They were then dehydrated to 100% methanol and stored in 100% methanol at -20^0 C. Whole-mount in situ hybridization was done as described (Welsh and O'Brien, 2000). Stained embryos were stored in PBS. In order to section, stained embryos were dehydrated in ethanol, cleared in xylene, embedded in paraffin and sectioned on a microtome at 20μM. The *Nodal, Lefty, Pitx2, Pax6, Pax3, T* and *Shh* probes used in this study were provided by Hiroshi Hamada, Tom Gridley, Peter Gruss, Michael Shen and Andrew McMahon. For histological analysis embryos were dissected in cold PBS and fixed overnight in Bouin's fixative. Embryos were then dehydrated through an ethanol series to xylene and embedded in paraffin then sectioned at 6μM and stained with hematoxylin and eosin. For LacZ staining embryos were fixed 30 minutes in 0.1M phosphate buffer (pH 7.3) supplemented with 5mM EGTA, 2mM $MgCl_2$ and 0.2% Gluteraldehyde then washed in 0.1M phosphate buffer with 2mM $MgCl_2$. Embryos were stained in 0.1M phosphate butter with 2mM $MgCl_2$, 5mM $K_4Fe(CN)_6$-$3H_2O$, 5mM $K_3Fe(CN)_6$ and 1mg/mL X-gal overnight at 37^oC.

4.3 The phenotype of ENU 128-7 mutants

We identified the recessive lethal mutant, ENU 128-7, in our forward genetic screen to identify mutations affecting genes required for mouse development on distal chromosome 14. Embryos homozygous for the ENU-induced mutation display a number of morphological defects culminating in midgestation lethality between E10.5 and E12.5. Mutant embryos are smaller than their wildtype littermates and show defective axial rotation. The direction of heart looping is randomized as well as being delayed and incomplete. The pericardium and amnion are swollen and often contain blood (Figure 4.1 D). The fore- and midbrain regions of the mutant are dysmorphic, the branchial arches are reduced in size or missing and a subset of mutant embryos display neural tube closure defects (Figure 4.1 B, C). We have previously used complementation crosses to map the responsible mutation to the proximal half of the *Ednrb*$^{s\text{-}24Pub}$ deletion (Figure 4.1 A). This region is 8.7 Mb and contains 10 Refseq genes, including Progesterone induced blocking factor 1 (*Pibf1)*.

4.4 Positional cloning of ENU 128-7

There are a number of ways to pursue the positional cloning of an ENU mutant. One is direct sequencing of obvious candidate genes. For example, two lines of ENU-induced mutant mice that display an obesity phenotype, *Fatboy* and *Southbeach*, map to a region of chromosome 18 that contains the Melanocortin-4 receptor (*Mc4r)* gene (Meehan et al., 2006). *Mc4r* knockout mice display severe obesity, and sequencing found single amino acid changes in *Mc4r* for each line (Huszar et al., 1997). In the case of ENU 128-7, the critical mapping interval for the mutation contained two known essential genes, *Klf5* and *Dach1*. Unfortunately, direct sequencing of these candidate genes failed to identify mutations. Alternatively, the technology is currently available to use massively parallel sequencing to identify causative point mutations in ENU mutants. This has been demonstrated recently when

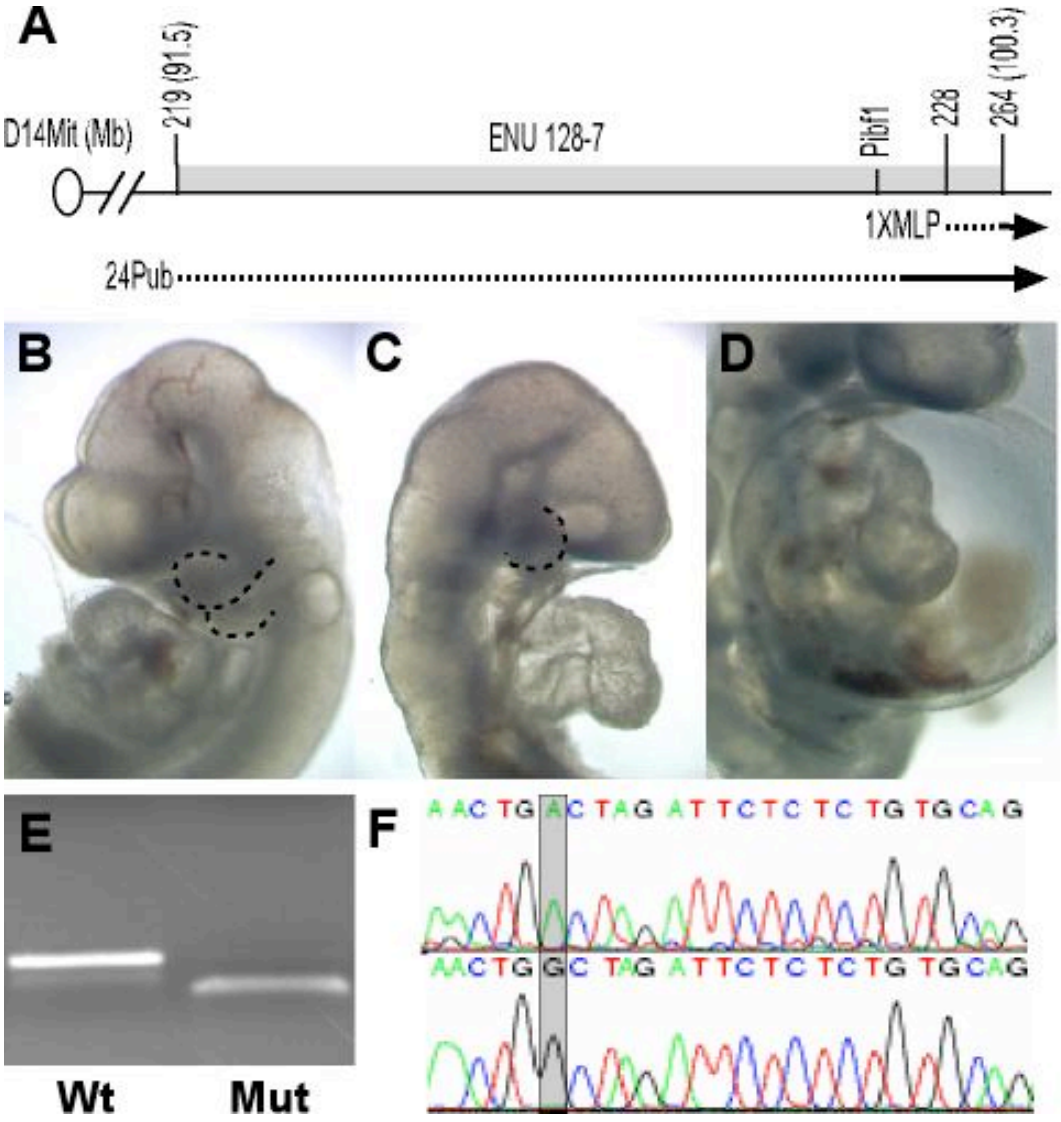

Figure 4.1 ENU 128-7 mutants exhibit multiple defects in embryonic development caused by a mutation in *Pibf1*. (A) Genetic mapping of ENU 128-7 to a 8.8 Mb region of mouse chromosome 14. (B,C) E10.5 wildtype (B) and 128-7 mutant (C) embryos showing dysmorphic head and branchial arch (dashed lines) structures. Disrupted heart morphogenesis is visible in C. (D) The pericardim is swollen and often contains blood. (E) RT-PCR of *Pibf1* from mouse embryos homozygous for the 128-7 ENU-induced mutation. *Pibf1* transcript is reduced in size and intensity compared to wildtype. (F) A single A to G nucleotide substitution is present 18 bases upstream of the splice acceptor at the beginning of exon 3 in *Pibf1*.

2.2 Mb of DNA was sequenced to identify a mutation in the gene *Megf8* (Zhang et al., 2009). We have chosen not to use this approach for our cloning efforts up to this point. Another high-throughput approach used for positional cloning efforts is denaturing high-performance liquid chromatography using the WAVE DNA fragment analysis system (Donohoe, 2005). This system uses UV absorbance to identify base-pair mismatches in PCR amplified DNA. We attempted using this system to identify the causative mutation in ENU 128-7 but were unsuccessful. Finally, since ENU mutants often contain nonsense mutations or splicing defects, and since these mutations can affect transcript size or stability, RT-PCR may identify changes in transcript size or abundance that lead to the responsible gene. This is the approach that proved successful for us.

RNA was collected from mutant and wildtype embryos and RT-PCR performed to look for reduced or altered transcript size or level for each of the ten genes within the critical genetic interval. One gene, *Pibf1*, showed reduced transcript levels as well as a smaller product (Figure 4.1 E). Sequencing RT-PCR products amplified from RNA isolated from mutant embryos demonstrated that the *Pibf1* transcript is missing exon 3 (data not shown). Exon 3 was sequenced from genomic DNA and an A to G mutation identified 18 bases upstream from the splice acceptor site at the beginning of exon 3 (Figure 4.1 F). The location of the mutation in the intron close to the splice site in addition to the loss of exon 3 in the mature transcript suggested a disruption of normal splicing between exons 2 and 3.

Splicing occurs by a series of transesterification reactions resulting in the joining of two exons and the release of the intron in the form of a lariat intermediate. The branch point sequence (BPS) is a conserved splicing signal important for spliceosome assembly and lariat formation and one of several recognition sequences required for accurate intron excision (Burge et al., 1999). The short BPS, located

between 10 and 50 bases upstream of the splice acceptor site, contains the adenosine residue at which the lariat is formed and has the consensus sequence YNYURAY. The sixth base of the branch point sequence is the base at which the 5' end of the intron binds and is the only base absolutely conserved within the branch point sequence. The base mutated in our ENU-induced mutant is the sixth base within a 7-base sequence matching the consensus sequence for the lariat branch point sequence, suggesting a disruption in lariat intron formation leading to a splicing defect in intron 2 of *Pibf1*.

It has been shown previously that introns may contain degenerate branch point sites as well as distal branch point sites (Harris and Senapathy, 1990). We confirmed that the mutated base in ENU 128-7 is in fact the branch point site by following a RT-PCR strategy to map the branch point site in intron 2. We designed RT primers oriented to capture the branched lariat structure (Figure 4.2 A,B) and used nested PCR to amplify the captured molecule (Figure 4.2 C). The resulting sequence confirms that the ENU-induced mutation identified in ENU 128-7 is at the branch point site in intron 2 of *Pibf1* (Figure 4.2 D). The splicing defect was confirmed by performing RT-PCR with primers in exons 2 and 3. In cDNA from mutant embryos the amount of *Pibf1* transcript is greatly decreased, demonstrating failure to properly splice between exons 2 and 3 (Figure 4.2 E). Loss of exon 3 is predicted to cause a shift in the reading frame of the transcript that generates a stop codon in exon 4. The resulting protein is predicted to contain 125 amino acids, compared to 756 for the wildtype protein, of which only the first 85 amino acids are identical to the wildtype protein. Due to the position of the premature stop codon and truncation of the resulting protein we presume the effect of the *Pibf1* mutation is likely a complete loss of function. (Figure 4.2 F).

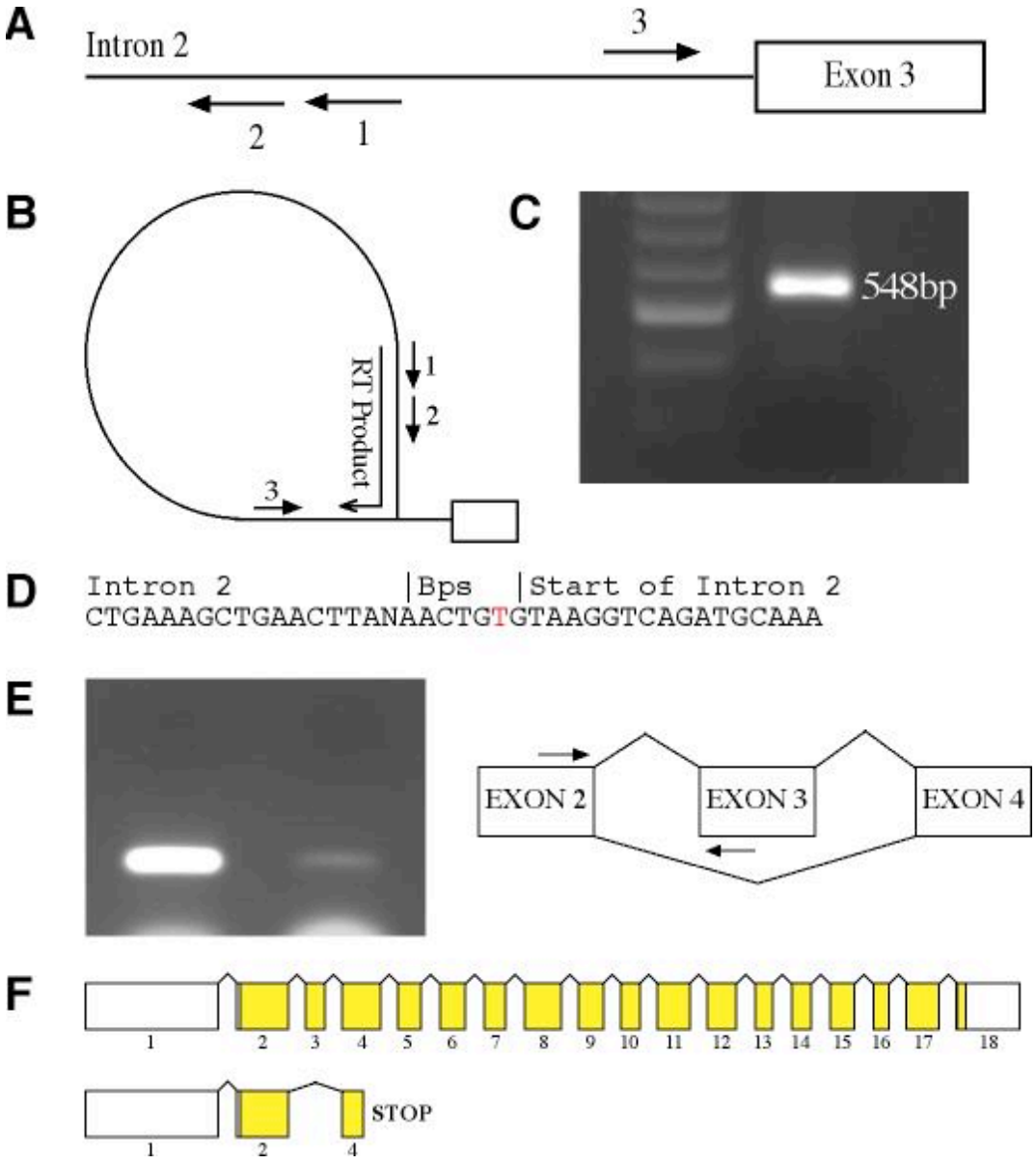

Figure 4.2 The point mutation in intron 2 of *Pibf1* is at the lariat branch point site and leads to a splicing defect in 128-7 mutant embryos. (A,B) The RT-PCR method to map the branch point site in intron 2 of *Pibf1*. Reverse transcription using a gene specific primer (primer 1) is used to capture the lariat and nested primers (primers 2 and 3) are then used to amplify the resulting cDNA and map the branch point. (C) The resulting amplicon from the strategy outlined in A and B. Primers 2 and 3 were predicted to yield a product of 548bp. (D) Sequence from amplicon in (C) confirming the based mutated in ENU 128-7 is the lariat branch point site in intron 2 of *Pibf1*. (E) RT-PCR with primers in exon 2 and 3 confirming the splicing defect in ENU 128-7 mutants. (F) Predicted result of loss of exon 3 of *Pibf1* is a frame shift generating a stop codon in exon 4 and presumably leading to the loss of coding sequence from exons 3-18.

4.4.1 Genetic confirmation of Pibf1 as the gene responsible for the phenotype of ENU 128-7 mutants

A fractionated dose of ENU gives 1 sequence change in 10^6 bases. Since the mouse genome contains 3,420 Mb of DNA, a single ENU mutagenized genome potentially contains over 3,000 mutations. Given this fact, identifying a single basepair change in an ENU mutant is insufficient to confirm that the identified gene is responsible for the phenotype of the mutant. Once a candidate gene is identified an efficient way to confirm the responsible gene is to perform a complementation cross to a mouse carrying a gene trap allele. Failure to complement between the ENU-induced mutation and the gene trap allele confirms the identity of the responsible gene. The International Gene Trap Consortium currently has lines containing tags that align to 38% of known genes in the mouse.

In order to confirm genetically that loss of *Pibf1* function is responsible for the phenotype of the ENU-induced mutation we generated a second mutant allele of *Pibf1* from an ES cell line (RRH031) containing a gene trap insertion in intron 10 of *Pibf1*. The location of the insertion site was confirmed by RT-PCR (data not shown). Mice heterozygous for the ENU-induced mutation were crossed to carriers of the RRH031 gene-trap insertion. The resulting compound heterozygous ($Pibf1^{128\text{-}7}/Pibf1^{RRH031}$) embryos were lethal at the same time as embryos homozygous for the ENU-induced mutation and displayed similar phenotypic defects (Figure 4.3). This genetic evidence confirms that loss of function of *Pibf1* is responsible for the phenotype of ENU 128-7 homozygous mutants.

4.5 Pibf1 is expressed in multiple embryonic regions patterned by Hedgehog signaling

The two most common alternatively spliced isoforms of *Pibf1* in murine tissues are the full-length cDNA and a splice variant that includes exons 1-5 and 17-18

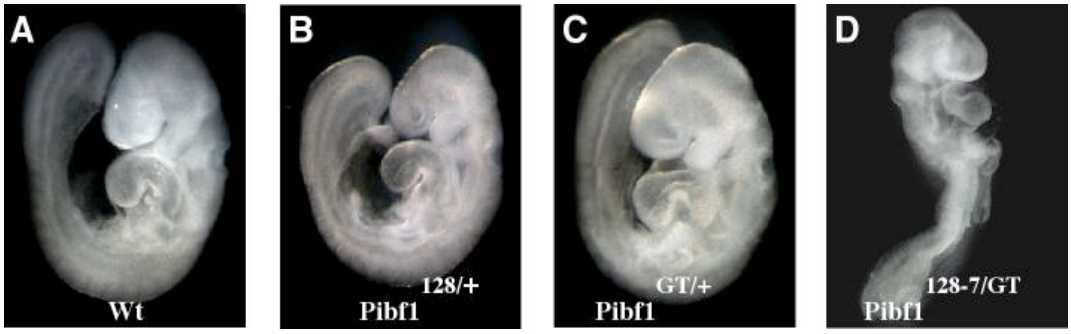

Figure 4.3 *Pibf1* gene trap allele fails to rescue the lethality of the ENU-induced mutation. The RRH031 ES Cell line containing a gene trap insertion in intron 10 of *Pibf1* was obtained from the Mutant Mouse Regional Resource Centers at UC-Davis. Germline mutant mice were generated by ES Cell microinjection using the service at the Cornell University Life Sciences Core Laboratories Center. (A) Wildtype littermate. (B) $Pibf1^{128\text{-}7}$ heterozygous embryo. (C) $Pibf1^{GT}$ heterozygous embryo. (E) $Pibf1^{128\text{-}7/GT}$ compound heterozygous embryos display a phenotype identical to the ENU-induced homozygous mutant embryos.

(Lachmann et al., 2004). These two splice variants are predicted to produce proteins with molecular weights of 90 and 35 kDa respectively. Presumably these two splice variants encode the 90 and 34 kDa PIBF1 proteins previously characterized. We examined expression of these two isoforms in midgestation embryos, but by RT-PCR we were only able to amplify the full-length isoform from murine whole-embryo RNA, even when PCR conditions were optimized in an attempt to amplify the shorter splice variant (data not shown). Therefore, we assume that the full-length *Pibf1* isoform is the most abundant splice-variant of *Pibf1* present in the developing embryo and that the 90kDa protein isoform is the functional isoform of PIBF1 during embryonic development. This is consistent with the previously published observation that the full-length isoform of *Pibf1* is the predominant isoform expressed in proliferative cells *in vitro* (Lachmann et al., 2004).

Pibf1 expression was assessed across a panel of developmental timepoints and tissues by RT-PCR. *Pibf1* is expressed at all developmental stages from E8.5 thru E18.5 but appears to be downregulated in most adult tissues (Figure 4.4 A). The only adult tissue tested that showed a high level of expression was the testis. *Pibf1* expression was not detected in brain, heart, lung or spleen and was only weakly detected in the liver.

Both LacZ staining and *in situ* hybridization were used to examine the spatial distribution of *Pibf1* expression in mouse embryos. We observed progressively restricted expression domains that are generally consistent regardless of the method used. At E8.5 *Pibf1* is highly expressed in the head, heart and embryonic midline with low levels of expression in the somites (Figure 4.4 B). Sectioned embryos showed a high level of expression throughout the neural tube, in the paraxial mesoderm, the heart and in the endodermal layer of the yolk sac (Figure 4.4 C). At E9.5 embryos show intense expression in the forebrain, hindbrain, branchial arches, somites and

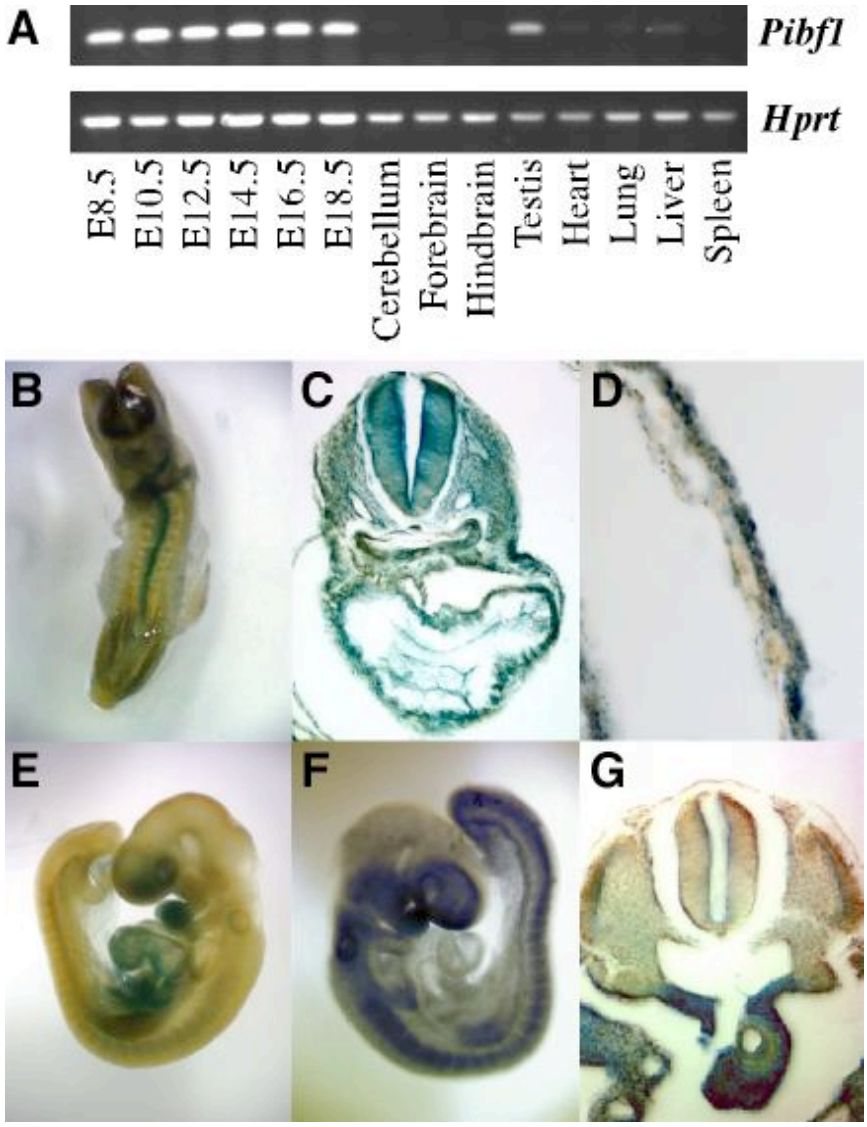

Figure 4.4 *Pibf1* expression pattern. (A) RT-PCR across a panel of developmental time points and adult tissues shows *Pibf1* is expressed throughout development but downregulated in most adult tissues, with the exception of testis. (B,C,D) At E8.5 *Pibf1* is expressed in the neural tube, paraxial mesoderm, heart and endodermal layer of the yolk sac. (E,F) At E9.5 *Pibf1* is expressed in the forebrain, branchial arches, somites, neural tube and limb buds. (G) By E10.5 *Pibf1* is expressed on the apical side of the neural tube, the myotomal layer of the somite and is highly expressed in the foregut. (B,C,D,E and G) are $Pibf1^{GT}$ carriers stained for LacZ while (F) is a wildtype embryo stained for *Pibf1* expression using whole-mount *in situ* hybridization.

limb buds (Figure 4.4 D). Sectioned E10.5 embryos show staining has become localized to the apical side of the neural tube as well as to the myotomal layer of the somite (Figure 4.4 E). Note that the Hedgehog signaling pathway has been shown to have a role in craniofacial development, limb bud patterning, neural tube patterning and somite development. Therefore there is a distinct overlap between regions requiring proper HH signaling and regions that show high levels of *Pibf1* expression.

4.6 Altered left/right patterning in Pibf1$^{128\text{-}7}$ mutant embryos

Defective axial rotation and heart looping morphogenesis in *Pibf1* mutant embryos are indicative of a failure to properly establish L/R asymmetry. In the mouse embryo the first known break in the symmetry of the L/R axis occurs on the ventral surface at the embryonic node at day E8.0. According to the nodal flow hypothesis the rotation of cilia tilted toward the posterior of the embryo generates leftward fluid flow that transports membrane-sheathed particles, nodal vesicular particles (NVPs), to the left side of the node. Signaling molecules contained in the NVPs, such as SHH and RA, act to generate L/R asymmetric patterns of gene expression (Hirokawa et al., 2006). Direct evidence for the nodal flow hypothesis was provided when an artificially generated rightward flow was shown to be sufficient to reverse the situs of wild-type embryos (Nonaka et al., 2002). The asymmetric distribution of signaling ligands at the node triggers transient L/R asymmetric expression at the margins of the node in the TGF-β-like signaling gene *Nodal*. This asymmetry in *Nodal* expression is then transferred to and stabilized in the lateral plate mesoderm (LPM).

Nodal expression in the left LPM is positively regulated by *Nodal* itself and expression rapidly extends along the anterior and posterior body axis until *Nodal* expression occupies most of the left LPM (Saijoh et al., 2005). In *Pibf1*$^{+/+}$ embryos *Nodal* is strongly expressed in the left LPM (Figure 4.5 A), while in all *Pibf1*$^{-/-}$ embryos observed *Nodal* expression is present in both the left and right LPM (Figure

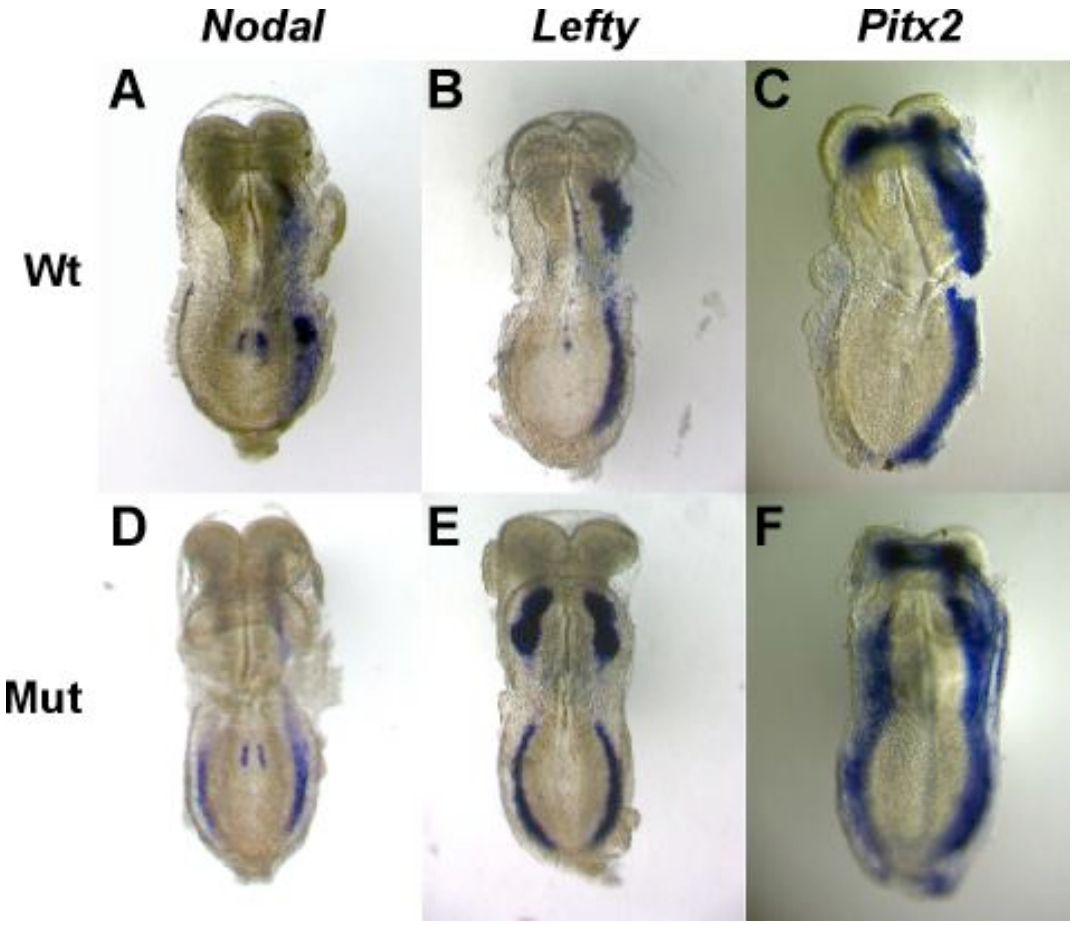

Figure 4.5 Proper expression of left-right patterning genes is lost in *Pibf1* mutant embryos. Ventral views of whole mount *in-situ* hybridization of E8.5 embryos. (A-C) *Nodal*, *Lefty2* and *Pitx2* are expressed asymmetrically in the left LPM and *Lefty1* is expressed in the midline in wildtype embryos. (D-F) *Nodal*, *Lefty2* and *Pitx2* are bilaterally expressed in *Pibf1* mutant embryos while *Lefty1* expression is lost in the left side of the floorplate.

4.5 D). NODAL induces the expression of its antagonists, *Lefty1* and *Lefty2* that are divergent ligands of the TGF-B family. *Lefty1* and *Lefty2* act to restrict *Nodal* expression to the left LPM as well as to limit its duration (Bisgrove et al., 1999). In *Pibf1*$^{+/+}$ embryos *Lefty1* is expressed in the floorplate of the neural tube and *Lefty2* is expressed in the left LPM (Figure 4.5 B). In *Pibf1*$^{-/-}$ embryos *Lefty1* expression is missing and *Lefty2* is bilaterally expressed (Figure 4.5 E). A direct target of NODAL is the paired-like homeodomain transcription factor *Pitx2* (Logan et al., 1998). *Pitx2* expression in the left LPM is maintained for much longer than either *Nodal* or *Lefty* and is believed to mediate the stabilization of L/R asymmetries. Similar to *Nodal* and *Lefty2*, expression of *Pitx2* is restricted to the left LPM in wildtype embryos but is bilaterally expressed in *Pibf1*$^{-/-}$ embryos (Figure 4.5 C, F). These results indicate that L/R patterning in *Pibf1*$^{-/-}$ embryos is disrupted at an early stage, even before gross anatomical defects are observed.

4.7 Midline defects in Pibf1$^{128\text{-}7}$ *embryos*

Loss of *Lefty1* expression in the midline and bilateral expression of *Nodal, Lefty2* and *Pitx2* suggest that the problem in left/right patterning in *Pibf1* mutants may be due to a disruption of the midline barrier. In order to test this hypothesis we first looked histologically at the embryonic structures that define the midline of the embryo, the notochord and the floorplate of the neural tube. During gastrulation epiblast cells initiate movement toward the caudal midline then ingress through the node and primitive streak. The notochord is formed from cells that remain in the midline as they exit the node. The notochord defines the embryonic midline and has dual roles as structural support and as a critical signaling center patterning the surrounding tissues. At E8.5 the notochords of both *Pibf1*$^{+/+}$ and *Pibf1*$^{-/-}$ embryos are clearly visible ventral to the neural tube and appear morphologically normal (Figure 4.6 A,B arrowheads). By E9.5 there are noticeable midline defects in mutant

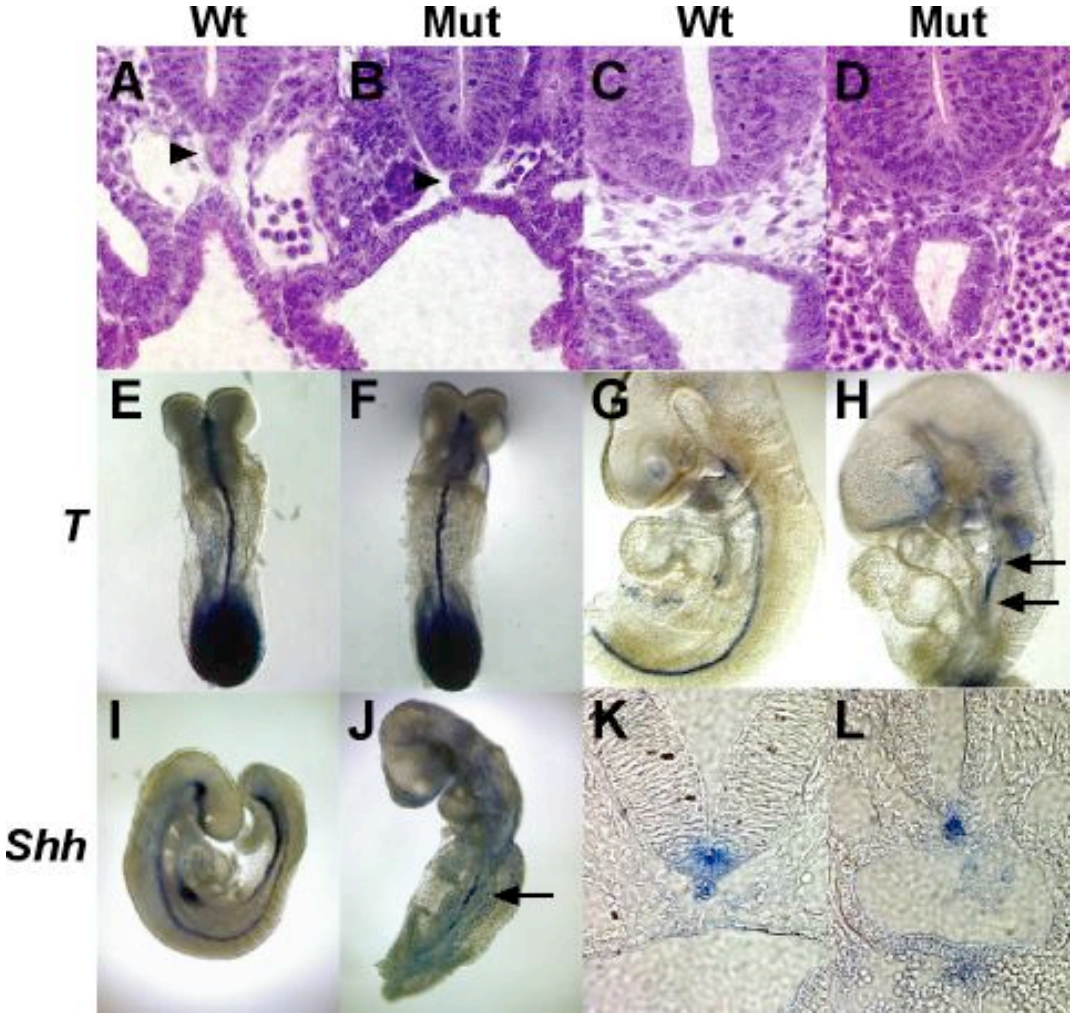

Figure 4.6 Premature degeneration of the notochord in *Pibf1* embryos. (A,B) H&E stained sections of wildtype and mutant embryos at E8.5. Morpholgy is normal in the mutant and in both cases the notochord (arrowhead) is clearly visible ventral to the neural tube. (C,D) H&E stained sections of wildtype and mutant embryos at E9.5. In the mutant the floor plate has failed to form, the notochord is not visible and cells are packed densely in the midline ventral to the neural tube. (E-H) Whole mount *in situ* hybridization for *T* expression. *T* is expressed in the nascent mesoderm and notochord in wildtype E8.5 embryos. Expression of *T* is normal in E8.5 mutant embryos. In E9.5 wildtype embryos *T* expression is visible in the notochord but in mutants is lost throughout most of the anterior/posterior extent of the embryo, with the exception of small portions where the notochord persists (H, arrows). (I-L) *Shh* expression at E9.5 in wildtype and mutant embryos. At E9.5 in wildtype embryos *Shh* is expressed in the notochord and the floor plate of the neural tube. *Shh* expression is lost in mutant embryos similar to *T*. *Shh* secreted from the notochord induces *Shh* expression in the floorplate in wildtype (K) but not in mutant (L) embryos.

embryos. In wildtype embryos the floorplate has formed and the cells of the floorplate have adopted a cuboidal cell shape while the space surrounding the notochord is sparsely populated with cells due to a robust extracellular matrix (Figure 4.6 C). In *Pibf1*$^{-/-}$ embryos the floorplate has failed to form and the cells at the ventral-most part of the neural tube retain a columnar shape. The mesenchyme ventral to the neural tube is densely packed, obscuring the notochord (Figure 4.6 D).

The mouse *Brachyury* (*T*) gene is required for early mesodermal patterning (Conlon et al., 1995). *T* is initially expressed in nascent mesoderm in the primitive streak. As the mesoderm differentiates *T* expression is down-regulated except in the cells of the notochord. In E8.5 wildtype embryos *T* is expressed throughout the nascent mesoderm at the posterior of the embryo as well as in the notochord and prechordal plate (Figure 4.6 E). E8.5 *Pibf1*$^{-/-}$ embryos have normal *T* expression, consistent with the normal notochord morphology in H&E sections (Figure 4.6 F). Wildtype E9.5 embryos retain *T* expression in the notochord and prechordal plate (Figure 4.6 G), but in E9.5 *Pibf1*$^{-/-}$ embryos *T* expression is lost through most of the A/P extent of the embryo, indicating the premature degeneration of the notochord (Figure 4.6 H). Expression of *T* often persists in small regions of the mutant embryo (Figure 4.6 G, arrows). This region of persistent *T* expression varies in size and location and suggests parts of the notochord are still present even though most of it has degenerated.

A well-characterized signaling molecule secreted from the notochord is SHH, one of the three ligands in the Hedgehog signal transduction pathway. SHH secreted from the notochord is important in patterning multiple surrounding tissues, including the neural tube, somites, endoderm and vasculature (Byrd et al., 2002; Dessaud et al., 2008; Marcelle et al., 1999). In wildtype embryos at E8.5 *Shh* is expressed in the notochord and prechordal plate. SHH produced by the notochord induces *Shh*

expression in the floor plate of the neural tube, and by E9.5 *Shh* is expressed in both the notochord and the floorplate of wildtype embryos (Figure 4.6 I, K). In *Shh* mutants *T* expression and notochord development is normal but starting at E8.0 *T* expression is progressively lost in a rostral to caudal direction, demonstrating SHH is required for notochord maintenance. *Shh* expression is normal at E8.5 in *Pibf1*$^{-/-}$ embryos (data not shown), but by E9.5 *Shh* expression is lost in the majority of the embryo along the A/P axis, similar to *T* expression in *Pibf1*$^{-/-}$ embryos (Figure 4.6 J). Also similar to *T*, some *Shh* expression within the notochord remains in the majority of *Pibf1*$^{-/-}$ embryos (Figure 4.6 J, arrow). Importantly, even in regions where *Shh* expression persists in the notochord it fails to induce *Shh* expression in the floorplate (Figure 4.6 L). The inability of notochord-derived Shh to induce expression of *Shh* in the floorplate strongly suggests that the defect in *Shh* signaling isn't merely due to loss of the notochord and consequent reduction in *Shh* expression, but that *Pibf1* is required for the HH signal to transmit from the notochord to the ventral neural tube and that the HH signal transduction mechanism is disrupted in *Pibf1*$^{-/-}$ embryos.

4.8 Embryological defects in Pibf1$^{128\text{-}7}$ *mutant embryos confirm a defect in Shh signaling*

It is well established that HH signaling is required for the patterning of numerous embryonic tissues within the developing embryos. In order to confirm that the loss of *Shh* observed in the floorplate of the neural tube was indicative of a global defect in HH signaling in *Pibf1* mutant embryos we characterized the phenotype of a number of tissues that are known to depend on HH signaling and compared the phenotype of *Pibf1* mutants with the phenotype of embryos with defects in the HH signaling pathway.

4.8.1 Vascular defects in Pibf1$^{-/-}$ mutants

The vascular system provides the developing embryo with required oxygen and nutrients as well as removing the waste from cellular metabolism. Its formation is a critical early step in murine embryogenesis. In the embryonic yolk sac endothelial cells form an initial network of vascular tubes of uniform diameter, the capillary plexus, which is later remodeled to form the mature vitelline vessels. In E9.5 wildtype yolk sacs large diameter vessels clearly demonstrate the remodeling associated with the formation of mature blood vessels. We have previously shown that in *Pibf1*$^{-/-}$ embryos there is no remodeling of the yolk sac vasculature with vessel formation arrested at the capillary plexus stage (See Figure 2.2 E,F). Expression of *Pibf1* in the endodermal layer of the yolk sac is consistent with a role for PIBF1 in the development of the yolk sac vasculature (See Figure 4.4 D). HH signaling has been demonstrated to have a role in the development of the yolk sac vasculature. Both *Ihh*$^{-/-}$ and *Smo*$^{-/-}$ mutants fail to form fully remodeled blood vessels (Byrd et al., 2002). *Ihh*$^{-/-}$ mutants form yolk sac blood vessels that are fewer in number and smaller than wildtype, while *Smo*$^{-/-}$ mutants fail to undergo any vascular remodeling in the yolk sac.

A further dysmorphic vascular phenotype in *Pibf1*$^{-/-}$ embryos lies in the morphology of the major blood vessels leading to the heart. The caudal end of the heart, the sinus venosus, arises within the septum transversum. The sinus venosus is fed by paired common cardinal veins that are in turn fed by caudal and cranial cardinal veins, umbilical veins and vitelline veins. In wildtype E9.5 embryos the left and right horns of the sinus venosus are visible in section just posterior to the heart (Figure 4.7 A). In *Pibf1*$^{-/-}$ embryos the common cardinal veins are fused and swollen, in some instances until the gut tube is nearly circumscribed, consistent with a defect in the circulation (Figure 4.7 B). The development of the major intraembryonic blood vessels also depends on HH signaling. In mouse *Smo*$^{-/-}$ mutants the anterior two-thirds

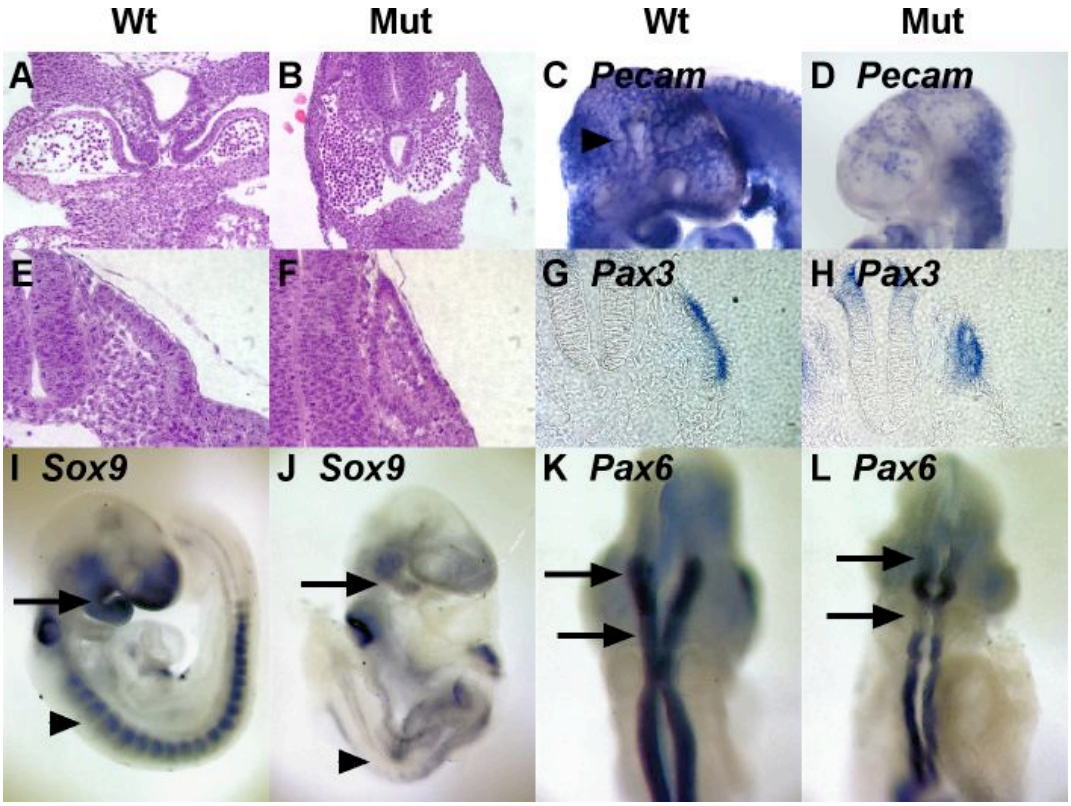

Figure 4.7 Patterning of HH signaling-dependent tissues is disrupted in *Pibf1* mutants. (A) In E9.5 wildtype embryos the sinus venosus divides into left and right horns just posterior to the caudal end of the developing heart. (B) In mutant E9.5 embryos the sinus venosus is swollen and dysmorphic compared to wildtype embryos. (C) E9.5 wildtype embryos contain mature vascular networks in the head as shown by staining for *Pecam*. (D) In E9.5 mutant embryos the vasculature contains immature blood vessels that fail to develop into a mature vasculature. (E,G) Somite morphology and resticted expression of myotomal marker *Pax3* in wildtype E9.5 embryos. (F,H) In mutant E9.5 embryos the somite persists as an epithelial block and ectopically expresses *Pax3* throughout the somite. (I,J) *Sox9* is expressed in the forebrain, branchial arches (arrow), otic vesicle and scleratome (arrowhead) in wildtype E9.5 embryos but expression is lost in the forebrain, branchial arches (arrow) and scleratome (arrowhead) in mutant embryos. (K,L) Dorsal view of *Pax6* expression in wildtype and mutant embryos at E9.5. Expression is greatly reduced in rhombomeres 2 and 4 in mutant embryos (arrows).

of the dorsal aortae are severely defective or absent while in zebrafish loss of *Shh* leads to the formation of a single large axial vessel expressing venous markers, rather than the normal dorsal aorta and cardinal vein, demonstrating a requirement for *Shh* in specifying arterial differentiation (Lawson et al., 2002).

In order to see if the vascular defects in the yolk sac and major blood vessels in *Pibf1*$^{-/-}$ mutants extend to the vasculature of the rest of the embryo we performed *in situ* hybridization to look at vascular development using *Pecam* as a marker for endothelial cells. Staining for *Pecam* in wildtype embryos shows developing vascular networks composed of organized blood vessels (Figure 4.7 C). In *Pibf1*$^{-/-}$ embryos the remodeling of endothelial cells into mature vascular networks is deficient, similar to that seen in the yolk sac (Figure 4.7 D). Defective vessel development in *Pibf1*$^{-/-}$ embryos is consistent with that reported for other mutants with HH signaling defects. The development of the vasculature in HH mutants is disrupted in numerous tissues, including the cephalic mesenchyme, outflow tract, aortic arches, and developing lungs (Kolesova et al., 2008; Pepicelli et al., 1998; Vokes et al., 2004).

4.8.2 Somite defects in Pibf1$^{-/-}$ *embryos*

Somites are epithelial blocks of paraxial mesoderm that give rise to the cartilage and bones of the ribs and vertebrae, skeletal muscles, the dermis of the dorsal body wall, smooth muscle, connective tissue surrounding the spinal cord and endothelial cells that contribute to blood vessels. Each somite is initially an epithelial cube, but the ventromedial half of each somite undergoes an epithelial to mesenchymal transition to form the scleratome. The superficial part of the somite becomes the dermamyotome. This patterning of somites is clearly visible in wildtype embryos at E9.5 (Figure 4.7 E). In *Pibf1*$^{-/-}$ embryos the somites fail to differentiate into scleratome and dermamyotome and instead persist as an epithelial block (Figure

4.7 F). Notably, *Gli1/Gli2* double mutants display a ventro-medial expansion of the epithelial dermamyotome similar to that seen in *Pibf1*$^{-/-}$ mutants (Buttitta et al., 2003).

The transcription factor *Pax3* is an important regulator of myogenic cell fate (Buckingham et al., 2006). *Pax3* is expressed in myogenic progenitor cells derived from the central dermamyotome. In wildtype embryos *Pax3* expression is restricted to the dorsolateral part of the somite (Figure 4.7 G). In *Pibf1*$^{-/-}$ embryos *Pax3* is ectopically expressed through the entire somite (Figure 4.7 H). *Shh* mutant mice also show expansion of the dermamyotomal marker *Pax3* ventrally along with reduced expression of the scleratomal marker *Pax1* (Chiang et al., 1996).

Sox9 is required for cartilage formation and is a marker for the scleratome (Bi et al., 1999). In wildtype E9.5 embryos *Sox9* is expressed in the scleratome, but in *Pibf1*$^{-/-}$ mutant embryos *Sox9* expression is lost, demonstrating a defect in scleratome development in *Pibf1*$^{-/-}$ mutants (Figure 4.7 I,J arrowheads). *Shh* mutant mice lack most scleratomal derivatives (Chiang et al., 1996) and *Smo* mutants fail to express scleratomal markers completely, displaying an absolute role for HH signaling in scleratome development (Zhang et al., 2001). The loss of *Sox9* and ectopic expression of *Pax3* demonstrates a failure of scleratome development in *Pibf1*$^{-/-}$ mutants strikingly similar to that seen in HH mutants.

4.8.3 Disrupted neural crest development in Pibf1$^{-/-}$ *embryos*

The neural crest are a population of mesenchymal cells that originate in the roof of the neural tube that then migrate to multiple regions, contributing to a heterogeneous group of derivative cell types, including neurons, secretory cells, pigment cells and connective tissue. Cephalic neural crest cells move peripherally and form connective tissues as well as cranial sensory ganglia. The movement of neural crest cells lateral to the pharynx creates the branchial arches. The maxillary and mandibular prominences of the first branchial arch elongate and fuse at the midline to

form the jaw. The first and second branchial arches are clearly visible in E9.5 wildtype embryos (Figure 4.1 B, dotted lines). In *Pibf1*$^{-/-}$ embryos the first arch is reduced in size and the second is missing (Figure 4.1 C, dotted line). *Shh*$^{-/-}$ mutant embryos also display a number of defects in pharyngeal arch-derived structures (Chiang et al., 1996). Virtually all of the structures derived from the first through sixth pharyngeal arches are abnormal or absent in *Shh*$^{-/-}$ mutant embryos (Washington Smoak et al., 2005). The defects in branchial arch development in *Shh*$^{-/-}$ mutants is due to the loss of neural crest cells, and *Shh* has been shown to be required for the survival of cranial neural crest (Ahlgren and Bronner-Fraser, 1999; Jeong et al., 2004).

The differentiation of cranial neural crest-derived cartilage is controlled by the transcription factor *Sox9*, which binds the promoter of *Col2a1* (Lefebvre et al., 1997). *Sox9* is expressed in cephalic neural crest cells and is required for the determination of the chondrogenic lineage in connective tissue derived from the branchial arches (Mori-Akiyama et al., 2003). In wildtype E9.5 embryos robust *Sox9* expression is visible in the forebrain and first branchial arch but is greatly reduced in *Pibf1*$^{-/-}$ mutant embryos, demonstrating a defect in the development of the neural crest in *Pibf1*$^{-/-}$ embryos (Figure 4.7 I,J arrows). Expression of *Sox9* is also lost in the branchial arches in *Shh*$^{-/-}$ mutant embryos (Washington Smoak et al., 2005).

The *Pax6* gene encodes a transcription factor that is expressed at E9.5 in the neural tube, prosencephalon and in rhombomeres 2 through 8 and has been shown to be required for neural crest migration (Mastick et al., 1997). *Pax6* mutants display a variety of craniofacial defects due to impaired migration of cranial neural crest cells. Strikingly, altered expression of *Pax6* is restricted to specific rhombomeres in *Pibf1*$^{-/-}$ mutants. The expression level in rhombomeres 3 and 5-8 appears normal, however *Pibf1* expression is downregulated in rhombomeres 2 and 4 (Figure 4.7 K,L arrows).

The dysmorphic morphology of the branchial arches in *Pibf1*$^{-/-}$ mutant embryos as well as loss of *Sox9* expression within the branchial arches supports the hypothesis that *Pibf1* is required for SHH signaling and maintenance of cranial neural crest. The loss of *Pax6* expression in the rhombomeres suggests that the defect in cranial neural crest development is due to a failure in neural crest migration. Lineage tracing experiments in chick embryos have shown that cranial neural crest cells in branchial arches 1, 2 and 3 are derived from neural crest cells migrating from rhombomeres 2, 4 and 6, respectively, while rhombomeres 3 and 5 release no neural crest cells (Lumsden et al., 1991). It has also been shown that some neural crest cells from rhombomere 1 migrate into branchial arch 1, and this may explain why the first branchial arch, although dysmorphic compared to wildtype, is present in *Pibf1*$^{-/-}$ mutants. The reduction of *Pax6* expression only in rhombomeres 2 and 4 suggests a rhombomere-specific defect in neural crest cell migration in *Pibf1*$^{-/-}$ mutant embryos.

4.8.4 Patterning of ventral neural tube progenitors is disrupted in Pibf1$^{-/-}$ *embryos*

Early work grafting pieces of floorplate and notochord showed SHH secreted from the notochord and floorplate is responsible for patterning the D/V axis of the ventral neural tube (Yamada et al., 1993; Yamada et al., 1991). SHH produced in the notochord and floorplate forms a gradient providing the spatial information necessary to confer positional identity to six distinct progenitor domains in the ventral neural tube (Dessaud et al., 2008). Loss of *Shh* leads to the dorsalization of the ventral neural tube, with expression of the alar plate marker *Pax3* expanded ventrally across the floorplate (Chiang et al., 1996). The identity of each domain is determined by the combination of transcription factors expressed. Markers for the six cell types within the ventral neural tube may be divided into two classes based on their mode of regulation by SHH. Class I genes are repressed by SHH signaling, while high levels of SHH signaling induce the expression of Class II genes. Many of these transcription

factors function as transcriptional repressors, and repressive interactions between class I and II proteins define the boundaries of ventral progenitor domains. For example, the class II transcription factor *Nkx6.1* is expressed in the p2 progenitor domain (Figure 4.8 E) and acts to repress the expression of *Nkx6.2*, which is expressed in the p1 progenitor domain (Figure 4.8 C). *Nkx6.2* acts to repress the expression of *Dbx1*, which is expressed in the p0 progenitor domain (Figure 4.8 A). A decrease in HH signaling would therefore be expected to reduce the gradient of HH in the neural tube and lead to the loss of ventral neural progenitor domains that require high levels of HH for their induction. In *Pibf1*$^{-/-}$ embryos *Nkx6.1* expression is lost (Figure 4.8 F) while *Nkx6.2* expression is expanded ventrally to the floorplate of the neural tube (Figure 4.8 D). This loss of class II transcription factors and ventral expansion of class I transcription factors demonstrates a dorsalization phenotype in the ventral neural tube in *Pibf1*$^{-/-}$ embryos indicative of a reduction in SHH signaling (Figure 4.8 G).

4.9 Pibf1 functions in SHH target cells downstream of Ptch1

SHH acts on target cells by binding to its receptor, PTCH1, and alleviating PTCH1 repression of SMO. PTCH1 function is required to keep the downstream signaling off in the absence of HH ligand. Loss of *Ptch1* leads to constitutive activation of *Smo* and upregulated SHH signaling. *Ptch1*$^{-/-}$ mutant mice are comparable in size with wildtype embryos and show normal axial rotation, but display a severe neural tube defect and overgrown headfolds at the anterior of the embryo (Figure 4.9 A,B). This is in contrast to the phenotype of *Pibf1*$^{-/-}$ mutants, which are smaller than wildtype littermates and show defective axial rotation, but in which the neural tube closes normally (Figure 4.9 C).

We used a genetic approach to determine if PIBF1 functions upstream of PTCH1, possibly with a role in production, secretion or trafficking of HH ligand, or downstream of PTCH1, serving to facilitate the transduction of the HH signal in the

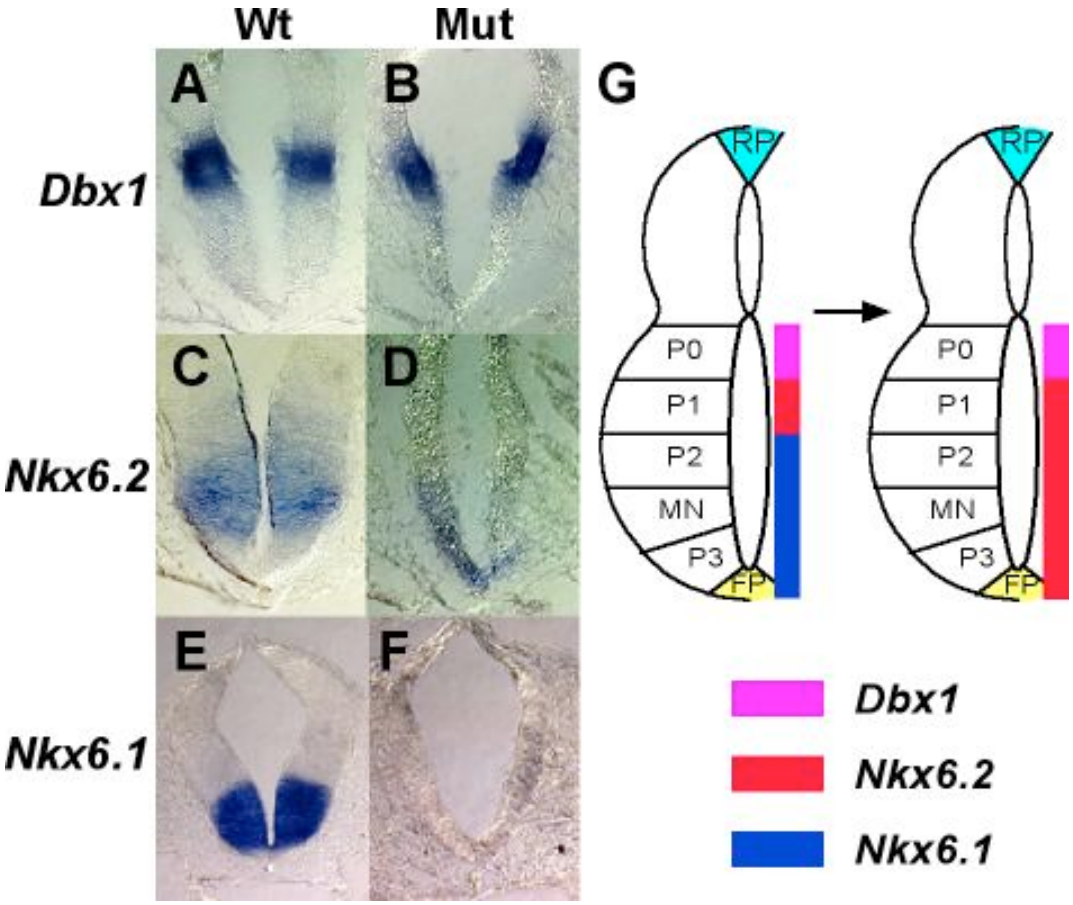

Figure 4.8 Ventral neural tube patterning is disrupted in *Pibf1* mutants. (A,B) *Dbx1* is expressed normally in the P0 progenitor domain in E9.5 *Pibf1* mutants. (C,D) *Nkx6.2* expressing V1 progenitors are expanded to the ventral-most neural tube in mutant E9.5 embryos compared to wildtype. (E,F) Expression of the class II transcription factor *Nkx6.1* is lost in mutant E9.5 embryos compared to wildtype. (G) A diagram of the ventralization phenotype seen in *Pibf1* mutants. Class II transcription factors are lost and Class I transcription factors are ectopically expressed ventrally.

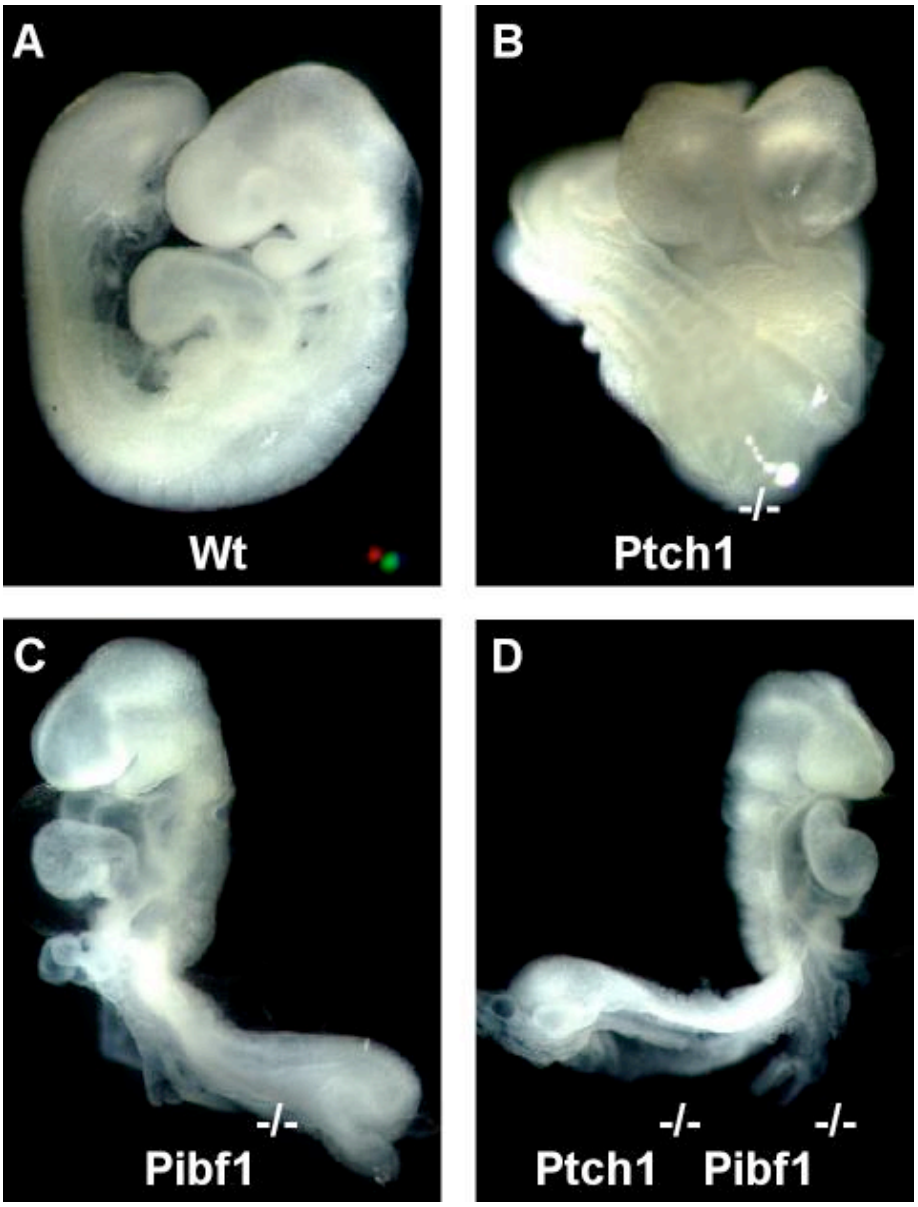

Figure 4.9 Double mutant analysis shows *Pibf1* functions in SHH-responsive cells downstream of *Ptch1*. (A) Wildtype E9.5 littermate. (B) E9.5 *Ptch1* mutant embryos have a severe neural tube defect with overgrown neural folds. (C) *Pibf1* mutant embryos are smaller than wildtype littermates, caudally truncated and fail to turn properly. (D) *Ptch1*/*Pibf1* double mutants display an identical phenotype to *Pibf1* mutant embryos, rescuing the *Ptch1* phenotype and demonstrating that loss of *Pibf1* is downregulating the constutive activation of SHH signaling that occurs as a result of loss of PTCH1 in the SHH-responsive cell.

HH-responsive cell. *Pibf1*$^{-/-}$*Ptch1*$^{-/-}$ double mutants display the same phenotype as *Pibf1*$^{-/-}$ mutants (Figure 4.9 D), rescuing the *Ptch1*$^{-/-}$ phenotype of gain of function in SHH signaling and suggesting SHH targets are not activated in *Pibf1*$^{-/-}$*Ptch1*$^{-/-}$ double mutants. This demonstrates that the constitutive activation of the SHH signaling pathway due to the loss of *Ptch1* is disrupted in *Pibf1*$^{-/-}$*Ptch1*$^{-/-}$ double mutants and that SHH signaling is being disrupted downstream of *Ptch1* in the SHH-responsive target cell in the *Pibf1* mutant.

4.10 Pibf1$^{128\text{-}7}$ *mutants have a severe reduction, but not a complete loss of Hedgehog signaling*

SHH produced in the notochord and floor plate forms a gradient providing the spatial information necessary to assign identity to progenitor domains in the ventral neural tube (Chamberlain et al., 2008; Dessaud et al., 2008). Each progenitor domain is marked by the expression of a distinct combination of transcription factors that differentially respond to the SHH signaling gradient. In *Pibf1* mutants we see the loss of class II transcription factors and a ventral shift in the expression domain of class I transcription factors. There is evidence that class I genes are activated by low levels of SHH and inhibited by high levels of SHH due to the repressive activity of class II genes (Pachikara et al., 2007; Persson et al., 2002). Thus, in *Pibf1* mutants SHH signaling is insufficient to induce class II transcription factor expression, yet it is possible that in the absence of class II transcription factor repression a low level of SHH signaling is sufficient to induce ectopic expression of class I transcription factors in the ventral neural tube, suggesting that some SHH signaling is present in *Pibf1* mutants.

The left-right patterning defects in *Pibf1* mutants also suggest a severe reduction rather than a complete loss of SHH signaling activity. Multiple components of the HH signaling pathway have been shown to be required for proper left-right

patterning. *Shh* mutants express *Pitx2* bilaterally while *Shh/Ihh* double mutants fail to express *Pitx2*. *Smo* mutants also fail to express *Nodal*, *Lefty* and *Pitx2* in the lateral plate mesoderm (Zhang et al., 2001). In *Pibf1* mutants *Nodal*, *Lefty* and *Pitx2* are bilaterally expressed rather than absent as seen with the complete loss of HH signaling in *Smo* mutants. The left-right patterning defects supports the inference that there is a low level of HH signaling in *Pibf1*$^{128\text{-}7}$ mutants and suggests that either *Pibf1* is not absolutely required for HH signaling or that the ENU-induced mutation does not result in the complete loss of *Pibf1* gene function. A low level of normally spliced transcript produced in *Pibf1*$^{128\text{-}7}$ mutants potentially provides a basis for a hypomorphic phenotype and embryonic defects consistent with a severe reduction in HH signaling (see Figure 4.2 E). In addition, although we mapped the lariat branch point in intron 2 of *Pibf1* to the base mutated in ENU 128-7 there is another sequence just upstream that also matches the consensus sequence for the lariat branch point sequence. It is possible that this sequence is serving as a low-fidelity branch point site that allows a small amount of normal transcript to be produced.

CHAPTER V

PIBF1 AND CYTOSKELETAL ORGANIZATION

5.1 Introduction

Changes in cell shape and structure take place throughout development and involve the reorganization of actin filaments and microtubules. Specialized cytoskeletal structures include organelles such as the microtubule-based cilia and actin-based microvilli formed on the apical surface of polarized epithelial cells. Furthermore, the efficient activity of various signaling pathways relies upon the association of pathway components with subcellular compartments and specialized structures formed by the cytoskeleton. The Notch receptor, Receptor/Jak complex and transcription factor STAT are enriched in apical or apicolateral membrane domains of polarized cells (Hombria and Sotillos, 2008; Levitan and Greenwald, 1998; Sotillos et al., 2008). Cilia are implicated in the switch between canonical and non-canonical WNT/planar cell polarity signaling (Bisgrove and Yost, 2006; Simons et al., 2005). In vertebrates, Hedgehog (HH) signal transduction is coupled to the formation of cilia (Corbit et al., 2005; Huangfu et al., 2003; Rohatgi et al., 2007).

Cilia are centriole-derived, membrane-bound projections from the cell containing an axonemal core composed of a microtubule scaffold (Satir and Christensen, 2007). Cilia may be motile or immotile. Epithelial cells may possess hundreds of 9+2 motile cilia with axonemes formed by nine doublet microtubules surrounding a pair of singlet microtubules. While motile cilia are formed by specialized cell types, nearly all mammalian cells are thought to form an immotile primary cilium (Wheatley et al., 1996). The immotile primary cilium is formed as a 9+0 axoneme of nine doublet microtubules that extend from the nine triplet microtubules of the basal body. Prior to primary cilia formation the mother centriole,

located in the centrosome, migrates and docks at the plasma membrane. The mother centriole becomes the basal body that serves as the microtubule organizing center during the growth of the ciliary axoneme (Santos and Reiter, 2008).

Dynamic intracellular remodeling events and the motor-driven distribution of component proteins are involved in the assembly and disassembly of cilia. The elongation of the ciliary axoneme requires intraflagellar transport (IFT) (Scholey, 2003). Multiple proteins, including IFT88 and IFT27, are transported up and down the cilia by microtubule-associated Kinesin-2 and Dynein motors. Loss of either the motor or basal body proteins leads to defects in ciliogenesis (Rosenbaum and Witman, 2002). In addition, the disruption of IFT proteins, basal body proteins, and subunits of the Kinesin molecular motors all impair Hedgehog signaling (Houde et al., 2006; Huangfu et al., 2003; Marszalek et al., 1999; Vierkotten et al., 2007). Importantly, multiple components of the SHH signaling pathway are enriched in cilia. In the absence of the SHH ligand the PTCH1 receptor is localized to cilia (Rohatgi et al., 2007). Upon SHH binding PTCH1 leaves the cilium followed by the accumulation of SMO at the cilium and activation of HH signaling (Corbit et al., 2005).

5.2 Materials and methods

Pibf1 expression vector and sub-cellular localization of PIBF1

Nucleotides 719 through 2210 of NM_029320.0, including the coding sequence of *Pibf1,* were amplified from mouse adult testis cDNA and cloned into the HA-tagged pKH3 vector. For transfection NIH3T3 cells were plated into 3cm dishes containing a 22x22mm glass coverslip and grown for 48 hours in DMEM without serum to induce the growth of cilia. Each dish was transfected with *Pibf1*-HA plasmid DNA using JetPEI transfection reagent (Polyplus) and incubated 24-48 hours before immunocytochemistry.

Immunocytochemistry

Coverslips were washed with PBS and fixed in 4% PFA. Cells were permeabilized in .25% Triton, blocked in 1% BSA and incubated sequentially for double immunofluorescence with primary and secondary antibodies in PBST plus 1% BSA, each followed by three washes in PBS. Antibodies used were rat a-HA (1:100), mouse a-acetylated tubulin (1:500), Texas Red donkey a-rat (1:500) and AF488 goat a-mouse (1:500). Nuclei were counterstained with DAPI, mounted in aqueous fluorescent mounting media and viewed on Zeiss Axio Imager Z1 fluorescent microscope using Axio Vision 4.0 software.

Scanning electron microscopy (SEM)

SEM was performed with the assistance of the Cornell Integrated Microscopy Center. Embryos were fixed overnight in 2.5% Gluteraldehyde in 0.1M sodium cacodylate pH 7.4. They were then washed in 0.1M sodium cacodylate and put in 1% osmium tetroxide for one hour at room temperature. Embryos were again washed then dehydrated through an ethanol series. Dehydrated embryos were critical-point dried, mounted on metal stubs and sputter coated before being visualized on the LEO DSM960 SEM.

5.3 Cilia are disrupted in Pibf1$^{128\text{-}7}$ mutant embryos

The phenotypic defects in *Pibf1*$^{-/-}$ mutants closely resemble those in *C2cd3*^{GT} mutants, which exhibit severe loss of cilia, and the loss of primary cilia has been shown to result in disruption of HH signaling and L/R patterning defects. Also, it has been previously shown that PIBF1 localizes to the centrosome in proliferating cells (Lachmann et al., 2004). The centrosome contains the centriole that translocates to the apical membrane and forms the basal body of cilia. Therefore we sought to determine whether *Pibf1* plays a role in cilia formation or function. Within the ventral node of

mammalian embryos each cell contains a single cilium. Node cilia are clearly visible in wildtype embryos using SEM (Figure 5.1 C). In *Pibf1*$^{-/-}$ mutant embryos the number of cilia at the node are greatly reduced and the cilia present appear dysmorphic compared to wildtype (Figure 5.1 D). Interestingly, the structure of the microvilli that line the apical cell wall are also disrupted in *Pibf1*$^{-/-}$ mutants. Microvilli are actin-based structures and this result suggests that the cortical actin network is disrupted in *Pibf1*$^{-/-}$ mutants in addition to the structure of the microtubule-based cilia.

5.4 PIBF1 is localized to the cilia

In order to better appreciate the role of PIBF1 in cilia function we constructed a HA-tagged *Pibf1* expression vector and used it to examine the subcellular localization of PIBF1 in ciliated cells. The HA-tagged PIBF1 protein localized to the ciliary axoneme, as demonstrated by co-localization with acetylated tubulin in NIH3T3 cells (Figure 5.1 E-G). Figure 5.1 E-G contains two cells, one that has been successfully transfected with the *Pibf1* expression vector and one control cell that has not. It is notable that within cells transfected with the HA-tagged *Pibf1* expression vector there is an excess of acetylated tubulin, as demonstrated by the ectopic green signal ventral to the cilium (Figure 5.1 E, arrow). This excess tubulin is not visible in control cells lacking expression vector (Figure 5.1 E, arrowhead; Figure 5.1 H).

5.5 Cilia loss contributes to, but does not fully explain the left/right patterning defects in Pibf1$^{128\text{-}7}$ *mutant embryos*

The morphological defects observed in *Pibf1*$^{-/-}$ mutants, including randomized turning direction and abnormal heart looping are typical of those seen in mutations disrupting L/R patterning (Krebs et al., 2003; Melloy et al., 1998; Nakaya et al., 2005; Zhang et al., 2004; Zhang et al., 2001). The symmetrical expression of genes such as *Nodal*, *Lefty2* and *Pitx2* demonstrates that *Pibf1* plays an essential role in L/R

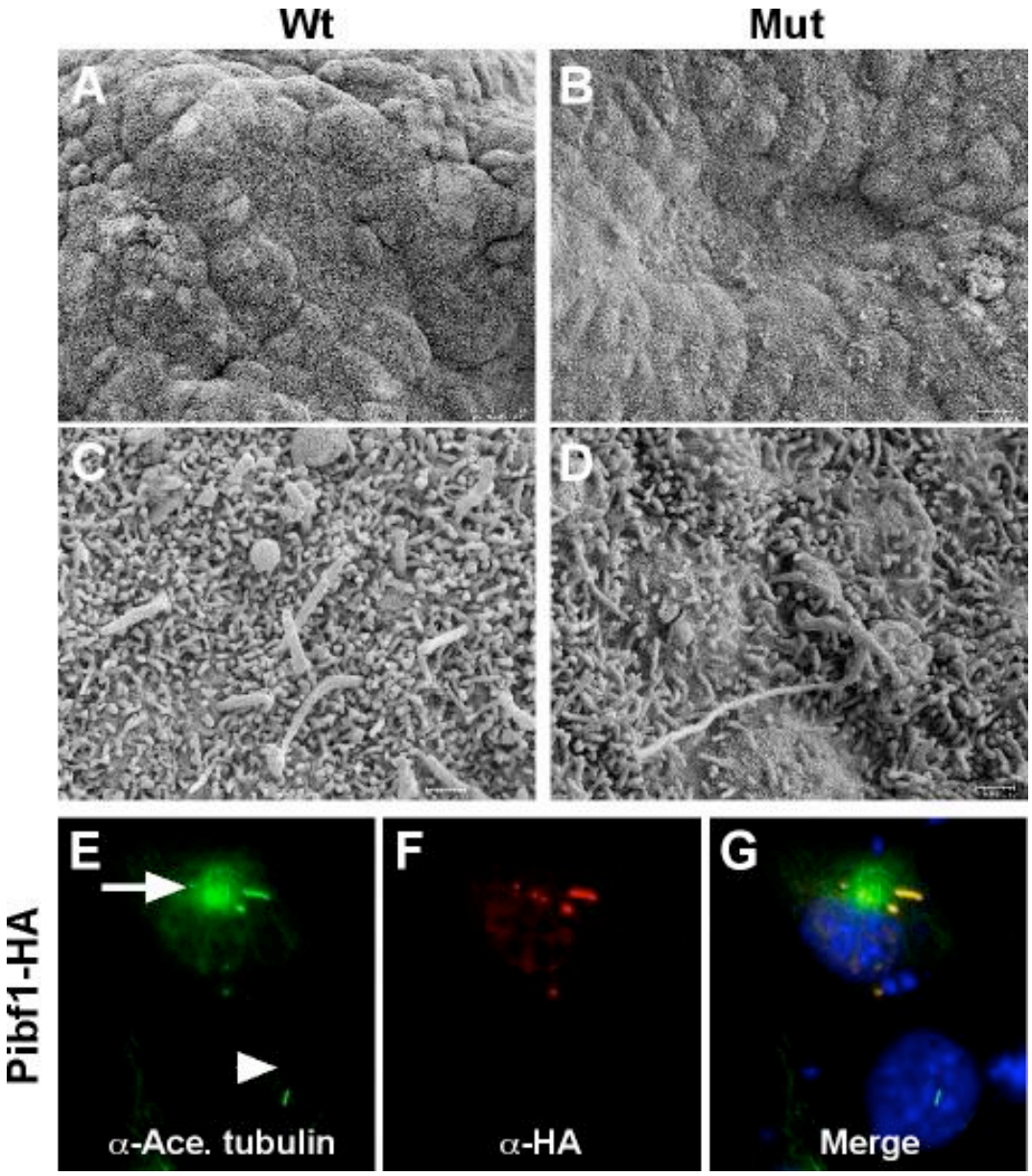

Figure 5.1 Loss of *Pibf1* causes a defect in cilia formation and PIBF1 localizes to the ciliary axoneme. (A,B) SEM images of the ventral node in wildtype and mutant E8.5 embryos. (C,D) magnified images of wildtype and mutant node cells showing cilia clearly visible in the wildtype node while cilia are reduced in number and dysmorphic in mutant node cells. Microvilli lining the apical membrane are also reduced in mutant cells. (E-G) Immunocytochemistry of NIH3T3 cells transfected with a HA-tagged *Pibf1* expression construct. Two cells are shown in the image, a *Pibf1*-HA transfected cell (top) and a cell that is not transfected (bottom). (E) shows localization of acetylated-tubulin (green) at the monocilia, (F) shows localization of PIBF1-HA and (G) shows the merged image. The yellow cilia in (G) demonstrates that PIBF1-HA is localizing to the ciliary axoneme. The nuclei are counterstained with DAPI (blue).

patterning. A number of genes that disrupt L/R patterning display randomized expression of *Nodal*, *Lefty* and *Pitx2*, but mouse mutants for genes such as *Kif3a*, *IFT88* and *IFT172* that are essential for the formation of monocilia display bilateral expression (Houde et al., 2006; Huangfu et al., 2003; Marszalek et al., 1999). In addition, genes required for proper cilia function, such as *Ftm*, also display bilateral expression of genes such as *Pitx2* (Vierkotten et al., 2007). Therefore, the bilateral pattern of expression of *Nodal*, *Lefty2* and *Pitx2* are consistent with disrupted cilia function in *Pibf1*$^{-/-}$ mutants.

Loss of cilia function is not the only cause of bilateral expression of *Nodal*, *Lefty2* and *Pitx2*. *Lefty1*$^{-/-}$ mutants fail to properly pattern the floorplate of the neural tube and also show bilateral expression of *Nodal*, *Lefty* and *Pitx2*, indicative of a failure to generate a midline barrier (Meno et al., 1998). These results suggest that bilateral expression of these three markers is due to either a loss of cilia function in the node and consequent disruption of nodal flow or the failure to properly construct a midline barrier to restrict asymmetric gene expression. Given that the phenotype of *Pibf1*$^{-/-}$ mutants is more severe than that described for *wimple* mutants, that lack nodal cilia, or of *Lefty1*$^{-/-}$ mutants, that lack a proper midline barrier, we suggest neither of these defects alone is sufficient to explain the phenotype of *Pibf1*$^{-/-}$ mutants and that *Pibf1* is required both for functional cilia and for development of the midline barrier. This hypothesis is supported by the observations that the structure that defines the midline of the embryo, the notochord, is prematurely degenerating, as well as by a reduced number of cilia within the node as revealed by SEM.

5.6 Identifying PIBF1 as a component of the ciliome

Given the diversity of roles performed by cilia and flagella, as well as the diverse range of cell types that contain them, a basic question that arises is how is ciliogenesis orchestrated, and to what extent do common mechanisms underlie this

process. Several groups have used genomic, proteomic or bioinformatics approaches to identify genes involved in ciliogenesis. Avidor-Reiss et al. used a global genomic approach comparing organisms with and without cilia, Broadhead et al. conducted a proteomic analysis of the trypanosome flagellum, Liu et al. analyzed the proteome of the mouse photoreceptor and Andersen et al. investigated the proteome of the human centrosome (Andersen et al., 2003; Avidor-Reiss et al., 2004; Broadhead et al., 2006; Liu et al., 2007). A search of the cilia proteome database (http://v3.ciliaproteome.org/) shows that *Pibf1* or a putative homolog of *Pibf1* was identified by each study as a component of the cilia. Not only does this provide additional evidence that PIBF1 is an important component of the cilia, it suggests that *Pibf1* is conserved as far back as protists, ciliated unicellular eukaryotes. In order to confirm the existence of a *Pibf1* homolog within the trypanosome genome a PBlast search using the amino acid sequence of mouse PIBF1 was conducted. The search yielded a single alignment with *Trypanosome brucei* (Figure 5.2 A). The alignment spanned 226 amino acids toward the C-terminal end of the 756-amino acid PIBF1 protein, from amino acids 487-692, and the region spanned by the alignment had 45% similarity between the two species with an E value of 4e-07 (Figure 5.2 B). The region of the PIBF1 protein conserved between mouse and *T. brucei* overlaps a SMC domain, which is a conserved protein domain from bacteria involved in chromosome segregation. It's worth noting that the Szekeres-Bartho lab has identified the N-terminal end of PIBF1 as the biologically active region of the protein (Figure 5.2 A, yellow highlight), but they were specifically looking at the inhibition of NK activity described as part of the immunomodulation in pregnant females triggered by Pibf1 (Polgar et al., 2003). The separation of the domain of PIBF1 required for immunological modulation and the conserved domain present in ancestral ciliated organisms suggests that the role of PIBF1 in cilia function may be separate from the role of PIBF1 in immunomodulation and the conserved

A

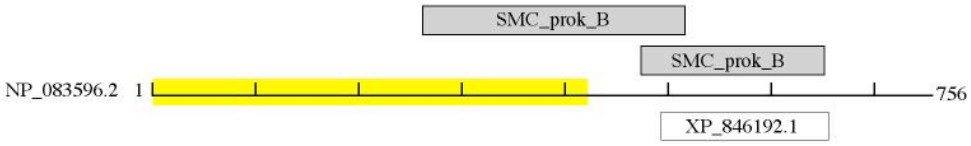

B

```
Pibf1   487  ECEKYQKKLEVLTKEFYSLQTSSEKRITELEAQNSEHQARLDIYEKLEKELDEIIMQTAE  546
             EC   ++KL++L  E+Y L+  + +RI ELEA     + +L     LE E +  I   A+
Sbjct   284  ECS--EQKLDILKGEYYELKLKNTQRIMELEACLRAAEEKLKTLSDLELESELFISNLAQ  341

Pibf1   547  IENEDEAERILYSYGYGANV------PTTA--------------KRRLKQSVHLARRVLQ  586
               +       + +   G  V      PT+                R+L  ++ + +R L
Sbjct   342  QADGQLTFSSMSAASAGGGVVGDKAAPTSTNALSSYESWLALPRSRKLAHTLTVTKRCLN  401

Pibf1   587  LEKQNSLILKDLDHQKNQVRQLSQELDRANSLLNQTQQPYRYLIESVRQRDAKIDSLMKS  646
             LE + + +  D++ +  Q+ +L   L+ A   LN T  P+  ++E        ++ L
Sbjct   402  LENRLTALQHDIEFKDKQLARLQTSLEMAREALNNTNSPF-AMVERT------VEKLTAD  454

Pibf1   647  TAQLEKDVSNLNKEKSALLQTKNQMALDLEQLLSHREEFAAMKQII  692
               +L   V NL++E + L Q   Q   D++ L +HR+E   +++I+
Sbjct   455  NEELHNKVMNLSEENALLRQRLEQRTTDVQVLCNHRKELLRIQRIL  500
```

Figure 5.2 *Pibf1* is conserved between mouse and *Trypanosome Brucei.* (A) A PBlast alignment between the amino acid sequence of PIBF1 (NP_083596) and an EST database from *T. Brucei* identifies a single alignment (with XP_846192.1) shown in the empty box under the PIBF1 sequence. Conserved protein domains are shown above the PIBF1 amino acid sequence. The highlighted region of the protein is the biologically active portion of the protein identified by Polgar et al., 2003. (B) The alignment between PIBF1 and XP_846192.1 is 205 amino acids in length and has 45% similarity.

domain of the protein may give a clue as to what part of the PIBF1 protein is important for its role in ciliogenesis.

5.7 Future studies of Pibf1 function

The disruption of both microtubule- and actin-based structures in *Pibf1* mutants suggests that *Pibf1* function is essential for the proper organization of the cytoskeleton. Cytoskeletal-based structures and domains are required for the efficient activity of multiple signaling pathways. We have identified *Pibf1* as a gene involved in HH signaling and the formation of cilia and microvilli on polarized epithelial cells. Further investigation of the role of *Pibf1* in the organization of the cytoskeleton provides an opportunity to define relationships between cilia morphogenesis, cell polarity and signal transduction.

5.7.1 Pibf1 and cell polarity

Cell polarity is critical for the asymmetric organization of molecular components that define subcellular signaling domains and modulate cell shape. Crosstalk between microtubule and actin networks forms a feedback loop to establish cortical polarity. Microtubules induce cortical polarity and cortical polarity proteins act to anchor microtubules and stabilize polarity (Siegrist and Doe, 2007). During directional cell migration microtubules set the position of actin-rich extensions at the leading edge and trigger the dissolution of actin stress fibers associated with focal adhesions at the rear of the cell (Kaverina et al., 1999; Kaverina et al., 1998; Small and Kaverina, 2003). Microtubules also induce apical cortical polarity and the clustering of cadherins at cell-cell junctions in epithelial cells (Rogers et al., 2004; Stehbens et al., 2006). Thus, microtubules interact with actin filaments to induce the formation of membrane-associated domains and structures in polarized cells. Microvilli are apical membrane protrusions that contain a dense bundle of cross-linked actin filaments and increase the surface area of cells. The altered structure of

microvilli on the apical surface of *Pibf1* deficient cells at the embryonic node suggests that *Pibf1* is required for the proper organization of the cortical actin network in these polarized epithelial cells (see Figure 5.1 D).

Primary cilium formation depends on the establishment of cell polarity. Actin networks are implicated in both breaking cell symmetry and the migration of centrioles to position the basal body at the apical membrane (Dawe et al., 2007; Li and Gundersen, 2008). Loss of the planar cell polarity pathway (PCP) protein Dishevelled (DVL) disrupts docking and planar polarization of basal bodies in ciliated cells in *Xenopus* (Park et al., 2008). Defective ciliogenesis in *Dvl* deficient cells is due to altered organization of the apical actin network leading to the mispositioning of the basal body. Also, treatment of ciliogenic oviducts with agents that inhibit actin polymerization prevents centriole migration (Boisvieux-Ulrich et al., 1989). Therefore, it is possible that defective ciliogenesis in *Pibf1* mutants is associated with the loss of apicobasal polarity. Impaired regulation of microtubule stability in *Pibf1* deficient cells potentially may disrupt the cortical actin network that is important for the positioning of the basal body and the formation of cilia and microvilli.

We intend to investigate the establishment of apical/basal polarity in *Pibf1* mutants in three ways. First, we will look for appropriate subcellular localization of PCP pathway components known to be asymmetrically distributed in polarized epithelial cells. Frizzled 3 (FZ3) and Dishevelled 2 (DVL2), both components of the PCP pathway, have been shown to localize to the apical cell membrane in mouse intestinal epithelium (Matsuyama et al., 2009). We will use immunohistochemistry to examine the distribution of these two proteins in polarized epithelial cells in *Pibf1* mutants. Second, we will check the integrity of the cortical actin network in polarized epithelial cells in *Pibf1* mutants. Polarized epithelial cells deposit dense actin filaments across the apical surface. We will stain sections of mouse node epithelia

with an antibody to actin and use 3D confocal data sets to examine whether the cortical actin network is intact in *Pibf1* mutants. Finally, we will use transmission electron microscopy (TEM) of ultrathin sections of mouse node to see if the centrioles are properly transported to the apical membrane prior to ciliogenesis. Improper trafficking of the centriole as a result of disrupted polarity has been shown to cause disrupted ciliogenesis (Park et al., 2008).

5.7.2 Investigating the role of Pibf1 in microtubule stability

Microtubules form a polarized and highly dynamic network of filaments that organize the cytoskeleton. Microtubules switch between phases of growth and shrinkage where maintenance of a GTP-tubulin cap at the growing end of filaments promotes stability. Microtubule-associated proteins bind mature regions or localize to the growing ends of microtubules to modulate activity and stability (Siegrist and Doe, 2007). Enrichment at the centrosome and the loss of PIBF1 in cells treated with agents that interfere with microtubule polymerization suggest that PIBF1 is a microtubule-associated protein (Lachmann et al., 2004). Proteins that modify the stability of microtubules can impact fundamental cellular processes including mitosis, intracellular trafficking, and the positioning of cytoskeletal protrusions that direct cell migration and neuronal growth cone formation. Artificially increasing microtubule stability is sufficient to induce axon formation and an increase in the stability of microtubules accompanies the expression of axonal markers during neurite outgrowth in cultured hippocampal neurons (Witte et al., 2008).

The dynamic assembly and disassembly of cilia depends on the regulation of microtubule growth and stability. The α-tubulin deacetylase, HDAC6, destabilizes microtubules and is required for the efficient disassembly of cilia. Chemical inhibition of HDAC6 blocks the disassembly of primary cilia *in vitro* (Pan et al., 2004; Pugacheva et al., 2007). Thus, stable axonemal microtubules are enriched in acetylated

α-tubulin and deacetylation destabilizes microtubules and promotes cilia disassembly (Ledizet and Piperno, 1991; Piperno et al., 1987; Webster and Borisy, 1989). We find that in ciliated cells PIBF1 is localized to the ciliary axoneme (see Figure 5.1 F). Furthermore, the ectopic accumulation of acetylated tubulin just beneath the ciliary axoneme in *Pibf1-HA* transfected cells suggests that altering levels of PIBF1 impacts microtubule stability (see Figure 5.1 E). A consequence of increased microtubule stability is a shift toward microtubule growth and an increase in cilia length. Indeed, in *Pibf1* transfected NIH3T3 cells there is a pronounced increase in cilia length (see Figure 5.1 G).

XMAP215 is a *Xenopus* protein with a demonstrated role in controlling microtubule dynamics, namely polymerizing microtubule growth by acting as a catalytic enzyme stabilizing association of new tubulin dimers (Gard and Kirschner, 1987). XMAP215, as well as its yeast homolog, STU2, are long, thin molecules that localize to the plus end of the microtubule (Al-Bassam et al., 2006; Cassimeris et al., 2001). XMAP215 was shown to affect microtubule assembly by mixing purified bovine brain tubulin and centrosomes from N115 cells on coverslips and measuring the length of the *in vitro* polymerized microtubules. In the presence of XMAP215 the length of microtubules increased. We would like to test whether PIBF1 can affect microtubule polymerization in a similar manner. In addition, a protocol has been described to measure microtubule assembly dynamics at molecular resolution (Kerssemakers et al., 2006).

As a reciprocal experiment to that described above, we will examine whether PIBF1 can influence the rate of Kinesin-13-catalyzed microtubule depolymerization. Conventional Kinesin is a motor protein that uses the energy from ATP hydrolysis to move along microtubule tracks (Vale et al., 1985). Of the ~100 eukaryotic proteins that contain a homologous catalytic ATPase domain, roughly 20% have been shown to

have motor activity. Kinesin-13, a member of the KIN I subfamily, has no motor activity. Kinesin-13 has been shown to depolymerize microtubules by the removal of the GTP-cap at the plus end of the microtubule (Desai et al., 1999). In vitro assays on dynamic microtubules nucleated off axonemes would allow us to test if the presence of PIBF1 can affect the stability of microtubules by interfering with Kinesin-13-catalyzed microtubule depolymerization. Such assays have been described previously (Hunter et al., 2003; Mitchison and Kirschner, 1984; Walker et al., 1988).

5.7.3 Compartmentalization of signaling molecules

The cilium is an apical, membrane-bound projection and the localization of PTCH1 to the base of the cilia implies an asymmetric distribution of HH pathway components. In fact, SHH ligand produced by the notochord must be trafficked across the basolateral membrane and to the apical membrane of the neural tube, and SHH ligand puncta have been observed on stabilized microtubules that span the ventral neural progenitors from basolateral to apical surfaces (Chamberlain et al., 2008). The establishment of cell polarity is also associated with the activity of additional signaling pathways, such as JAK/STAT and WNT (Simons et al., 2005; Sotillos et al., 2008). For example, an activated form of β-catenin in the kidney caused overproliferation and renal cysts, and elevated levels of β-catenin were reported in the cystic kidneys caused by conditional deletion of *Kif3a* (Lin et al., 2003; Saadi-Kheddouci et al., 2001). However, the phenotype of mice that lack cilia demonstrates that cilia cannot be essential for either canonical or noncanonical WNT signaling. Mouse mutants that lack canonical WNT signaling die early in gastrulation, and mutants lacking noncanonical WNT signaling have a shortened body axis and an inability to close the neural tube in the trunk region. These phenotypes are not seen in mice that lack cilia. It has been suggested that instead of cilia being required for WNT signaling, WNT signaling (more specifically PCP signaling) may be required to establish apical/basal

polarity and construct normal cilia. Fuzzy and Inturned are PCP proteins in *Xenopus* that when mutated lead to a neural tube defect due to both a loss of HH signaling and a loss of cilia in the neural tube (Park et al., 2006). A requirement for PCP in cilia formation would also explain how the cilia of the mouse node are asymmetrically positioned and tilted toward the rear to generate nodal flow.

Components of the JAK/STAT pathway have been localized to apicolateral membrane domains in polarized cells in *Drosophila* (Sotillos et al., 2008). In *Drosophila* the JAK/STAT pathway is composed of only three ligands, one receptor (*dome*) and one JAK (*hop*). In the ectoderm cells of both the hindgut and posterior spiracles *dome* localizes to the apical membrane. *Hop* is cytoplasmic, but after coexpression with *dome* both proteins localize to the apical membrane, and apical polarization of JAK/STAT components is required for full signaling efficiency. In addition, PIBF1 has been shown to induce JAK/STAT signaling through the IL-4R receptor and activation of STAT6 (Kozma et al., 2006).

We would like to investigate whether the components of the JAK/STAT signaling pathway are localized to the cilia and whether the signaling pathway can function in the absence of cilia. We would first test cell lines that can be induced to grow cilia, starting with NIH3T3, to see if they express components of the JAK/STAT signaling pathway, in particular IL-4R and STAT6, the components of the JAK/STAT pathway that are activated by secreted PIBF1 ligand. We will then perform immunohistochemistry to examine the subcellular localization of these proteins. This would provide evidence to support the hypothesis that JAK/STAT polarization in epithelia is a general feature and that the pathway components are compartmentalized at the cilia for the localized activation of the signaling pathway.

CHAPTER VI

SUMMARY AND CONCLUSIONS

Regional forward genetic screens provide a number of opportunities to gain knowledge about a defined genomic interval. Our mutagenesis screen tested 952 pedigrees of G1 females and recovered 7 lethal mutations. The mutant lines were fine-mapped within the piebald region through complementation crosses with a number of overlapping deletion lines. Each line was then characterized to determine a time-of-death, identify morphological or physiological defects, and assign the seven lines to four complementation groups. The ENU-induced mutations recovered in the screen included a line with a defect in the patterning of the left/right axis as well as a line containing a mutation in the mouse ortholog of the human gene PAM.

We used the number of complementation groups recovered from our screen to predict the number of essential genes mapping to the piebald region. A high essential gene density in contrast to a low overall gene density characterizes the piebald region. Comparing the essential gene density of the piebald region with essential gene densities from a number of other genomic intervals, along with investigations comparing the level of conservation and genomic organization between the regions, led us to identify an interesting and distinctive organization to the piebald region, and provides a further appreciation of the unique functional genomic characteristics of the piebald region. Combined with ongoing work in the O'Brien lab identifying coordinately regulated genes in the region and the *cis* regulatory elements that control their expression, these studies have the potential to help us better understand the regulatory landscape of distal mouse chromosome 14.

The primary benefit of genetic screens is the creation of novel mutant alleles that help to reveal gene function. After positional cloning one of our mutants, ENU

128-7, and confirming genetically the identity of the responsible gene, I have focused on studying this novel mutation in Progesterone induced blocking factor 1. My work with the ENU-induced mutation in *Pibf1* allowed me to identify *Pibf1* as an essential gene required for ciliogenesis and Hedgehog signaling. I described defects in *Pibf1* mutants in the patterning of the left/right axis consistent with reduced HH signaling. This led to the observation that the notochord is prematurely degenerating in mutant embryos, and that SHH secreted from the notochord of mutant embryos fails to induce *Shh* expression in the floorplate of the neural tube. This demonstrated that normal signaling between these two tissues is disrupted and gave the initial insight that *Pibf1* may be required for HH signaling. Embryological defects present in *Pibf1* mutants provided evidence from four separate tissues that require HH signaling in their patterning and development that was consistent with disrupted SHH signaling. Genetic evidence for loss of HH signaling is shown in an epistasis experiment using *Pibf1*$^{-/-}$*Ptch1*$^{-/-}$ double mutants. This showed that HH signaling is being disrupted downstream of *Ptch1*, consistent with loss of cilia, and provided strong genetic evidence that PIBF1 is required for HH signaling.

Cilia have been shown to be required for full responsiveness to ligands of the Hedgehog signaling pathway. As a consequence of loss of cilia, proper subcellular localization of HH pathway components is lost and HH signaling is disrupted. The role of *Pibf1* in cilia formation and/or function is demonstrated by the loss of cilia on the cells of the murine node. In addition, cells transfected with a HA-tagged *Pibf1* expression vector demonstrated that PIBF1 localizes to the ciliary axoneme, consistent with a role in cilia function. Finally, *Pibf1* homologues have been identified in a number of genomic and proteomic studies of the ciliome, and *Pibf1* appears to be conserved in ciliated organisms as far back as the protist *T. Brucei*. I hypothesized that the role of PIBF1 in ciliogenesis may be due to its previously identified role as a

microtubule-associated protein. Preliminary data showed that increased expression of *Pibf1* leads to an upregulation of markers of microtubule stability. Increased cilia length in cells expressing the HA-tagged *Pibf1* expression vector supported the hypothesis that *Pibf1* may affect microtubule stability. In summary, evidence based on my characterization of the *Pibf1* mutant phenotype supports that HH signaling is disrupted in *Pibf1* mutants and that *Pibf1* is required for ciliogenesis and Hedgehog signaling.

In addition to eliminating gene function, ENU mutagenesis screens also provide the opportunity to develop allelic series containing unexpected hypo-, hyper- and neomorphic mutations to further inform us of the roles of genes. Given that *Pibf1* has multiple known functions in mammals, including in ciliogenesis and HH signaling, as well as a role in immunomodulation in pregnant females, such an allelic series is potentially highly informative in understanding the gene's function. As a result of our screen we have an additional five ENU-induced mutations in the interval containing *Pibf1,* four of which give evidence of being hypomorphic. The further characterization of these mutants has the potential of being highly useful in the further dissection of either *Pibf1* function or the function of the other genes in the region. The development of resources that provide reagents for ongoing experimentation is a major benefit of mutagenesis screens and should help us further annotate the functional genomics of distal mouse chromosome 14.

BIBLIOGRAPHY

Ahlgren, S. C. and Bronner-Fraser, M. (1999). Inhibition of sonic hedgehog signaling in vivo results in craniofacial neural crest cell death. *Curr Biol* **9**, 1304-14.

Al-Bassam, J., van Breugel, M., Harrison, S. C. and Hyman, A. (2006). Stu2p binds tubulin and undergoes an open-to-closed conformational change. *J Cell Biol* **172**, 1009-22.

Allen, J. W. (1990). Biology of mammalian germ cell mutagenesis. In *Banbury Report*, vol. 34 (ed. Cold Spring Harbor, N.Y.: Cold Spring Harbor Laboratory Press.

Andersen, J. S., Wilkinson, C. J., Mayor, T., Mortensen, P., Nigg, E. A. and Mann, M. (2003). Proteomic characterization of the human centrosome by protein correlation profiling. *Nature* **426**, 570-4.

Aponte, J. L., Sega, G. A., Hauser, L. J., Dhar, M. S., Withrow, C. M., Carpenter, D. A., Rinchik, E. M., Culiat, C. T. and Johnson, D. K. (2001). Point mutations in the murine fumarylacetoacetate hydrolase gene: Animal models for the human genetic disorder hereditary tyrosinemia type 1. *Proc Natl Acad Sci U S A* **98**, 641-5.

Avidor-Reiss, T., Maer, A. M., Koundakjian, E., Polyanovsky, A., Keil, T., Subramaniam, S. and Zuker, C. S. (2004). Decoding cilia function: defining specialized genes required for compartmentalized cilia biogenesis. *Cell* **117**, 527-39.

Backman, M., Machon, O., Van Den Bout, C. J. and Krauss, S. (2003). Targeted disruption of mouse Dach1 results in postnatal lethality. *Dev Dyn* **226**, 139-44.

Beier, D. R. (2000). Sequence-based analysis of mutagenized mice. *Mamm Genome* **11**, 594-7.

Bi, W., Deng, J. M., Zhang, Z., Behringer, R. R. and de Crombrugghe, B. (1999). Sox9 is required for cartilage formation. *Nat Genet* **22**, 85-9.

Bisgrove, B. W., Essner, J. J. and Yost, H. J. (1999). Regulation of midline development by antagonism of lefty and nodal signaling. *Development* **126**, 3253-62.

Bisgrove, B. W. and Yost, H. J. (2006). The roles of cilia in developmental disorders and disease. *Development* **133**, 4131-43.

Bloom, A. J., Miller, B. R., Sanes, J. R. and DiAntonio, A. (2007). The requirement for Phr1 in CNS axon tract formation reveals the corticostriatal boundary as a choice point for cortical axons. *Genes Dev* **21**, 2593-606.

Broadhead, R., Dawe, H. R., Farr, H., Griffiths, S., Hart, S. R., Portman, N., Shaw, M. K., Ginger, M. L., Gaskell, S. J., McKean, P. G. et al. (2006). Flagellar motility is required for the viability of the bloodstream trypanosome. *Nature* **440**, 224-7.

Buckingham, M., Bajard, L., Daubas, P., Esner, M., Lagha, M., Relaix, F. and Rocancourt, D. (2006). Myogenic progenitor cells in the mouse embryo are marked by the expression of Pax3/7 genes that regulate their survival and myogenic potential. *Anat Embryol (Berl)* **211 Suppl 1**, 51-6.

Bultman, S., Gebuhr, T., Yee, D., La Mantia, C., Nicholson, J., Gilliam, A., Randazzo, F., Metzger, D., Chambon, P., Crabtree, G. et al. (2000). A Brg1 null mutation in the mouse reveals functional differences among mammalian SWI/SNF complexes. *Mol Cell* **6**, 1287-95.

Bultman, S. J., Gebuhr, T. C. and Magnuson, T. (2005). A Brg1 mutation that uncouples ATPase activity from chromatin remodeling reveals an essential role for SWI/SNF-related complexes in beta-globin expression and erythroid development. *Genes Dev* **19**, 2849-61.

Burge, C. B., Tuschl, T. and Sharp, P. A. (1999). Splicing of Precursors to mRNAs by the spliceosomes. In *The RNA World, Second Edition*, (ed. R. F. Gesteland T. R. Cech and J. F. Atkins), pp. 525-560. Cold Spring Harbor, NY: Cold Spring Harbor Laboratory Press.

Burgess, R. W., Peterson, K. A., Johnson, M. J., Roix, J. J., Welsh, I. C. and O'Brien, T. P. (2004). Evidence for a conserved function in synapse formation reveals Phr1 as a candidate gene for respiratory failure in newborn mice. *Mol Cell Biol* **24**, 1096-105.

Burke, R., Nellen, D., Bellotto, M., Hafen, E., Senti, K. A., Dickson, B. J. and Basler, K. (1999). Dispatched, a novel sterol-sensing domain protein dedicated to the release of cholesterol-modified hedgehog from signaling cells. *Cell* **99**, 803-15.

Buttitta, L., Mo, R., Hui, C. C. and Fan, C. M. (2003). Interplays of Gli2 and Gli3 and their requirement in mediating Shh-dependent sclerotome induction. *Development* **130**, 6233-43.

Byrd, N., Becker, S., Maye, P., Narasimhaiah, R., St-Jacques, B., Zhang, X., McMahon, J., McMahon, A. and Grabel, L. (2002). Hedgehog is required for murine yolk sac angiogenesis. *Development* **129**, 361-72.

Cassimeris, L., Gard, D., Tran, P. T. and Erickson, H. P. (2001). XMAP215 is a long thin molecule that does not increase microtubule stiffness. *J Cell Sci* **114**, 3025-33.

Chamberlain, C. E., Jeong, J., Guo, C., Allen, B. L. and McMahon, A. P. (2008). Notochord-derived Shh concentrates in close association with the apically positioned basal body in neural target cells and forms a dynamic gradient during neural patterning. *Development* **135**, 1097-106.

Chiang, C., Litingtung, Y., Lee, E., Young, K. E., Corden, J. L., Westphal, H. and Beachy, P. A. (1996). Cyclopia and defective axial patterning in mice lacking Sonic hedgehog gene function. *Nature* **383**, 407-13.

Conlon, F. L., Wright, C. V. E. and Robertson, E. J. (1995). Effects of the T-Wis Mutation on Notochord Formation and Mesodermal Patterning. *Mechanisms of Development* **49**, 201-209.

Corbit, K. C., Aanstad, P., Singla, V., Norman, A. R., Stainier, D. Y. and Reiter, J. F. (2005). Vertebrate Smoothened functions at the primary cilium. *Nature* **437**, 1018-21.

Davis, R. J., Shen, W., Sandler, Y. I., Amoui, M., Purcell, P., Maas, R., Ou, C. N., Vogel, H., Beaudet, A. L. and Mardon, G. (2001). Dach1 mutant mice bear no gross abnormalities in eye, limb, and brain development and exhibit postnatal lethality. *Mol Cell Biol* **21**, 1484-90.

Dawe, H. R., Farr, H. and Gull, K. (2007). Centriole/basal body morphogenesis and migration during ciliogenesis in animal cells. *Journal of Cell Science* **120**, 7-15.

Desai, A., Verma, S., Mitchison, T. J. and Walczak, C. E. (1999). Kin I kinesins are microtubule-destabilizing enzymes. *Cell* **96**, 69-78.

Dessaud, E., McMahon, A. P. and Briscoe, J. (2008). Pattern formation in the vertebrate neural tube: a sonic hedgehog morphogen-regulated transcriptional network. *Development* **135**, 2489-503.

DiAntonio, A., Haghighi, A. P., Portman, S. L., Lee, J. D., Amaranto, A. M. and Goodman, C. S. (2001). Ubiquitination-dependent mechanisms regulate synaptic growth and function. *Nature* **412**, 449-52.

Donohoe, E. (2005). Denaturing High-Performance Liquid Chromatography Using the WAVE DNA Fragment Analysis System. In *Hypertension*, pp. 173-187.

Favor, J. (1999). Mechanisms of mutation induction in germ cells of the mouse as assessed by the specific locus test. *Mutat Res* **428**, 227-36.

Garcia-Garcia, M. J., Eggenschwiler, J. T., Caspary, T., Alcorn, H. L., Wyler, M. R., Huangfu, D., Rakeman, A. S., Lee, J. D., Feinberg, E. H., Timmer, J. R. et al. (2005). Analysis of mouse embryonic patterning and morphogenesis by forward genetics. *Proc Natl Acad Sci U S A* **102**, 5913-9.

Gard, D. L. and Kirschner, M. W. (1987). A microtubule-associated protein from Xenopus eggs that specifically promotes assembly at the plus-end. *J Cell Biol* **105**, 2203-15.

Goldowitz, D., Frankel, W. N., Takahashi, J. S., Holtz-Vitaterna, M., Bult, C., Kibbe, W. A., Snoddy, J., Li, Y., Pretel, S., Yates, J. et al. (2004). Large-scale mutagenesis of the mouse to understand the genetic bases of nervous system structure and function. *Brain Res Mol Brain Res* **132**, 105-15.

Haffter, P., Granato, M., Brand, M., Mullins, M. C., Hammerschmidt, M., Kane, D. A., Odenthal, J., van Eeden, F. J., Jiang, Y. J., Heisenberg, C. P. et al. (1996). The identification of genes with unique and essential functions in the development of the zebrafish, Danio rerio. *Development* **123**, 1-36.

Hagge-Greenberg, A., Snow, P. and O'Brien, T. P. (2001). Establishing an ENU mutagenesis screen for the piebald region of mouse Chromosome 14. *Mamm Genome* **12**, 938-41.

Harris, N. L. and Senapathy, P. (1990). Distribution and consensus of branch point signals in eukaryotic genes: a computerized statistical analysis. *Nucleic Acids Res* **18**, 3015-9.

Hentges, K. E., Pollock, D. D., Liu, B. and Justice, M. J. (2007). Regional variation in the density of essential genes in mice. *PLoS Genet* **3**, e72.

Hilliard, S. A., Yu, L., Gu, S., Zhang, Z. and Chen, Y. P. (2005). Regional regulation of palatal growth and patterning along the anterior-posterior axis in mice. *J Anat* **207**, 655-67.

Hirokawa, N., Tanaka, Y., Okada, Y. and Takeda, S. (2006). Nodal flow and the generation of left-right asymmetry. *Cell* **125**, 33-45.

Hitotsumachi, S., Carpenter, D. A. and Russell, W. L. (1985). Dose-repetition increases the mutagenic effectiveness of N-ethyl-N-nitrosourea in mouse spermatogonia. *Proc Natl Acad Sci U S A* **82**, 6619-21.

Hombria, J. C. and Sotillos, S. (2008). Disclosing JAK/STAT links to cell adhesion and cell polarity. *Semin Cell Dev Biol* **19**, 370-8.

Hooper, J. E. and Scott, M. P. (2005). Communicating with Hedgehogs. *Nature Reviews Molecular Cell Biology* **6**, 306-317.

Hosoda, K., Hammer, R. E., Richardson, J. A., Baynash, A. G., Cheung, J. C., Giaid, A. and Yanagisawa, M. (1994). Targeted and natural (piebald-lethal) mutations of endothelin-B receptor gene produce megacolon associated with spotted coat color in mice. *Cell* **79**, 1267-76.

Houde, C., Dickinson, R. J., Houtzager, V. M., Cullum, R., Montpetit, R., Metzler, M., Simpson, E. M., Roy, S., Hayden, M. R., Hoodless, P. A. et al. (2006). Hippi is essential for node cilia assembly and Sonic hedgehog signaling. *Dev Biol* **300**, 523-33.

Hough, R. B., Lengeling, A., Bedian, V., Lo, C. and Bucan, M. (1998). Rump white inversion in the mouse disrupts dipeptidyl aminopeptidase-like protein 6 and causes dysregulation of Kit expression. *Proc Natl Acad Sci U S A* **95**, 13800-5.

Huangfu, D., Liu, A., Rakeman, A. S., Murcia, N. S., Niswander, L. and Anderson, K. V. (2003). Hedgehog signalling in the mouse requires intraflagellar transport proteins. *Nature* **426**, 83-7.

Hunter, A. W., Caplow, M., Coy, D. L., Hancock, W. O., Diez, S., Wordeman, L. and Howard, J. (2003). The kinesin-related protein MCAK is a microtubule depolymerase that forms an ATP-hydrolyzing complex at microtubule ends. *Mol Cell* **11**, 445-57.

Huszar, D., Lynch, C. A., Fairchild-Huntress, V., Dunmore, J. H., Fang, Q., Berkemeier, L. R., Gu, W., Kesterson, R. A., Boston, B. A., Cone, R. D. et al. (1997). Targeted disruption of the melanocortin-4 receptor results in obesity in mice. *Cell* **88**, 131-41.

Ingham, P. W. (2008). Hedgehog signalling. *Current Biology* **18**, R238-R241.

Jacob, L. and Lum, L. (2007). Deconstructing the hedgehog pathway in development and disease. *Science* **318**, 66-68.

Jeong, J., Mao, J., Tenzen, T., Kottmann, A. H. and McMahon, A. P. (2004). Hedgehog signaling in the neural crest cells regulates the patterning and growth of facial primordia. *Genes Dev* **18**, 937-51.

Kasarskis, A., Manova, K. and Anderson, K. V. (1998). A phenotype-based screen for embryonic lethal mutations in the mouse. *Proc Natl Acad Sci U S A* **95**, 7485-90.

Kaverina, I., Krylyshkina, O. and Small, J. V. (1999). Microtubule targeting of substrate contacts promotes their relaxation and dissociation. *Journal of Cell Biology* **146**, 1033-1043.

Kaverina, I., Rottner, K. and Small, J. V. (1998). Targeting, capture, and stabilization of microtubules at early focal adhesions. *Journal of Cell Biology* **142**, 181-190.

Kerssemakers, J. W., Munteanu, E. L., Laan, L., Noetzel, T. L., Janson, M. E. and Dogterom, M. (2006). Assembly dynamics of microtubules at molecular resolution. *Nature* **442**, 709-12.

Kile, B. T., Hentges, K. E., Clark, A. T., Nakamura, H., Salinger, A. P., Liu, B., Box, N., Stockton, D. W., Johnson, R. L., Behringer, R. R. et al. (2003). Functional genetic analysis of mouse chromosome 11. *Nature* **425**, 81-6.

Kile, B. T. and Hilton, D. J. (2005). The art and design of genetic screens: mouse. *Nat Rev Genet* **6**, 557-67.

Klein, O. D., Minowada, G., Peterkova, R., Kangas, A., Yu, B. D., Lesot, H., Peterka, M., Jernvall, J. and Martin, G. R. (2006). Sprouty genes control diastema tooth development via bidirectional antagonism of epithelial-mesenchymal FGF signaling. *Dev Cell* **11**, 181-90.

Kolesova, H., Roelink, H. and Grim, M. (2008). Sonic hedgehog is required for the assembly and remodeling of branchial arch blood vessels. *Dev Dyn* **237**, 1923-1934.

Kozma, N., Halasz, M., Polgar, B., Poehlmann, T. G., Markert, U. R., Palkovics, T., Keszei, M., Par, G., Kiss, K., Szeberenyi, J. et al. (2006). Progesterone-induced blocking factor activates STAT6 via binding to a novel IL-4 receptor. *J Immunol* **176**, 819-26.

Krebs, L. T., Iwai, N., Nonaka, S., Welsh, I. C., Lan, Y., Jiang, R., Saijoh, Y., O'Brien, T. P., Hamada, H. and Gridley, T. (2003). Notch signaling regulates left-right asymmetry determination by inducing Nodal expression. *Genes Dev* **17**, 1207-12.

Kurihara, L. J., Semenova, E., Miller, W., Ingram, R. S., Guan, X. J. and Tilghman, S. M. (2002). Candidate genes required for embryonic development: a comparative analysis of distal mouse chromosome 14 and human chromosome 13q22. *Genomics* **79**, 154-61.

Lachmann, M., Gelbmann, D., Kalman, E., Polgar, B., Buschle, M., Von Gabain, A., Szekeres-Bartho, J. and Nagy, E. (2004). PIBF (progesterone induced blocking factor) is overexpressed in highly proliferating cells and associated with the centrosome. *Int J Cancer* **112**, 51-60.

Lawson, N. D., Vogel, A. M. and Weinstein, B. M. (2002). sonic hedgehog and vascular endothelial growth factor act upstream of the Notch pathway during arterial endothelial differentiation. *Dev Cell* **3**, 127-36.

Ledizet, M. and Piperno, G. (1991). Detection of Acetylated Alpha-Tubulin by Specific Antibodies. *Methods in Enzymology* **196**, 264-274.

Lee, J. J., Ekker, S. C., von Kessler, D. P., Porter, J. A., Sun, B. I. and Beachy, P. A. (1994). Autoproteolysis in hedgehog protein biogenesis. *Science* **266**, 1528-37.

Lee, M. S. (1999). Molecular clock calibrations and metazoan divergence dates. *J Mol Evol* **49**, 385-91.

Lefebvre, V., Huang, W., Harley, V. R., Goodfellow, P. N. and de Crombrugghe, B. (1997). SOX9 is a potent activator of the chondrocyte-specific enhancer of the pro alpha1(II) collagen gene. *Mol Cell Biol* **17**, 2336-46.

Levitan, D. and Greenwald, I. (1998). LIN-12 protein expression and localization during vulval development in C. elegans. *Development* **125**, 3101-9.

Li, R. and Gundersen, G. G. (2008). Beyond polymer polarity: how the cytoskeleton builds a polarized cell. *Nature Reviews Molecular Cell Biology* **9**, 860-873.

Lin, F., Hiesberger, T., Cordes, K., Sinclair, A. M., Goldstein, L. S., Somlo, S. and Igarashi, P. (2003). Kidney-specific inactivation of the KIF3A subunit of kinesin-II inhibits renal ciliogenesis and produces polycystic kidney disease. *Proc Natl Acad Sci U S A* **100**, 5286-91.

Lin, X. (2004). Functions of heparan sulfate proteoglycans in cell signaling during development. *Development* **131**, 6009-21.

Liu, Q., Tan, G., Levenkova, N., Li, T., Pugh, E. N., Jr., Rux, J. J., Speicher, D. W. and Pierce, E. A. (2007). The proteome of the mouse photoreceptor sensory cilium complex. *Mol Cell Proteomics* **6**, 1299-317.

Logan, M., Pagan-Westphal, S. M., Smith, D. M., Paganessi, L. and Tabin, C. J. (1998). The transcription factor Pitx2 mediates situs-specific morphogenesis in response to left-right asymmetric signals. *Cell* **94**, 307-317.

Lumsden, A., Sprawson, N. and Graham, A. (1991). Segmental origin and migration of neural crest cells in the hindbrain region of the chick embryo. *Development* **113**, 1281-91.

Marcelle, C., Ahlgren, S. and Bronner-Fraser, M. (1999). In vivo regulation of somite differentiation and proliferation by Sonic Hedgehog. *Developmental Biology* **214**, 277-287.

Marszalek, J. R., Ruiz-Lozano, P., Roberts, E., Chien, K. R. and Goldstein, L. S. (1999). Situs inversus and embryonic ciliary morphogenesis defects in mouse mutants lacking the KIF3A subunit of kinesin-II. *Proc Natl Acad Sci U S A* **96**, 5043-8.

Mastick, G. S., Davis, N. M., Andrew, G. L. and Easter, S. S., Jr. (1997). Pax-6 functions in boundary formation and axon guidance in the embryonic mouse forebrain. *Development* **124**, 1985-97.

Matsuyama, M., Aizawa, S. and Shimono, A. (2009). Sfrp controls apicobasal polarity and oriented cell division in developing gut epithelium. *PLoS Genet* **5**, e1000427.

Meehan, T. P., Tabeta, K., Du, X., Woodward, L. S., Firozi, K., Beutler, B. and Justice, M. J. (2006). Point mutations in the melanocortin-4 receptor cause variable obesity in mice. *Mamm Genome* **17**, 1162-71.

Melloy, P. G., Ewart, J. L., Cohen, M. F., Desmond, M. E., Kuehn, M. R. and Lo, C. W. (1998). No turning, a mouse mutation causing left-right and axial patterning defects. *Dev Biol* **193**, 77-89.

Meno, C., Shimono, A., Saijoh, Y., Yashiro, K., Mochida, K., Ohishi, S., Noji, S., Kondoh, H. and Hamada, H. (1998). lefty-1 is required for left-right determination as a regulator of lefty-2 and nodal. *Cell* **94**, 287-97.

Mitchison, T. and Kirschner, M. (1984). Dynamic instability of microtubule growth. *Nature* **312**, 237-42.

Mori-Akiyama, Y., Akiyama, H., Rowitch, D. H. and de Crombrugghe, B. (2003). Sox9 is required for determination of the chondrogenic cell lineage in the cranial neural crest. *Proc Natl Acad Sci U S A* **100**, 9360-5.

Muller, H. J. (1927). Artificial transmutation of the gene. *Science* **46**, 84-7.

Murphy, W. J., Larkin, D. M., Everts-van der Wind, A., Bourque, G., Tesler, G., Auvil, L., Beever, J. E., Chowdhary, B. P., Galibert, F., Gatzke, L. et al. (2005). Dynamics of mammalian chromosome evolution inferred from multispecies comparative maps. *Science* **309**, 613-7.

Nadeau, J. H., Balling, R., Barsh, G., Beier, D., Brown, S. D., Bucan, M., Camper, S., Carlson, G., Copeland, N., Eppig, J. et al. (2001). Sequence interpretation. Functional annotation of mouse genome sequences. *Science* **291**, 1251-5.

Nakaya, M. A., Biris, K., Tsukiyama, T., Jaime, S., Rawls, J. A. and Yamaguchi, T. P. (2005). Wnt3a links left-right determination with segmentation and anteroposterior axis elongation. *Development* **132**, 5425-36.

Niswander, L., Yee, D., Rinchik, E. M., Russell, L. B. and Magnuson, T. (1989). The albino-deletion complex in the mouse defines genes necessary for development of embryonic and extraembryonic ectoderm. *Development* **105**, 175-82.

Nobrega, M. A., Ovcharenko, I., Afzal, V. and Rubin, E. M. (2003). Scanning human gene deserts for long-range enhancers. *Science* **302**, 413.

Nonaka, S., Shiratori, H., Saijoh, Y. and Hamada, H. (2002). Determination of left-right patterning of the mouse embryo by artificial nodal flow. *Nature* **418**, 96-9.

Nusslein-Volhard, C. and Wieschaus, E. (1980). Mutations affecting segment number and polarity in Drosophila. *Nature* **287**, 795-801.

O'Brien, T. P., Metallinos, D. L., Chen, H., Shin, M. K. and Tilghman, S. M. (1996). Complementation mapping of skeletal and central nervous system abnormalities in mice of the piebald deletion complex. *Genetics* **143**, 447-61.

Pachikara, A., Dolson, D. K., Martinu, L., Riccomagno, M. M., Jeong, Y. and Epstein, D. J. (2007). Activation of Class I transcription factors by low level Sonic hedgehog signaling is mediated by Gli2-dependent and independent mechanisms. *Dev Biol* **305**, 52-62.

Pan, J. M., Wang, Q. and Snell, W. J. (2004). An aurora kinase is essential for flagellar disassembly in Chlamlydomonas. *Developmental Cell* **6**, 445-451.

Panakova, D., Sprong, H., Marois, E., Thiele, C. and Eaton, S. (2005). Lipoprotein particles are required for Hedgehog and Wingless signalling. *Nature* **435**, 58-65.

Park, T. J., Haigo, S. L. and Wallingford, J. B. (2006). Ciliogenesis defects in embryos lacking inturned or fuzzy function are associated with failure of planar cell polarity and Hedgehog signaling. *Nat Genet* **38**, 303-11.

Park, T. J., Mitchell, B. J., Abitua, P. B., Kintner, C. and Wallingford, J. B. (2008). Dishevelled controls apical docking and planar polarization of basal bodies in ciliated epithelial cells. *Nature Genetics* **40**, 871-879.

Pepicelli, C. V., Lewis, P. M. and McMahon, A. P. (1998). Sonic hedgehog regulates branching morphogenesis in the mammalian lung. *Curr Biol* **8**, 1083-6.

Pepinsky, R. B., Zeng, C., Wen, D., Rayhorn, P., Baker, D. P., Williams, K. P., Bixler, S. A., Ambrose, C. M., Garber, E. A., Miatkowski, K. et al. (1998). Identification of a palmitic acid-modified form of human Sonic hedgehog. *J Biol Chem* **273**, 14037-45.

Persson, M., Stamataki, D., te Welscher, P., Andersson, E., Bose, J., Ruther, U., Ericson, J. and Briscoe, J. (2002). Dorsal-ventral patterning of the spinal cord requires Gli3 transcriptional repressor activity. *Genes Dev* **16**, 2865-78.

Peterson, K. A., King, B. L., Hagge-Greenberg, A., Roix, J. J., Bult, C. J. and O'Brien, T. P. (2002). Functional and comparative genomic analysis of the piebald deletion region of mouse chromosome 14. *Genomics* **80**, 172-84.

Piperno, G., Ledizet, M. and Chang, X. J. (1987). Microtubules Containing Acetylated Alpha-Tubulin in Mammalian-Cells in Culture. *Journal of Cell Biology* **104**, 289-302.

Polgar, B., Kispal, G., Lachmann, M., Paar, C., Nagy, E., Csere, P., Miko, E., Szereday, L., Varga, P. and Szekeres-Bartho, J. (2003). Molecular cloning and immunologic characterization of a novel cDNA coding for progesterone-induced blocking factor. *J Immunol* **171**, 5956-63.

Pollock, D. D. and Larkin, J. C. (2004). Estimating the degree of saturation in mutant screens. *Genetics* **168**, 489-502.

Porter, J. A., Ekker, S. C., Park, W. J., von Kessler, D. P., Young, K. E., Chen, C. H., Ma, Y., Woods, A. S., Cotter, R. J., Koonin, E. V. et al. (1996). Hedgehog patterning activity: role of a lipophilic modification mediated by the carboxy-terminal autoprocessing domain. *Cell* **86**, 21-34.

Potter, M. D., Shinpock, S. G., Popp, R. A., Godfrey, V., Carpenter, D. A., Bernstein, A., Johnson, D. K. and Rinchik, E. M. (1997). Mutations in the murine fitness 1 gene result in defective hematopoiesis. *Blood* **90**, 1850-7.

Poulin, F., Nobrega, M. A., Plajzer-Frick, I., Holt, A., Afzal, V., Rubin, E. M. and Pennacchio, L. A. (2005). In vivo characterization of a vertebrate ultraconserved enhancer. *Genomics* **85**, 774-81.

Pugacheva, E. N., Jablonski, S. A., Hartman, T. R., Henske, E. P. and Golemis, E. A. (2007). HEF1-Dependent aurora a activation induces disassembly of the primary cilium. *Cell* **129**, 1351-1363.

Quwailid, M. M., Hugill, A., Dear, N., Vizor, L., Wells, S., Horner, E., Fuller, S., Weedon, J., McMath, H., Woodman, P. et al. (2004). A gene-driven ENU-based approach to generating an allelic series in any gene. *Mamm Genome* **15**, 585-591.

Rinchik, E. M. and Carpenter, D. A. (1999). N-ethyl-N-nitrosourea mutagenesis of a 6- to 11-cM subregion of the Fah-Hbb interval of mouse chromosome 7: Completed testing of 4557 gametes and deletion mapping and complementation analysis of 31 mutations. *Genetics* **152**, 373-83.

Rinchik, E. M., Carpenter, D. A. and Johnson, D. K. (2002). Functional annotation of mammalian genomic DNA sequence by chemical mutagenesis: a fine-structure genetic mutation map of a 1- to 2-cM segment of mouse chromosome 7 corresponding to human chromosome 11p14-p15. *Proc Natl Acad Sci U S A* **99**, 844-9.

Rinchik, E. M., Russell, L. B., Copeland, N. G. and Jenkins, N. A. (1986). Molecular genetic analysis of the dilute-short ear (d-se) region of the mouse. *Genetics* **112**, 321-42.

Rogers, S. L., Wiedemann, U., Hacker, U., Turck, C. and Vale, R. D. (2004). Drosophila RhoGEF2 associates with microtubule plus ends in an EB1-dependent manner. *Curr Biol* **14**, 1827-33.

Rohatgi, R., Milenkovic, L. and Scott, M. P. (2007). Patched1 regulates hedgehog signaling at the primary cilium. *Science* **317**, 372-6.

Roix, J. J., Hagge-Greenberg, A., Bissonnette, D. M., Rodick, S., Russell, L. B. and O'Brien, T. P. (2001). Molecular and functional mapping of the piebald deletion complex on mouse chromosome 14. *Genetics* **157**, 803-15.

Rosenbaum, J. L. and Witman, G. B. (2002). Intraflagellar transport. *Nature Reviews Molecular Cell Biology* **3**, 813-825.

Russell, L. B. (1961). Genetics of mammalian sex chromosomes. *Science* **133**, 1795-803.

Russell, L. B. (1971). Definition of functional units in a small chromosomal segment of the mouse and its use in interpreting the nature of radiation-induced mutations. *Mutation Research/Fundamental and Molecular Mechanisms of Mutagenesis* **11**, 107-123.

Russell, W. L. (1951). X-ray-induced mutations in mice. *Cold Spring Harb Symp Quant Biol* **16**, 327-36.

Russell, W. L., Kelly, E. M., Hunsicker, P. R., Bangham, J. W., Maddux, S. C. and Phipps, E. L. (1979). Specific-locus test shows ethylnitrosourea to be the most potent mutagen in the mouse. *Proc Natl Acad Sci U S A* **76**, 5818-9.

Russell, W. L., Russell, L. B. and Kelly, E. M. (1958). Radiation dose rate and mutation frequency. *Science* **128**, 1546-50.

Saadi-Kheddouci, S., Berrebi, D., Romagnolo, B., Cluzeaud, F., Peuchmaur, M., Kahn, A., Vandewalle, A. and Perret, C. (2001). Early development of polycystic kidney disease in transgenic mice expressing an activated mutant of the beta-catenin gene. *Oncogene* **20**, 5972-81.

Saijoh, Y., Oki, S., Tanaka, C., Nakamura, T., Adachi, H., Yan, Y. T., Shen, M. M. and Hamada, H. (2005). Two nodal-responsive enhancers control left-right asymmetric expression of Nodal. *Developmental Dynamics* **232**, 1031-1036.

Santos, N. and Reiter, J. F. (2008). Building it up and taking it down: the regulation of vertebrate ciliogenesis. *Dev Dyn* **237**, 1972-81.

Satir, P. and Christensen, S. T. (2007). Overview of structure and function of mammalian cilia. *Annual Review of Physiology* **69**, 377-400.

Schimenti, J. C., Libby, B. J., Bergstrom, R. A., Wilson, L. A., Naf, D., Tarantino, L. M., Alavizadeh, A., Lengeling, A. and Bucan, M. (2000). Interdigitated deletion complexes on mouse chromosome 5 induced by irradiation of embryonic stem cells. *Genome Res* **10**, 1043-50.

Scholey, J. M. (2003). Intraflagellar transport. *Annual Review of Cell and Developmental Biology* **19**, 423-443.

Schumacher, A., Faust, C. and Magnuson, T. (1996). Positional cloning of a global regulator of anterior-posterior patterning in mice. *Nature* **384**, 648.

Semenova, E., Wang, X., Jablonski, M. M., Levorse, J. and Tilghman, S. M. (2003). An engineered 800 kilobase deletion of Uchl3 and Lmo7 on mouse chromosome 14 causes defects in viability, postnatal growth and degeneration of muscle and retina. *Hum Mol Genet* **12**, 1301-12.

Shim, K., Minowada, G., Coling, D. E. and Martin, G. R. (2005). Sprouty2, a mouse deafness gene, regulates cell fate decisions in the auditory sensory epithelium by antagonizing FGF signaling. *Dev Cell* **8**, 553-64.

Shindo, T., Manabe, I., Fukushima, Y., Tobe, K., Aizawa, K., Miyamoto, S., Kawai-Kowase, K., Moriyama, N., Imai, Y., Kawakami, H. et al. (2002). Kruppel-like zinc-finger transcription factor KLF5/BTEB2 is a target for angiotensin II signaling and an essential regulator of cardiovascular remodeling. *Nat Med* **8**, 856-63.

Shopland, L. S., Lynch, C. R., Peterson, K. A., Thornton, K., Kepper, N., Hase, J., Stein, S., Vincent, S., Molloy, K. R., Kreth, G. et al. (2006). Folding and organization of a contiguous chromosome region according to the gene distribution pattern in primary genomic sequence. *J Cell Biol* **174**, 27-38.

Siegrist, S. E. and Doe, C. Q. (2007). Microtubule-induced cortical cell polarity. *Genes Dev* **21**, 483-96.

Simon, J. (1995). Locking in stable states of gene expression: transcriptional control during Drosophila development. *Curr Opin Cell Biol* **7**, 376-85.

Simons, M., Gloy, J., Ganner, A., Bullerkotte, A., Bashkurov, M., Kronig, C., Schermer, B., Benzing, T., Cabello, O. A., Jenny, A. et al. (2005). Inversin, the gene product mutated in nephronophthisis type II, functions as a molecular switch between Wnt signaling pathways. *Nat Genet* **37**, 537-43.

Small, J. V. and Kaverina, I. (2003). Microtubules meet substrate adhesions to arrange cell polarity. *Curr Opin Cell Biol* **15**, 40-7.

Sotillos, S., Diaz-Meco, M. T., Moscat, J. and Castelli-Gair Hombria, J. (2008). Polarized subcellular localization of Jak/STAT components is required for efficient signaling. *Curr Biol* **18**, 624-9.

Stehbens, S. J., Paterson, A. D., Crampton, M. S., Shewan, A. M., Ferguson, C., Akhmanova, A., Parton, R. G. and Yap, A. S. (2006). Dynamic microtubules regulate the local concentration of E-cadherin at cell-cell contacts. *J Cell Sci* **119**, 1801-11.

Sturtevant, A. H. (1965). A history of genetics: Harper & Row.

Szekeres-Bartho, J., Autran, B., Debre, P., Andreu, G., Denver, L. and Chaouat, G. (1989). Immunoregulatory effects of a suppressor factor from healthy pregnant women's lymphocytes after progesterone induction. *Cell Immunol* **122**, 281-94.

Szekeres-Bartho, J., Kilar, F., Falkay, G., Csernus, V., Torok, A. and Pacsa, A. S. (1985). The mechanism of the inhibitory effect of progesterone on lymphocyte cytotoxicity: I. Progesterone-treated lymphocytes release a substance inhibiting cytotoxicity and prostaglandin synthesis. *Am J Reprod Immunol Microbiol* **9**, 15-8.

Szekeres-Bartho, J., Par, G., Dombay, G., Smart, Y. C. and Volgyi, Z. (1997a). The antiabortive effect of progesterone-induced blocking factor in mice is manifested by modulating NK activity. *Cell Immunol* **177**, 194-9.

Szekeres-Bartho, J., Par, G., Szereday, L., Smart, C. Y. and Achatz, I. (1997b). Progesterone and non-specific immunologic mechanisms in pregnancy. *Am J Reprod Immunol* **38**, 176-82.

Szekeres-Bartho, J. and Wegmann, T. G. (1996). A progesterone-dependent immunomodulatory protein alters the Th1/Th2 balance. *J Reprod Immunol* **31**, 81-95.

Vale, R. D., Reese, T. S. and Sheetz, M. P. (1985). Identification of a novel force-generating protein, kinesin, involved in microtubule-based motility. *Cell* **42**, 39-50.

Venter, J. C. Adams, M. D. Myers, E. W. Li, P. W. Mural, R. J. Sutton, G. G. Smith, H. O. Yandell, M. Evans, C. A. Holt, R. A. et al. (2001). The sequence of the human genome. *Science* **291**, 1304-51.

Vierkotten, J., Dildrop, R., Peters, T., Wang, B. and Ruther, U. (2007). Ftm is a novel basal body protein of cilia involved in Shh signalling. *Development* **134**, 2569-77.

Vogel, J., Hess, W. R. and Borner, T. (1997). Precise branch point mapping and quantification of splicing intermediates. *Nucleic Acids Res* **25**, 2030-1.

Vokes, S. A., Yatskievych, T. A., Heimark, R. L., McMahon, J., McMahon, A. P., Antin, P. B. and Krieg, P. A. (2004). Hedgehog signaling is essential for endothelial tube formation during vasculogenesis. *Development* **131**, 4371-80.

Walker, R. A., O'Brien, E. T., Pryer, N. K., Soboeiro, M. F., Voter, W. A., Erickson, H. P. and Salmon, E. D. (1988). Dynamic instability of individual microtubules analyzed by video light microscopy: rate constants and transition frequencies. *J Cell Biol* **107**, 1437-48.

Washington Smoak, I., Byrd, N. A., Abu-Issa, R., Goddeeris, M. M., Anderson, R., Morris, J., Yamamura, K., Klingensmith, J. and Meyers, E. N. (2005). Sonic hedgehog is required for cardiac outflow tract and neural crest cell development. *Dev Biol* **283**, 357-72.

Waterston, R. H. Lindblad-Toh, K. Birney, E. Rogers, J. Abril, J. F. Agarwal, P. Agarwala, R. Ainscough, R. Alexandersson, M. An, P. et al. (2002). Initial sequencing and comparative analysis of the mouse genome. *Nature* **420**, 520-62.

Webster, D. R. and Borisy, G. G. (1989). Microtubules Are Acetylated in Domains That Turn over Slowly. *Journal of Cell Science* **92**, 57-65.

Welsh, I. C., Hagge-Greenberg, A. and O'Brien T, P. (2007). A dosage-dependent role for Spry2 in growth and patterning during palate development. *Mech Dev*.

Welsh, I. C. and O'Brien, T. P. (2000). Loss of late primitive streak mesoderm and interruption of left-right morphogenesis in the Ednrb(s-1Acrg) mutant mouse. *Dev Biol* **225**, 151-68.

Wheatley, D. N., Wang, A. M. and Strugnell, G. E. (1996). Expression of primary cilia in mammalian cells. *Cell Biol Int* **20**, 73-81.

Wilson, L., Ching, Y. H., Farias, M., Hartford, S. A., Howell, G., Shao, H., Bucan, M. and Schimenti, J. C. (2005). Random mutagenesis of proximal mouse chromosome 5 uncovers predominantly embryonic lethal mutations. *Genome Res* **15**, 1095-105.

Witte, H., Neukirchen, D. and Bradke, F. (2008). Microtubule stabilization specifies initial neuronal polarization. *Journal of Cell Biology* **180**, 619-632.

Wright, T. R. (1970). The genetics of embryogenesis in Drosophila. *Adv Genet* **15**, 261-395.

Yamada, T., Pfaff, S. L., Edlund, T. and Jessell, T. M. (1993). Control of cell pattern in the neural tube: motor neuron induction by diffusible factors from notochord and floor plate. *Cell* **73**, 673-86.

Yamada, T., Placzek, M., Tanaka, H., Dodd, J. and Jessell, T. M. (1991). Control of cell pattern in the developing nervous system: polarizing activity of the floor plate and notochord. *Cell* **64**, 635-47.

You, Y., Bergstrom, R., Klemm, M., Lederman, B., Nelson, H., Ticknor, C., Jaenisch, R. and Schimenti, J. (1997). Chromosomal deletion complexes in mice by radiation of embryonic stem cells. *Nat Genet* **15**, 285-8.

Zhang, M., Bolfing, M. F., Knowles, H. J., Karnes, H. and Hackett, B. P. (2004). Foxj1 regulates asymmetric gene expression during left-right axis patterning in mice. *Biochem Biophys Res Commun* **324**, 1413-20.

Zhang, X. M., Ramalho-Santos, M. and McMahon, A. P. (2001). Smoothened mutants reveal redundant roles for Shh and Ihh signaling including regulation of L/R asymmetry by the mouse node. *Cell* **105**, 781-92.

Zhang, Z., Alpert, D., Francis, R., Chatterjee, B., Yu, Q., Tansey, T., Sabol, S. L., Cui, C., Bai, Y., Koriabine, M. et al. (2009). Massively parallel sequencing identifies the gene Megf8 with ENU-induced mutation causing heterotaxy. *Proc Natl Acad Sci U S A* **106**, 3219-24.

Zhen, M., Huang, X., Bamber, B. and Jin, Y. (2000). Regulation of presynaptic terminal organization by C. elegans RPM-1, a putative guanine nucleotide exchanger with a RING-H2 finger domain. *Neuron* **26**, 331-43.

Zheng, B., Sage, M., Cai, W. W., Thompson, D. M., Tavsanli, B. C., Cheah, Y. C. and Bradley, A. (1999). Engineering a mouse balancer chromosome. *Nat Genet* **22**, 375-8.